uOttawa

L'Université canadienne
Canada's university

FACULTÉ DES ÉTUDES SUPÉRIEURES ET POSTOCTORALES

uOttawa

L'Université canadienne
Canada's university

FACULTY OF GRADUATE AND POSDOCTORAL STUDIES

François Brind'Amour
AUTEUR DE LA THÈSE / AUTHOR OF THESIS

M.A.Sc. (Mechanical Engineering)
GRADE / DEGREE

Department of Mechanical Engineering
FACULTÉ, ÉCOLE, DÉPARTEMENT / FACULTY, SCHOOL, DEPARTMENT

Navigation Sensor for Collaborative Mobile Robots

TITRE DE LA THÈSE / TITLE OF THESIS

Atef Fahim
DIRECTEUR (DIRECTRICE) DE LA THÈSE / THESIS SUPERVISOR

CO-DIRECTEUR (CO-DIRECTRICE) DE LA THÈSE / THESIS CO-SUPERVISOR

EXAMINATEURS (EXAMINATRICES) DE LA THÈSE / THESIS EXAMINERS

Rafik Goubran

Dan Necsulescu

Gary W. Slater
LE DOYEN DE LA FACULTÉ DES ÉTUDES SUPÉRIEURES ET POSTDOCTORALES /
DEAN OF THE FACULTY OF GRADUATE AND POSTDOCORAL STUDIES

Navigation Sensor for Collaborative Mobile Robots

François Brind'Amour

A thesis submitted to the Faculty of Graduate and Postdoctoral Studies in partial fulfillment of the requirements for the degree of

Master of Applied Science

in Mechanical Engineering

Ottawa-Carleton Institute for Mechanical and Aerospace Engineering
University of Ottawa
Ottawa, Canada

September 2005

©2005 François Brind'Amour

Library and Archives Canada

Published Heritage Branch

395 Wellington Street
Ottawa ON K1A 0N4
Canada

Bibliothèque et Archives Canada

Direction du Patrimoine de l'édition

395, rue Wellington
Ottawa ON K1A 0N4
Canada

Your file Votre référence
ISBN: 0-494-11226-3
Our file Notre référence
ISBN: 0-494-11226-3

NOTICE:
The author has granted a non-exclusive license allowing Library and Archives Canada to reproduce, publish, archive, preserve, conserve, communicate to the public by telecommunication or on the Internet, loan, distribute and sell theses worldwide, for commercial or non-commercial purposes, in microform, paper, electronic and/or any other formats.

The author retains copyright ownership and moral rights in this thesis. Neither the thesis nor substantial extracts from it may be printed or otherwise reproduced without the author's permission.

AVIS:
L'auteur a accordé une licence non exclusive permettant à la Bibliothèque et Archives Canada de reproduire, publier, archiver, sauvegarder, conserver, transmettre au public par télécommunication ou par l'Internet, prêter, distribuer et vendre des thèses partout dans le monde, à des fins commerciales ou autres, sur support microforme, papier, électronique et/ou autres formats.

L'auteur conserve la propriété du droit d'auteur et des droits moraux qui protège cette thèse. Ni la thèse ni des extraits substantiels de celle-ci ne doivent être imprimés ou autrement reproduits sans son autorisation.

In compliance with the Canadian Privacy Act some supporting forms may have been removed from this thesis.

While these forms may be included in the document page count, their removal does not represent any loss of content from the thesis.

Conformément à la loi canadienne sur la protection de la vie privée, quelques formulaires secondaires ont été enlevés de cette thèse.

Bien que ces formulaires aient inclus dans la pagination, il n'y aura aucun contenu manquant.

Canada

Abstract

This thesis presents a possible inexpensive and simple solution for humanitarian demining in developing countries. It consists of a group of mobile robots that can advance and interact collaboratively with each other in a mine field. A base station controls the group and can map their position with the aid of a long range positioning system, thus, identify the landmine position when one is detected by a robot. A short range positioning system is used within the group to measure the distance separating them from one another and the geometry of the formation.

A prototype battery powered mobile robot platform has been developed and tested. Electronic hardware and software was designed and built to allow for low level control of the movements of the vehicle and for wireless communications with a base station. The base station exercises high level control over the mobile robot. A positioning system consisting of a long and a short range positioning system has been designed. The short range positioning system, which uses sonic waves within the audible frequency range, has been implemented and tested. Operating within the audible frequency range reduces the sensory system cost and results in an omni-directional range measuring system. The system provides sub-wavelength precision with an absolute error less than 2 cm for distances from 1 m to 4 m at a 5 KHz frequency.

Acknowledgements

This thesis could not have been realized without the help of many persons. The Author would like to thank particularly some of the greatest contributors for their direct or indirect help to this work.

The support staff from the Department of Mechanical Engineering of the University of Ottawa was of great help. Thanks to Michel Robert and Alan Stewart for their help with building the electronic modules. Thanks to Madan Makasare, Leo Denner and Gregg for their involvement in building the physical robot. Thanks to Kristian Ewen for helping me conducting surveys on the SRPS, enduring cold weather.

Special thanks go to Jessy Fleurent for his help in theoretical and practical advices concerning electronics and mathematics.

I would like to thank especially Dr. Atef Fahim for his advices, support, and guidance throughout this thesis.

Finally, I must thank Andréane for being so supportive of my choice of doing graduated studies, especially in the final stages of this work.

Table of Contents

List of Figures

List of Tables

Nomenclature

0x	Identifier for hexadecimal numbers (ex: 0x7F2A is equivalent to 32554)
%	Identifier for binary numbers (ex: %01001100 is equivalent to 38)
AGV	Autonomous Guided Vehicle
AP	Anti-personnel
ATD	Analog-To-Digital
CCD	Charge-Couple Device
DC	Direct Current
DGPS	Differential Global Positioning System
EEPROM	Electrically-Erasable Programmable Read-Only Memory
FNA	Fast Neutron Analysis
GPR	Ground Penetrating Radar
GPS	Global Positioning System
IMAS	International Mine Action Standards
IMS	Ion Mobility Spectrometer
ISR	Interrupt Service Routine
LED	Light-Emitting Diode
LIFO	Last In First Out
LRPS	Long Range Positioning System
MCU	Microcontroller Unit
MOSFET	Metal-Oxide-Semiconductor Field-Effect Transistor
NGO	Non-Governmental Organization
NQR	Nuclear Quadrupole Resonance
PC	Personal Computer
PCB	Printed Circuit Board
PI	Proportional-Integral
PWM	Pulse Width Modulation
RAM	Random Access Memory
RF	Radio Frequency
SA	Selective Availability
SNR	Signal-to-Noise Ratio
SRPS	Short Range Positioning System
TCNT	Timer Count Register
TMA	Thermal Neutron Analysis
UN	United Nations
UWR	Ultra-Wideband Radar
UXO	Unexploded Ordnance
VJT	Vector Jump Table

1 Introduction

1.1 Landmines

For over a century, landmines have been used in wars for many purposes. Among them, preventing enemies from passing or entering certain areas, to force them to go through certain areas, or slow them altogether. During numerous conflicts in Europe, Africa, Asia, the Middle East, Central and South America, landmines have been laid. During 2002, there were over 11,700 new casualties due to landmines and unexploded ordnances (UXO), and among them, over 2,649 children [18].

While in theory the location of mines should be well documented and mapped by the layer, in the chaos of the aftermath of a war or conflict, often, their location is forgotten, and they remain functional for many years. Up until recently, persistent mines where the only ones available. Persistent mines are a type of landmines that does not deactivate themselves over time. By opposition, a non-persistent mine will self-deactivate within hours or days after being used. They theoretically do not pose a threat to civilians after the end of a conflict.

The presence of mines in an area prevents local habitants from reclaiming their home back after the conflicts subside, rebuild what was destroyed or to cultivate the land, or, when they do come back, civilians are wounded or killed. Those desperate or brave enough to attempt a come back are wounded, maimed or killed. It affects men, women, and children, without distinction.

The only known method of deactivating persistent land mines is by removal or clearing. General mine clearing techniques can be divided into two classes: military and civilian mine clearing. Both are very different in their objectives and methods, and are not necessarily compatible with one another.

As a general definition, military mine clearance calls for clearing a path through a minefield. The main objective is the advancement of troops and equipment. The demining must be done quickly, as the goal is to advance. It relies on mechanical devices, such as mechanized plows, flails or rollers to explode or disable the mines. For military purposes, a clearance rate of 80% is considered sufficient and limited casualties are considered as acceptable [5]. The state of the terrain after the passage of the equipment is also of minor importance.

As opposed to military landmine clearance whose goal is to clear a limited area to create a path, civilian landmine clearing operations must ensure that a large area is safe and suitable for agriculture or construction. The standards are much higher than for military mine clearance. Standards for civilian mine clearing practices has been formulated by the United Nations.

Since civilian mine clearing is not within the mandate of the military, and is not commercially profitable, it is generally left to the local population or to Non-Governmental Organizations (NGO) or Aid organizations. Such organizations are generally heavily under funded. Consequently, the equipment that is generally used for civilian mine clearing tends to be very inexpensive, and the techniques used tend to be primitive and rely heavily on manual labour.

1.2 Thesis Outline

This thesis presents a robotic platform that could be used for civilian mine clearing in certain environments. It consists of a group of small, very inexpensive robots that exert small ground pressure, that can interact together, and serve as a platform for landmine detection equipment. The concept includes a base station controlling a group of robots. A long range positioning system, based on a camera with image analysis that permits to the base station to know where is the group of robots in the landmine affected area. A short range positioning system, based on the time of flight of sound, permits the robots to know the distance separating each robot from the others, and by proxy, the exact configuration of the robots formation. The maximum error obtained for this short range positioning system is about 2 cm for distances up to 4 m.

Chapter 2 presents a review of the present knowledge about landmines, current demining techniques and technology, demining robots and positioning systems.

Chapter 3 outlines the reasons leading to the choice of the system presented in the remaining of this thesis. It also describes the general architecture of the system that is developed further in the thesis.

Chapter 4 presents a detailed evaluation of suitable positioning systems for this project, and the particular choice that was made for this work.

Chapter 5 explains the principles of a long range positioning system. A short range positioning system is required for the long range positioning system to work. This short range positioning system is details the design and the development of short and long range positioning systems. The short range positioning system is based on the speed of audible waves in air, and can attain sub-wavelength accuracy.

Chapter 6 describes the design of the mechanical and electronic subsystems of the robotic platform. Many electronic modules were designed to control the robot movements, control the communications with other robots and the base station, and to implement the short range positioning system.

Chapter 7 describes the software developed for control of the robot functions and wireless communication with the base station.

Chapter 8 presents the results of tests carried out to prove the concept of the short range positioning system.

Chapter 9 concludes the thesis by providing a summary and a discussion of the work. The chapter also outlines future work that could remedy deficiencies and improve the performance of the demining system.

2 Literature Review

2.1 Landmines

2.1.1 The Landmine Problem

Landmines have been used extensively during 20^{th} century for many reasons. They have been used both in military and civilian conflicts. When used by non-military groups, it is to prevent people from returning to their home. The military mines used can be also harmful to civilians when they are not removed or de-activated at the end of the conflict, and their location is forgotten.

About 100 million mines have already been laid in more than 60 countries [14], [31]. Landmines have economic, medical, social and environmental consequences on the affected populations. A commonly used figure is that landmines cost about $3 to produce, and up to $1,000 to remove. At the present removal rate, it will take decades to remove all landmines. However, not all mined areas are problematic. Areas are generally classified as high, medium, and low priority minefields.

In 1997, in Ottawa, Canada, a total of 122 governments signed the Mine Ban Treaty, officially titled: *"The 1997 Convention on the Prohibition of the Use, Stockpiling, Production and Transfer of Anti-Personnel Mines and on Their Destruction"*, sometimes referred to as the Ottawa Convention. As of 31 July 2003, a total of 134 countries were State Parties to the Mine Ban Treaty, and another 13 had signed but not yet ratified [18].

The Landmine Monitor Report [18] is an annual report that presents the current state of the use of landmines around the world. It includes information about countries using landmines, countries possessing landmines, mine action funding and other humanitarian demining data. The section "Major Findings" presents a summary about countries still producing and using landmines, stockpile landmines, mine-affected countries, state of mine action funding.

The United States Department of State presents, in an annual report [39], the accomplishments of the U.S. Humanitarian Mine Action Program. It provides detailed information about landmine-affected countries, country-by-country. It also provides information about the Humanitarian Demining Training Center, a facility located at Fort Leonard Wood, Missouri, USA. It is a center whose primary mission is to train U.S. military personnel in accordance with International Mine Action Standards. Their approach is to "Train-the-Trainer". They train an initial team from a host country in mine clearing techniques. This initial team is then made responsible for training indigenous groups.

2.1.2 Organizations

A host of organizations dedicate their efforts to demining operation, and to helping victims of mines. A list of these is provided in Appendix A.

2.1.3 Demining Techniques

As stated in Section 2.1.1, mine affected areas must first be prioritized, based on the impact of the minefield on the area. Places like uninhabited borders or deserts are less important to demine than fields that could serve for agriculture. From [14], 5 basic parts compose the humanitarian landmine clearing process:

1. Locate and identify the minefield
2. Prepare and clean the minefield (cut vegetation, remove metal fragments from surface, etc.)
3. Locate and mark individual landmines
4. Neutralize landmines by removal or in-place detonation
5. Ensure there is no mine left (quality control)

The quality control is an important step. International Mine Action Standards (IMAS, www.mineactionstandards.org) is a set of standards developed by the United Nations (UN). The UN standards for quality of a mine removal operation changed in 2001. Before that, it was required that 99.6% of all landmines must be removed. Now, the standard states that all landmines have to be removed to a depth of 200 mm below original ground level (IMAS 09.10). Local populations must also have confidence that demining has been done properly, so it is reported that they sometimes organize a soccer match on the now cleaned minefield to prove that the area is safe [31].

There are many ways to detect and remove landmines, and there is a general consensus in affirming that there is no single tool that is appropriate for every situation. References [6], [14] and [22] provide a good overview of demining techniques.

Landmine Field Identification

By virtue of the design of mines, minefields are not easily identified. Once laid, their location is often unknown except to those who laid them. Landmine field locations can be found if some mines are exposed due to ground erosion. Already exploded mines can also facilitate the identification of a minefield [22]. Oral tradition (soldiers, accidents, local population) can also help in identifying minefields [31].

Manual Probing

Manual probing consists of prodding the ground with a thin steel shaft at a shallow angle (~30°) at short regular intervals (~2 cm). When a hard object is detected, the deminer has to carefully dig around the suspect object to identify it. It is a very slow and meticulous task, and deminers have to stay concentrated. A single deminer can clear 20-50 m^2 per day using this method. Since the manual probing method is very extensive, it is considered the only way that can guarantee complete detection of landmines [22]. Even if manual probing does not seem to be a high technology method, it is widely employed and research in this domain is important (protective gear, vegetation cutting equipment, prodding and excavation tools, etc.) because it can make a rapid difference in minefield cleaning efforts [6].

Metal Detectors

Metal detectors are devices capable of detecting very small amounts of metal (under 1 g) in the ground at shallow depths. They are therefore capable of detecting minimum metal content landmines, in which often only the striker pin is made of metal [5]. This advantage is also an inconvenience because minefields are usually cluttered with small metal parts, like shrapnel. These increase dramatically the amount of false alarms, and every one of them must be carefully checked, and its source identified. The false alarm rate is in the order of 1 landmine for every 1,000 alarms. The accuracy of metal detectors also heavily depends on the nature of the soil and the amount of water in it [6], [14], [15].

Dogs

Dogs are considered very good at landmine detection. Their nose is orders of magnitude more sensitive than human ones. They can detect quantities of 10^{-12} to 10^{-13} g of explosives [5]. They also do not suffer from malfunctions due to the hostile and dirty environment as high technology electronic or mechanical equipment, and are usually well accepted by local demining groups. However, dog training is extremely difficult and expensive, and they treat landmine detection as a game, which could have deadly consequences. They cannot be used for extended periods of time, as they become tired and bored quickly. They are therefore used for quality control, after mine clearing activities, and for minefield delimitation (finding roughly the limits of a minefield) [6].

Flails

Instead of trying to locate precisely the landmines, this technique deals with detonating or exploding them. A rotating drum with attached chains rotates rapidly in front of a blast-protected vehicle. The chains hit the ground to a controlled depth, detonating or breaking the landmines apart. Prices for those vehicles are very high (starting at ~500,000 €) [6].

Other Sensors

Many other types of sensors are in development, but they are not yet widely used, either due to their high cost, because their technology is not mature enough, or because of operating complexities. Table 2.1 was adapted from [6] and presents a survey of landmine detection technologies, their maturity and their cost. This information was compiled in 1999. As there is active research conducted in those areas, the information contained in this table is subject to change rapidly in the future.

Table 2.1 Landmine Detection Technologies, Maturity and Costs

Sensor technology	Maturity	Cost	Comments
Dogs	High	High-Very High	Used in practice
Prodding / Excavation	High	Very Low	Used in practice
Magnetic Devices	High	Medium	Used in practice
Metal Detectors	High	Low	Used in practice
Metal Detector Array	High	High-Very High	Used in practice?
Passive mm Wave	Low-Medium	Very High	EU HOPE project claims low cost
mm Wave Radar	Low	Very High	Cost based on lab equipment
Passive Infrared	Medium-High	High	Cost is decreasing
Polarized Infrared	Medium	Very High	
Multispectral	Low	Very High	
Ground Penetrating Radar (GPR)	High	Medium-High	
Ultra-Wideband Radar (UWR)	Low-Medium	High-Very High	
GPR Array	Medium-High	Very High	
Nuclear Quadrupole Resonance (NQR)	Medium	High	
Thermal Neutron Analysis (TMA)	Medium	Very High	
Fast Neutron Analysis (FNA)	Low-Medium	Very High	
Ion Mobility Spectrometer (IMS)	Medium	Medium-High	
Biosensor	Medium-High	Medium	

Those sensors are described in, amongst others, references [5], [6], and [22]. These references also present a good summary of future landmine detection methods.

2.2 Demining Robots

Many robots have been built for humanitarian demining. Unfortunately, few, if any of them are actually used. This is because of their high initial and operating costs, their operating complexity, or because they are difficult to repair on location in the third world countries in which they have to operate. Another reason is their poor adaptability to the different terrains on which they have to navigate. Reference [8] presents a good summary of the numerous attempts to use robots for demining.

The Dervish (www.dervish.org) is a vehicle meant to detonate mines. It is made of three wheels, with their respective axis pointed at the center of the robot. The robot circles in spirals, evolving at about 1 meter per minute, and applying a pressure high enough to detonate the anti-personnel landmines. It is resistant to the blast of an anti-personnel landmine.

Professor J. Trevelyan, from the University of Western Australia, proposed a suspended pole robot. Three or four poles are positioned at the edge of a mined area. Cables attached to the poles suspend a tool that can be moved over the minefield, much like a traffic light is suspended over an intersection. The tool can either be a passive probe used to detonate mines by touching the ground at regular spaced intervals, or an active probe, such as ground penetrating radar [38].

Of interest is a class of robots used as a mobile platform that can be used for many sensor types. The Pemex robot (http://www.maechler.ch/philip/epfl/pemex/index.html), by Prof. J. Nicoud and P. Mächler of Swiss Federal Institute of Technology, is a robot that runs on two bicycle wheels, and has a sensor head that can be swept left and right. The sensor head is a hemisphere containing the detector and electronics, and it is gliding on the ground.

The WHEELEG robot (http://www.scg.dees.unict.it/giovanni/WHEELEG.HTM) is made for rough terrain, using both wheels and legs to move itself. Its intended applications are humanitarian demining and exploration on rough terrain.

Reference [8] is a thesis done on the design of landmine detection machines. It presents two possible designs, Lizard and Worm, which are small robots. Their shape, as their name state it, are based on small animals that can easily move on irregular ground and through vegetation.

2.3 General Positioning Systems

For autonomous robotic systems, knowing the position of a robot with respect to other robots or with respect to surroundings is a problem to which many solutions were proposed. The most applicable of these systems are discussed below.

2.3.1 Dead Reckoning

The most basic system used is dead reckoning. Its basis is to determine the present position based on a known traveled distance, velocity, and direction from a known starting point. It is also known as odometry. The required information to determine the present position can be deduced from wheel rotation, number of steps of a leg, etc. The error associated with this technique is incremental, since the absolute position is not known directly from this technique. If there is a wheel slip, or the robot moves on uneven or rough terrain, the error can grow rapidly. Even though dead reckoning is prone to incremental error, it can be used in conjunction with other techniques to periodically null out the error. If conditions are good, it can be very precise on short distances [2].

Advanced mathematical treatment of the signal can lead to drastic reduction in accumulated error [9]. This is accomplished through Kalman filters and careful calibration. Attention must also be given in the wheel design itself. Some robots include knife-edged non-driven wheels to minimize wheel slippage.

2.3.2 Heading

Heading is often an important piece of information that can be combined with odometry through sensors fusion. Heading information can be known by many types of sensors.

Mechanical gyroscopes are based on a rotating disc suspended in a gimbal. If the gimbal frame is rotated, the disc rotation axis will tend to stay the same. An optical gyroscope functions in a similar way, except that it relies on interfering patterns of light travelling in a closed-loop optical fiber. Like for dead reckoning, gyroscopes are subject to drift from friction and earth rotation. The earth rotation can be corrected for if the latitude is known [2].

Geomagnetic sensors are devices that measure the magnetic field orientation of earth. They give an absolute heading value, and are not subject to drift. Mechanical magnetic compasses are the most widely known form of geomagnetic sensors, but other types of sensors are also available [2].

The polarized light emitted by the blue sky can also serve as a base for heading sensors used in robotics [35]. This polarization varies with the position of the sun and clouds, but it is an information used by the honeybee and the desert ants to find their way.

2.3.3 Global Positioning System

The Global Positioning System (GPS) is a satellite-based one developed by the U.S. Department of Defense. The position is determined by a technique based on triangulation of signals from a number of reference satellites in known orbital positions [2]. Selective Availability (SA) was initially used to intentionally decrease positioning accuracy to about 100 m. SA has been turned off on May 2, 2000 [26] and, at the time of the writing of the thesis, the relative accuracy of GPS is now about 15 m [11], [23].

2.3.4 Beacons Systems

Triangulation or trilateration are techniques that can give position information within an area delimited by beacons whose locations are known. Triangulation is achieved by measuring the angle of reception of a signal from three or more beacons. Trilateration is achieved by measuring the distance to known beacons. There are many ways to measure distance to the beacons, or angle between them. The angles for triangulation can be found by using a rotating laser with reflective beacons where the rotation angle is captured once the beam is reflected. The distance for trilateration can be found through the time of flight of signals received by the robot and emitted from emitters located on each beacon, or vice versa. [2]. Using trigonometric relationships, the location of the robot with respect to the known locations of the beacons would be determined.

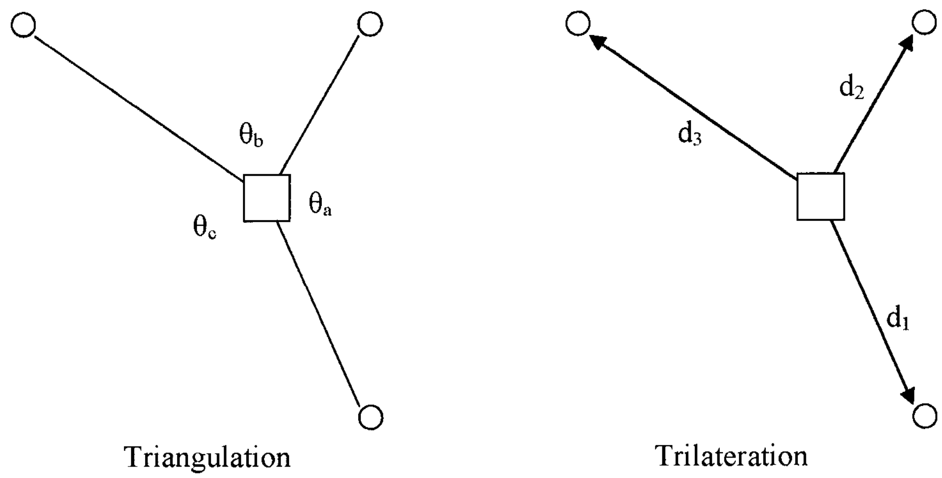

Figure 2.1Triangulation and Trilateration Positioning Systems

2.4 Sound-Based Positioning Systems

For mobile robotics, ultrasonic ranging systems are often used because of their convenience and ruggedness. The ultrasonic ranging system is based on the speed of an acoustical wave (sonic, ultrasonic) propagating in a medium (air, water, etc.). In sonar (or pulse-echo mode) applications, a burst of waves is emitted, reflected by an object and detected. From the total time-of-flight of the wave, it is possible to deduce the distance, since the speed of the wave in the medium is known. In transmit-receive mode, the emitter and the receiver are placed at the two ends from which it is desired to know the distance. Both configurations are shown in Figure 2.2.

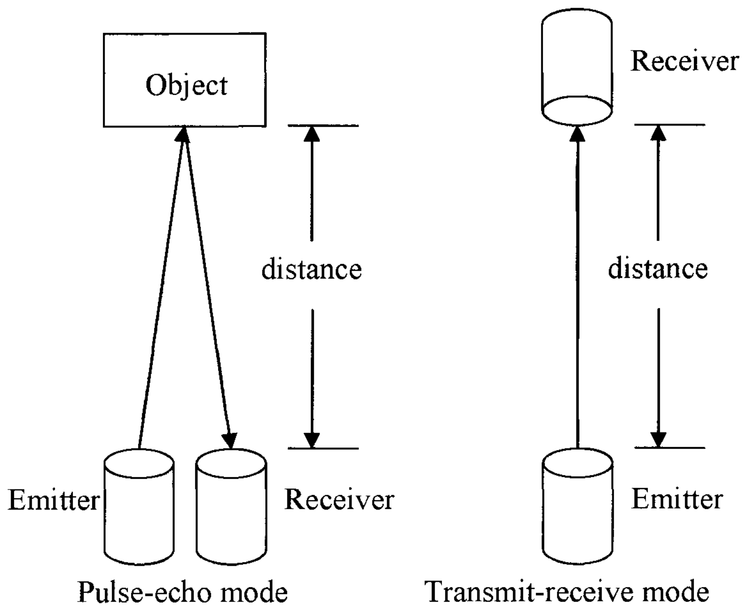

Figure 2.2 Comparison of Pulse-Echo Mode vs Transmit-Receive Mode

2.4.1 Time of Flight Detection

Several problems are associated with each method. The first one has to do with precision. Very often, a small burst of a few waves at a certain frequency is emitted. The start of the emission is known, and the incoming wave is detected after some time by the receiver, which now knows the time elapsed for the wave to travel the distance (or twice the distance in sonar applications). The problem is to know the exact time of arrival, since the receiver only detects the presence of the frequency. Often, a threshold is used to achieve this detection, and this method is sensitive to the intensity of the incoming wave. Those problems are discussed in [1], [10], [13], [17], [29], [34], [37], and [42].

Figure 2.3 shows that a simple fixed threshold can affect the time of arrival detection. If the overall wave amplitude was, even slightly, lower or higher, a different time of arrival would have been detected, thus inducing a variability decreasing precision.

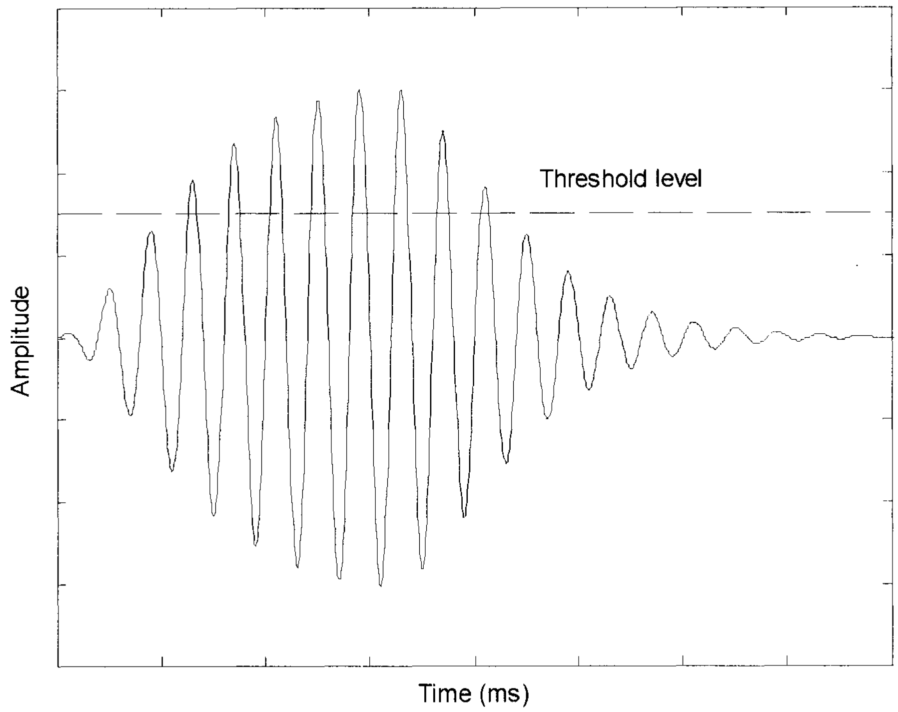

Figure 2.3 Effect of Threshold on Time of Arrival Detection

Several techniques are used to overcome this problem. Some deal with phase detection. However, this technique is ambiguous if the distance is greater that one wavelength, such that several solutions exist. Figueroa and Barbieri [10] used a high frequency signal, modulated by a low frequency signal. This technique permits to combine the precision of the frequency based technique with the range of the amplitude based technique.

Some other authors ([13], [34], and [37]) use methods to detect either the signal envelope or the phase within the burst of wave, achieving precisions similar to phase detection, but for distances greater than one wavelength.

2.4.2 Directionality

Ultrasonic systems usually found in mobile robotics and other ranging applications are highly directional. That is to say, both the emitter and the receiver have to be facing one another. In this application, where the robot's orientation can be random, this means that the system has to cover 360°. Numerous solutions have been proposed. Wang et al. [41] propose a system where a laser rangefinder scans an area by using two servomechanisms. Ureña et al. propose to use sets of 8 transducers, operating in both emitting and receiving mode, to cover 240° per module. By adding overlap for each module of 8 transducers to add redundancy, they use 4 of those modules to cover a full 360°. Kleeman [19] also uses multiple emitter-receiver modules, and steers them with servomotors. They add a feature consisting in cross-correlating the received echo with an echo template to distinguish between the emissions of the different modules.

2.4.3 Speed of Sound

As the ranging system is based on the speed of sound, this quantity must be known with sufficient precision. It is known that the speed of sound is mainly affected by temperature, and, to a lesser extent, by humidity. Temperature can be compensated for very easily by measuring it, and so can humidity. Humidity is rarely compensated for, due to minimal influence on the speed of sound. A temperature gradient is very difficult to measure, and can pose a challenge for a distance measurement based on the speed of sound. A method is described in [24] and [25] to deduce speed of sound by using more receivers than necessary. An emitter generates a pulse that is received by many receivers. A formulation is presented to calculate the distance from each receiver to the emitter, along with the speed of sound.

3 Proposed Platform for Mine Detection

3.1 Requirements

As has been mentioned earlier, the goal of mine clearing is to identify mined areas, and remove or destroy landmines. This process can be accomplished in two radically different ways. Either it is done by military organizations or humanitarian organizations.

3.2 Other Considerations

Landmines are laid in many different parts of the world and come in many different models. Therefore many different ways of removing them are necessary [16]:

"Field experience confirms that the search for the single, comprehensive machine that can respond in all contexts and against all threats is not only unrealistic but may also delay innovation."

Even if the perfect machine for mine removal does not exist, it is possible to make a contribution to humanitarian mine clearing, while advancing in the field of mobile robotics.

3.3 Minerats Concept

The landmine trigger mechanism is activated by virtue of a force acting on it. The magnitude of that force is adjusted to the weight of the intended target. For example, antipersonnel mines have their trigger mechanism adjusted to the weight of a person, while anti-tank mines are designed to detonate under a heavier weight. By far, anti-personnel mines have the most sensitive trigger mechanism. Hence, a solution that would prevent the mine from being detonated is that of the Minerats concept. Following the Minerats concept, robots that are light enough such that they do not trigger the mines while going over them are used for demining.

Furthermore, according to this concept, a multitude of small inexpensive robots move in tandem in a mine field to detect mines. This idea was first described by [40] in 1995. Applying this concept and pushing it further, it is proposed to have a team of small, lightweight and inexpensive robots that could move coordinated and autonomously in a formation, scanning a minefield and detecting the landmines for further removal. Since the robots do not have to remove the mines, they do not need to be mechanically complicated.

3.4 Global Architecture

In order to effectively realize the Minerats Concept, many components are needed. The first one is a vehicle group, operating as a team. This way, it becomes possible to scan a whole area in a reasonable amount of time. Those vehicles should be rugged, simple, and exert low enough ground pressure to avoid detonating the landmines. They should have some means for working together, either by having a base station coordinate their formation, or whereby each robot having a mean to know the position of the other robots and to be able to communicate with each one another. This implies some kind of positioning system.

Because of vulnerability to possible explosions, the robot cost should be kept as low as possible. To achieve this goal, a good solution is to build the robots with as few high-cost decision making controllers as possible, and locate the high-cost decision making controllers in a base station. The base station controls the group of robots via remote control through a radio communication link. The base station would be located out of harm's way. This approach requires means for the base station to know the position of each robot. It should be note, however, that this was true at the time of the design of the robots. Ongoing trend in increasing processing power and decreasing prices may render feasible the use of more complex processors on the robots in the future.

This way, a group of robots will be sent to a minefield, controlled by a base station that has some way of knowing their position. The group of robots will therefore be able to scan the minefield, looking for landmines with some kind of detection device. The group of robots needs to be at a safe distance from the base station, to avoid damages to it in case of explosion. The more robots there are scanning the minefield, the faster the demining process will be.

Since the typical safe fragmentation radius is generally below 100 m for personal landmines [7], a maximum working distance of 200 m would provide a minimum of 100 m between the group of robots and the base station. The usable working range is depicted in Figure 3.1. The maximum working distance is a preliminary value used for design of positioning system and robots, and is subject to revision as the project goes on and further technological advancements are made.

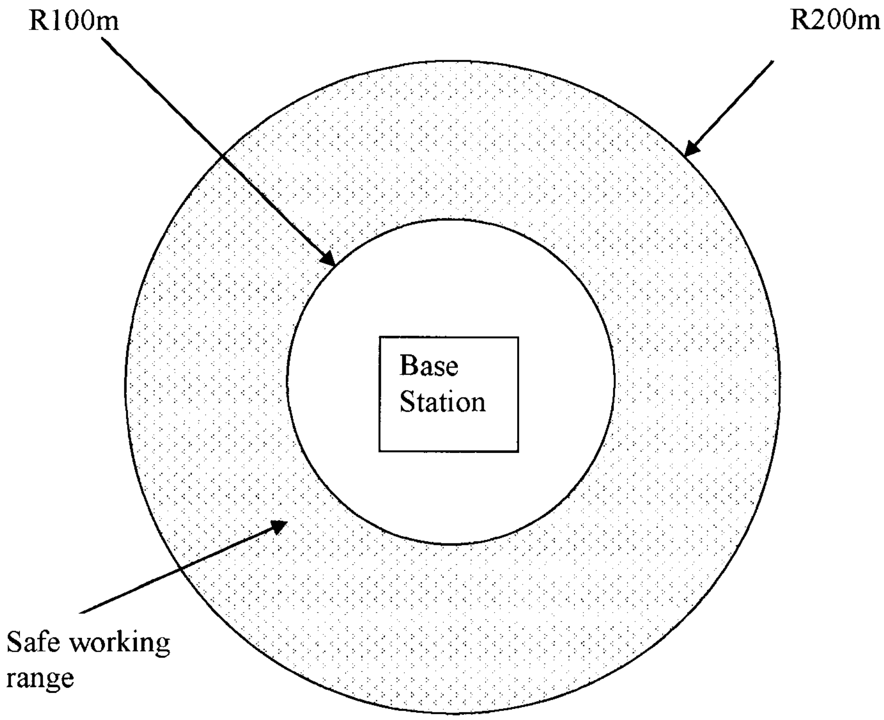

Figure 3.1 Safe Working Range Relative to Base Station

3.5 Mine Detection Hardware

Some kind of landmine detection hardware should be installed on the robots. This way, they could mark the location of detected landmines for further removal. The robots should therefore have payload capacity to install these detectors. However, it is outside the scope of this thesis to work on the mine detection hardware.

4 Positioning System

4.1 The Need for a Positioning System

As stated in Chapter 3, the demining system is composed of a base station controlling a team of robots crawling in formation in a minefield to detect landmines. For purposes of coordination, there must be some kind of communication between the base station and the robots, and preferably also between the robots themselves. Also, in order to properly control the robots, the base station must know where the robots are, and where they are going. Therefore, some kind of positioning system is needed.

It was also stipulated in Chapter 3 that the working range of the group of robots from the base station has to be from 100 m to 200 m. Since the goal of the project is to detect and mark the locations of landmines for later removal, the position of the robots must be known to a certain precision. If the position of a landmine is known to within less than 1 m, it should be easy to locate for removal afterwards. The more precise the location of the landmine, the easier and safer it will be to neutralize or remove it with minimal hazard.

4.2 Considered Principles

4.2.1 Global Positioning System

The GPS system would provide each robot with an absolute and independent positioning system. However, the precision is about 15 m [11], [23].

Differential GPS (DGPS) is a technique than can be used to reduce the error in position to 4 to 6 m. For that, a DGPS station must remain stationary at a known position, and transmits a correction signal to a DGPS-capable receiver within range of less than about 10 km. The cost of such a system is about $2,000 for a differential-capable GPS receiver, and between $10,000 and $20,000 for the DGPS station [2].

However, this system is quite expensive, as a GPS receiver would have to be mounted on each robot. A GPS receiver currently costs about $200 and hence is deemed too expensive, since each robot is exposed to destruction and must be very inexpensive. Also, at 15 m precision, the accuracy of this system is also much lower than the target goal of about 1 meter.

Again, as stated in section 3.4, improvements in the GPS will certainly have an effect of increasing the precision and decreasing the costs associated with it. It might become a possible solution later on.

4.2.2 Laser Ranging System

Laser ranging uses time-of-flight type of system based on the speed of light. The target whose distance is to be measured is illuminated with a laser pulse. The laser is then reflected back to the emitter, and the total time taken is measured. The distance from laser to target can then be calculated as shown below [4]:

$$R = \frac{v \cdot \Delta T}{2} \tag{1}$$

Where
R is the distance from emitter to target (m)
v is the wave propagation velocity (m/s)
ΔT is the total wave front travel time (s)

Here, the wave propagation velocity if laser is used is approximately 3×10^8 m/s in vacuum [4]. If a resolution of 1 meter is desired, ΔT can be calculated to 6.7×10^{-9} s. As the frequency is the inverse of time, a clock of 150 MHz is required to measure elapsed time with the necessary resolution. A technique called *"time transformation"* can be used to stretch the measured time, hence requiring slower clock to obtain the same resolution [4]. Typical spreads of 1:100,000 are common in short range applications. That would mean the ΔT for 1 m would become 667×10^{-6} s, or a clock of 1.5 kHz, which is well within the range of small microcontrollers.

The laser ranging system could be usable if combined with another system permitting one to aim the laser on a suitable surface on each target. The laser system in this case would be located at the base station, and would sample the distance to each robot sequentially. The distance between the robots and their formation can then be inferred from their distances and the angle of pointing.

Alternatively, each robot would be equipped with a laser system and would sequentially sample the distance to each of the other robots and to the base station. While this approach would increase the accuracy of the system, it would also increase its cost considerably.

4.2.3 Two Cameras with Triangulation

This system consists of two cameras situated at the base station, and looking at a robot. Both cameras are separated by a known distance, and are equipped with angle measuring device. The two cameras and the robot form a triangle with two known included angles and one known side. Figure 4.1 shows the general idea.

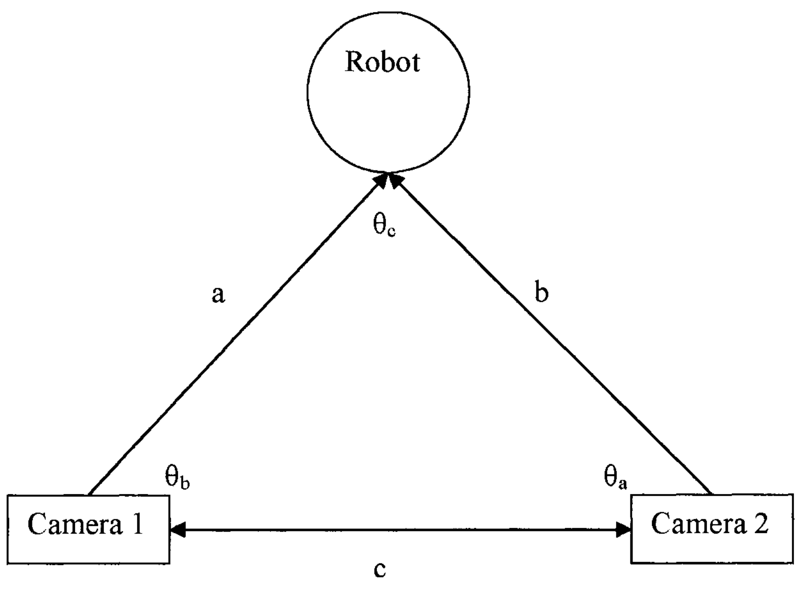

Figure 4.1 Two Cameras with Triangulation Positioning System

The position of the robot can then be deduced by the cosine law. With reference to Figure 4.1, the distance of the robot from a camera system is given by the Sine Law:

$$\frac{a}{\sin(\theta_a)} = \frac{b}{\sin(\theta_b)} = \frac{c}{\sin(\theta_c)} \tag{2}$$

By knowing angles θ_a and θ_a, and dimension c, it is possible to find the position of the robot with respect to the camera system.

4.2.4 One Camera and Known Focal Length

For this system, a camera with a variable zoom is needed. The focal length of the camera must also be known. If the camera looks at two or more robots, and the distance between the robots is known, along with the focal length, then, the distance from the camera to the robots can be computed. This system has the advantage of needing only one camera with a tracking mechanism to keep the robot formation in view. The zoom capability is needed to maximize the projection of the target behind the lens and increase accuracy. The distance to the robots can be inferred from the size of the formation, the size of its projection, and the focal length as follows:

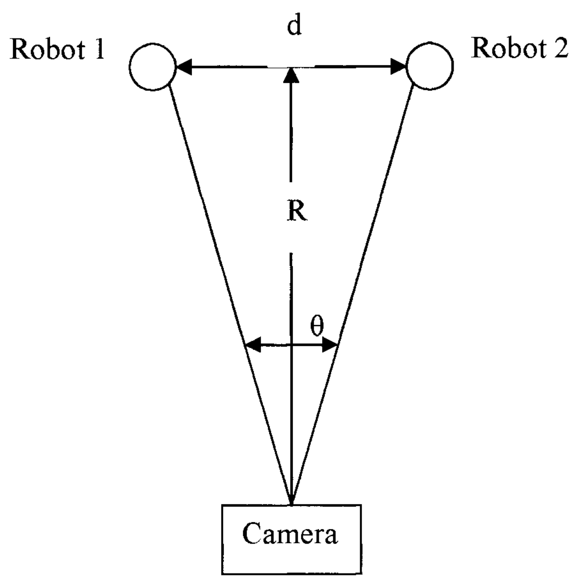

Figure 4.2 Explanation of Ranging with One Camera

$$R = \frac{d}{2 \cdot \tan\left(\frac{\theta}{2}\right)} \qquad (3)$$

Where

R is the distance from camera to the robots

d is the distance between the robots

θ is the angular separation between the robots

The distance d has to be known. This could be found using a short range positioning system. The angle can be found by using the distance separating the robots in the image (using image analysis algorithms) and the focal length.

4.3 Short Range Positioning Systems

From both cost and complexity perspective, the system using only one camera would seem ideal. In this case, the more expensive equipment is kept secure from possible explosions by staying close to the base station. However, this approach requires some kind of equipment installed on the robots to measure the distance between them. Hence, a short range positioning system is needed. Many options are to be considered, and are listed below.

Polaroid-Type Sonar (pulse-echo mode)

This system is a sonar based on the time of flight of an ultrasonic burst. This system was developed and used first on Polaroid cameras to find the correct focal distance. The system is now available commercially as a package shown in Figure 4.3.

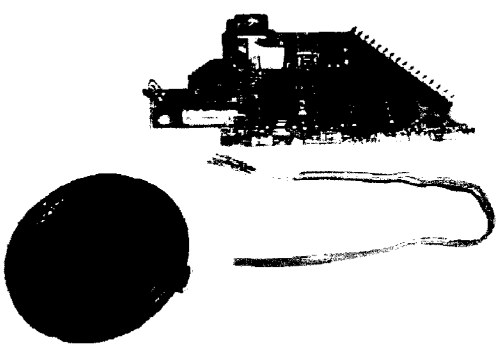

Figure 4.3 Polaroid 6500 series Ultrasonic Ranging System

A single transducer is used in this system. The transducer is first put in emitting mode, and generates a burst of 16 pulses at 50 kHz. The transducer then acts as a receiver. The ultrasonic burst is reflected from the target, and propagates towards the transducer. A band pass filter must remove all other frequencies but the one that was generated. When a 50 kHz signal is detected and exceeds a set threshold, the time elapsed between the emission and the reception of the pulse can then be converted to a distance by knowing the speed of sound. The speed of sound can be calculated using Equation (4) [36]:

$$c = \sqrt{\gamma \cdot R \cdot T} \tag{4}$$

Where

c is the speed of sound in a gas

γ is the gas specific ratio (1.4 for air)

R is the universal gas constant (287.05 J / kg K)
T is the gas absolute temperature, in Kelvin

The distance can then be calculated using Equation (1) by replacing the laser propagation velocity with the speed of sound c.

For air at 20°C, the speed of sound is 343.11 m/s. Unless there is a large change in humidity such that it would significantly affect the value of γ, the speed of sound is only dependent on temperature. That is true, unless the air is moving, which is a condition that can happen frequently outside. The speed of air can probably be eliminated by using the average of distance in two opposite directions.

Ultrasonic Emitter-Receiver (Transmit-Receive Mode)

The transmit-receive mode operates in a similar way to the pulse-echo mode described earlier, with the exception that the receiver is not installed on the same object as the emitter. An emitter generates an ultrasonic pulse, and the start time of that pulse is known by some kind of way. When a receiver, located at some distance from the emitter, detects the incoming pulse, the elapsed time since the start of the pulse is measured. The distance can be calculated as follows:

$$\text{distance} = c \cdot \Delta t \qquad (5)$$

As with every system based on ultrasonic waves, the speed of sound must be known. The transmit-receive mode pose another problem. The emitter and the receiver must be synchronized in order to measure the time of flight of the signal. The exact moment of a pulse must be known by the receiver. A typical method that can be used for such an application is a light or radio wave burst signalling the beginning of the sonic wave burst. Such a wave travel at approximately $3\text{x}10^8$ m/s. This is orders of magnitude faster than sound. Consequently, the error resulting is insignificant and can be ignored.

Audible Emitter-Receiver (Transmit-Receive Mode)

The same principle for an ultrasonic emitter-receiver could be applied to audible sounds. It is possible to have greater omni-directionality with audible sounds because of the relation between the wavelength and the transducer size. If the transducer size is small compared to the wavelength, it will act more closely as a point source [42]. The wavelength can be calculated as follows:

$$\lambda = \frac{c}{f} \tag{6}$$

Where

λ is the wavelength

c is the speed of the wave

f is the frequency of the signal

For a typical 5 kHz signal, the wavelength would be around 680 mm.

It can be more complicated to determine with sufficient precision the time of arrival of the signal. If a filter simply detects the presence of a certain frequency, it will take a certain number of wavelengths, therefore yielding a precision on the order of the wavelength itself. A technique using phase detection [37] could be adapted to obtain a higher precision than the wavelength itself and yield acceptable precision. Moreover, since they are widely used, audible transducers cost much less than ultrasonic transducers.

4.4 Chosen Principles

4.4.1 Long Range Positioning System

The laser ranging system is interesting for its high range, except that it has extreme directionality. To be usable, it would have to be combined with a very precise aiming system. The other solutions considered are much less complex.

A GPS system would carry a too great cost to be applicable. A GPS receiver would have to be installed on each robot, and they are vulnerable to explosion. It also does not have the sufficient accuracy (around 15 meters of precision). It is inappropriate for this application.

The two cameras system was not retained. It involves having two cameras, doubling the cost of an already expensive part, while similar results can be obtained using only one camera with variable zoom, if combined with a short range positioning system.

The camera with variable zoom was chosen for this system because of its simplicity in hardware terms, its relative low cost, and possible precision. It only needs one camera that can be tied to the base station, and the whole base station is not exposed to explosions. However, it needs additional information, which is the distance between each robot. Therefore, a short positioning system is needed.

4.4.2 Short Range Positioning System

The Polaroid-type sonar was found to be not very suitable for this application. As with the laser system, it would be difficult to know which other robot reflected the echo received. The high directivity of the system is also a concern, since the emitter-receiver pair would have to be rotated to cover all the surrounding of each robot. It would also be difficult to identify which of the robots reflected the pulse, and, even worse, if it is a foreign object that generated the echo. The cost is also high (~$100 per module), since each robot needs a module, and they are exposed to hazards from the detonation of a landmine.

The ultrasonic emitter receiver system could be applied, because it does not need many components, and does not require a great deal of processing power. The same holds true for the audible emitter-receiver system. Both are inexpensive, although audible transducers (~$5 each) tend to cost less than ultrasonic transducers (~$15 each). Directionality problems can be solved by using a conical acoustic reflector, as described in [30]. The ultrasonic sound system relies on a shorter wavelength, improving the precision over audible sound system. However, with proper phase detection technology, acceptable precision can be achieved even with audible sound system, and it uses cheaper transducers, so this solution was retained.

5 Positioning System Design

5.1 Global Concept

The underlying principle of the positioning system is based on the sensor fusion between a short range positioning system (SRPS) and a long range positioning system (LRPS). The group of at least three robots moves in a triangle formation. The distance between each robot is dictated by the mine detection system. However, the scope of this thesis concerns the construction of the robots, the design of the LRPS, and the design and implementation of the SRPS. Mine detection is outside the scope of this thesis, so a distance of between 1 and 4 meters between robots will be assumed.

5.2 Long Range Positioning System

As stated in Section 4.4.1, the chosen LRPS is composed of a camera with a variable zoom looking at a group of robots. Since the group is relatively far (between 100 and 200 m, Figure 3.1) and the camera is positioned slightly above ground level, say 2 m, the robots will appear lying on a same horizontal line in the image generated by the camera, as shown in Figure 5.1.

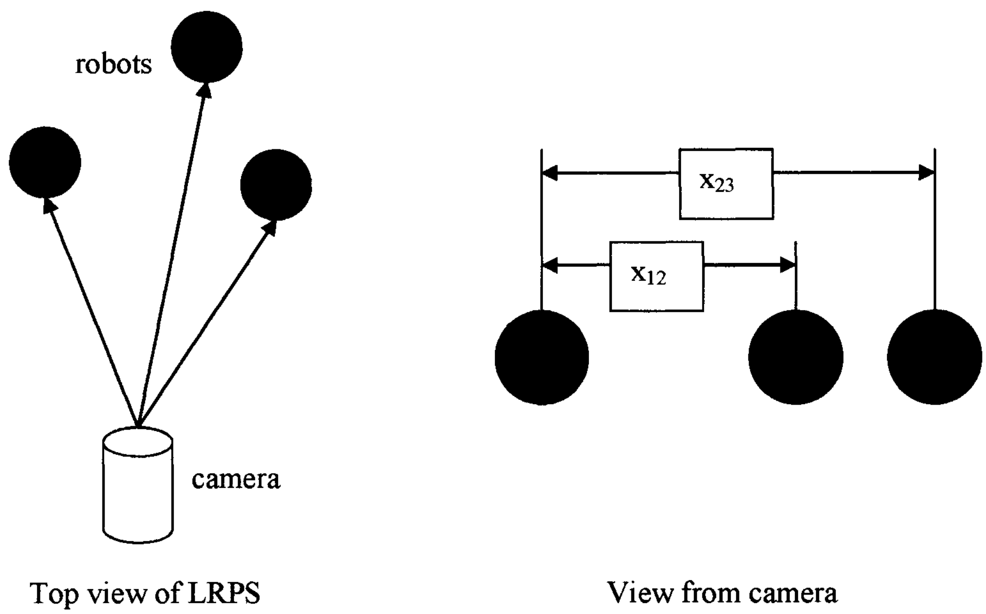

Figure 5.1 Camera Looking at a Formation of Three Robots

The actual distance between each robot is known from a SRPS, which is described in Section 5.3. Each robot in the image will appear separated by a distance. This distance is proportional to actual distance between each robot, and the orientation of that distance with the camera line of sight. Figure 5.2 presents the symbols used for the calculations of the LRPS.

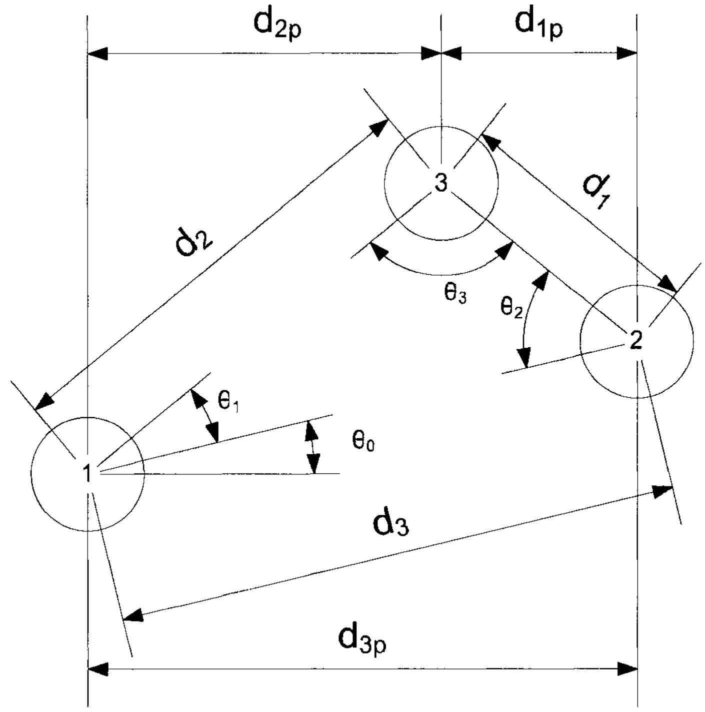

Figure 5.2 Symbols Used for LRPS

Where

d_1, d_{1p} are the distance between robots 2 and 3 and its projection on a plane respectively

d_2, d_{2p} are the distance between robots 1 and 3 and its projection on a plane respectively

d_3, d_{3p} are the distance between robots 1 and 2 and its projection on a plane respectively

θ_1 is the angle of separation between robots 2 and 3, as seen from robot 1

θ_2 is the angle of separation between robots 1 and 3, as seen from robot 2

θ_3 is the angle of separation between robots 1 and 2, as seen from robot 3

θ_0 is the angle between line connecting robots 1 and 2, and line perpendicular to camera line of sight

Note: When the suffix "*i*" is appended to a dimension, it indicates that it is the projection of the dimension on the camera CCD.

Information from the SRPS provides the distances d_1, d_2 and d_3. θ_1, θ_2 and θ_3 can be deduced from the cosine law, Equations (7), (8), and (9).

$$\theta_1 = a\cos\left(\frac{d_2^2 + d_3^2 - d_1^2}{2 \cdot d_2 \cdot d_3}\right) \quad (7)$$

$$\theta_2 = a\cos\left(\frac{d_1^2 + d_3^2 - d_2^2}{2 \cdot d_1 \cdot d_3}\right) \quad (8)$$

$$\theta_3 = a\cos\left(\frac{d_1^2 + d_2^2 - d_3^2}{2 \cdot d_1 \cdot d_2}\right) \quad (9)$$

Image recognition software is used to locate the robots in the image. Several such softwares are readily available from Matrox (www.matrox.com), National Instruments (www.ni.com), and many other vendors and are commonly used for machine vision in industrial applications.

Once the robot triad is in the field of view, the camera focal length is adjusted so as to maximize the size of the triad within the field of view. This allows full pixel as well as sub-pixel analysis to locate more precisely the robots centroid within the robot's images, as well as the location of centroids with respect to the field of view, and yields a smaller relative error on the dimension d_{3pi}.

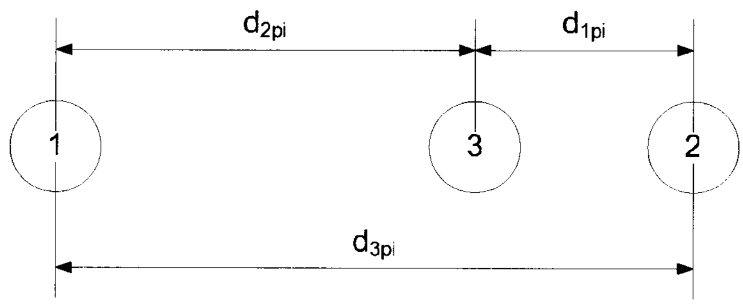

Figure 5.3 View of Robots in Image From Camera

As shown in Figure 5.3, the robots will appear nearly on the same horizontal line in the image from the camera. The projections of the distances d_{1p}, d_{2p} and d_{3p}, between the corners of the robot triad on the camera's CCD are named d_{1pi}, d_{2pi} and d_{3pi}, respectively. There is a correspondence between those actual distances and their projection on the CCD. They are related to the distance separating the camera, the camera sensor size and the camera focal length.

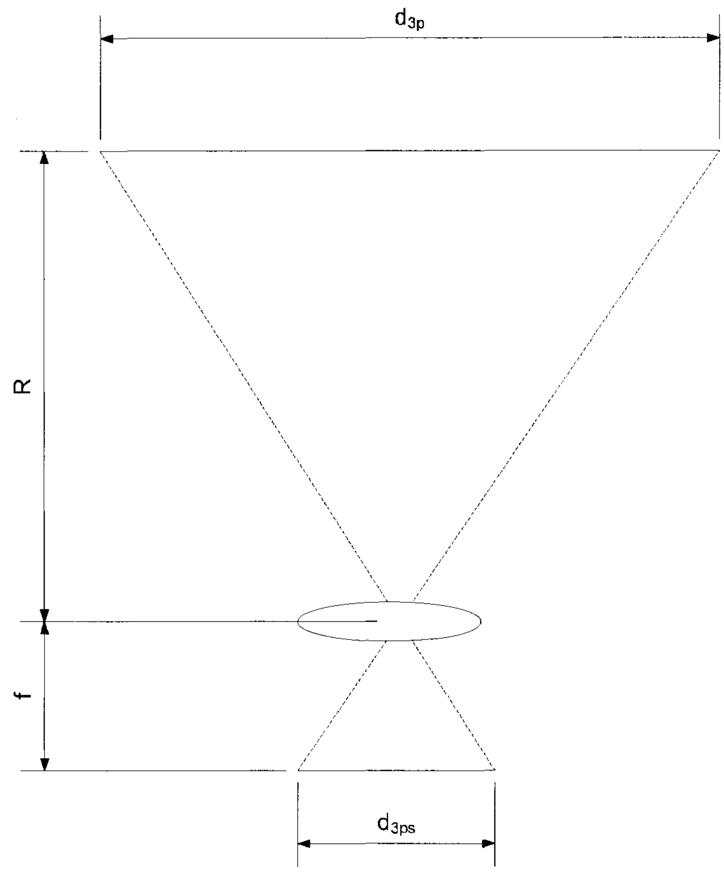

Figure 5.4 Focal Length Symbols

When the distance d_{3p} is projected on the sensor, because of focal length and distance between camera and object, it will appear to have a length given by:

$$d_{3ps} = \frac{d_{3p} \cdot f}{R} \tag{10}$$

Where

d_{3p} is the projected distance, perpendicular to camera line of sight

d_{3ps} is the dimension of projected d_{3p} on the sensor
R is the range from camera to object
f is the camera focal length

For full pixel analysis, if the sensor has a width of S_w, and has a horizontal definition of S_{dh} (in pixels), then, the distance d_{3pi} (in pixels) will be:

$$d_{3pi} = \frac{d_{3ps}}{S_w} \cdot S_{dh} \tag{11}$$

It should be noted that for the same scene, increasing the camera resolution increases the accuracy of the measurements.

At this point, d_{3p} is still not known, as it is dependent on the orientation of the triangle of robots, θ_0. The value of the ratio d_{2p}/d_{1p} varies with the triangle orientation θ_0, and it can be used to calculate θ_0.

The following equations can be deduced from Figure 5.2 and trigonometry:

$$d_{1p} = d_1 \cdot \cos(\theta_2 - \theta_0) \tag{12}$$

$$d_{2p} = d_2 \cdot \cos(\theta_1 + \theta_0) \tag{13}$$

$$d_{3p} = d_3 \cdot \cos(\theta_0) \tag{14}$$

From observation of the projected image (Figure 5.3), the ratio $\frac{d_{2p}}{d_{1p}}$ can be found. The values of d_1 and d_2 are known from the SRPS. The value of θ_0 can be obtained by Equations (12) and (13):

$$\frac{d_{2p}}{d_{1p}} = \frac{d_2 \cdot \cos(\theta_1 + \theta_0)}{d_1 \cdot \cos(\theta_2 - \theta_0)} \tag{15}$$

A trigonometric identity can be used to develop the cosine of a sum of angles:

$$\cos(x \pm y) = \cos(x) \cdot \cos(y) \mp \sin(x) \cdot \sin(y) \tag{16}$$

Developing the equation with trigonometric identities and re-arranging:

$$\theta_0 = \arctan\left(\frac{\cos(\theta_1) - \cos(\theta_2) \cdot \frac{d_{2p}}{d_{1p}} \cdot \frac{d_1}{d_2}}{\sin(\theta_1) + \sin(\theta_2) \cdot \frac{d_{2p}}{d_{1p}} \cdot \frac{d_1}{d_2}} \right) \tag{17}$$

An ambiguity as to whether robot 3 is closer or further from the camera with respect to the line joining robots 1 and 2 remains to be solved. This can be resolved by having robot 3 move away from the camera. If the angles θ_1 and θ_2 increase, then its initial position was further from the camera with respect to the line joining robots 1 and 2. If the angles θ_1 and θ_2 decrease, then the robot was closer with respect to said line.

At this point, the value of θ_0 is known, so the values d_{1p}, d_{2p}, and d_{3p} can be calculated, and the value of the distance separating the robots from the camera can be calculated using Equations (10) and (11).

5.3 Short Range Positioning System

5.3.1 General Considerations

As explained in Section 4.4.2, the system chosen for short range positioning system uses the time of flight of audible sound waves. The main reason of this choice is its omni directional quality, its simplicity for mobile robotic applications and the lower cost of the hardware used when compared to an ultrasonic time of flight system. Using audible sound waves presents one major obstacle to precision. According to Equation (6), the length of an audible sound wave at 5 kHz is around 68 mm. Thus, a system detecting the sound within ±1 wavelength will achieve poor accuracy. To improve the accuracy, a system detecting the sound within less than 1 wavelength is needed.

Moreover, since the robots must emit and receive omni-directional sound pulses, the whole system has to be designed to accomplish this. The audible transducer consists of a small electret condenser microphone cartridge coupled with a piezo audio transducer, generating an audible wave at 5 kHz. This system is compact, with the microphone at about 10 mm diameter, and the piezo transducer at about 16 mm diameter. The microphone and the piezo transducer face upward, and an inverted aluminium cone faces each device. The arrangement can be seen in Figure 5.5 and Figure 5.6. This setup is also used for the Milibots [12], a team of small heterogeneous robots.

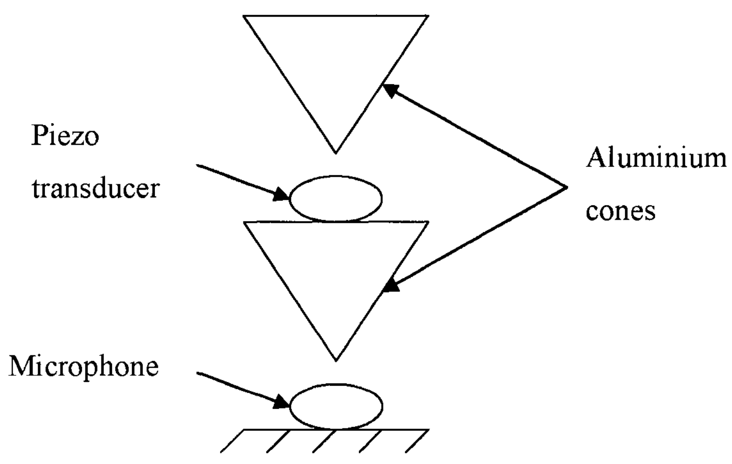

Figure 5.5 Arrangement of Piezo Transducer and Microphone with Aluminium Cones

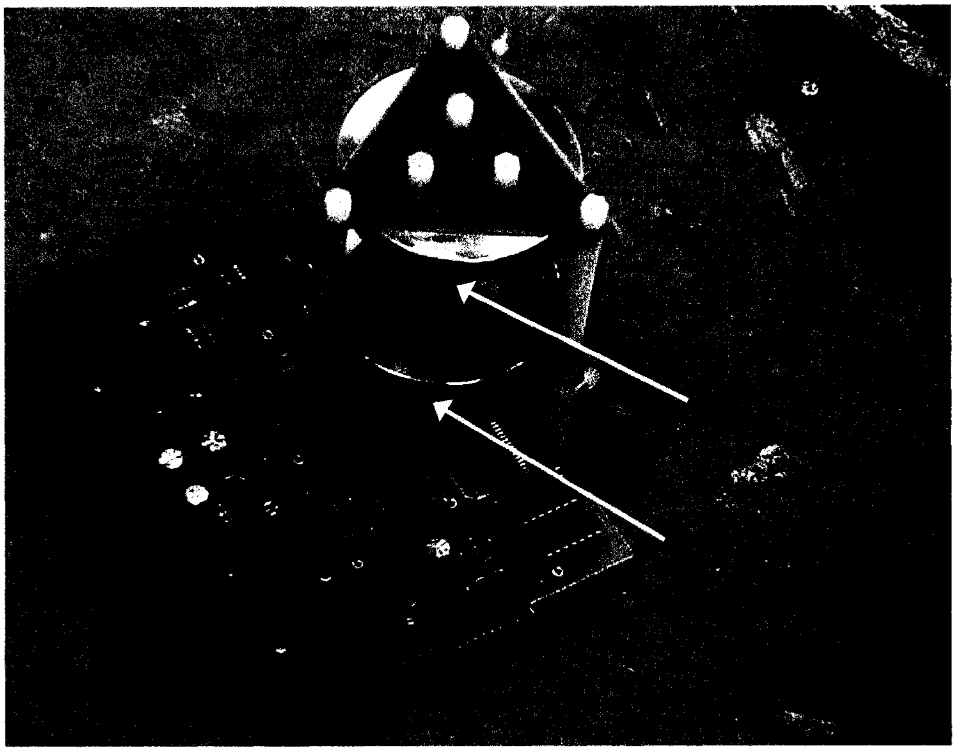

Figure 5.6 Ranging System Module

The choice of a ranging system working on an audible frequency at 5 kHz, rather than the usual 40 kHz ultrasonic frequency poses some problems of filtering. Usually, there is not a lot of noise at ultrasonic frequencies, and it is easy to extract the signal coming from the emitter. However, a microphone listening for a 5 kHz will pick up a lot of noise and it becomes difficult to differentiate between ambient noise and the desired signal. To overcome this difficulty, the signal has to be made as strong as possible. The piezo transducer used is a CUI CEP-1152 with a maximum operating voltage of 20 V peak-to-peak. It is driven by a square 12 V amplitude signal, with a 330 Ω resistor in series with the transducer to limit the voltage amplitude to 20 V.

The receiver part consists in a Panasonic WM-54B electret condenser microphone cartridge. The audio signal received by the microphone is filtered by a very sharp bandpass filter to ensure that only the selected frequency goes through the detection circuit. A pre-amplifier increases the signal from the microphone to get a better signal to noise ratio. Then, two sharp cascaded bandpass filters are implemented. The signal coming from the filtering section passes through a peak detection circuit. The peak detection circuit comprises three sub circuits; a low gain post amplifier, a high gain amplifier, and a threshold circuit. The received signal path is depicted in Figure 5.7.

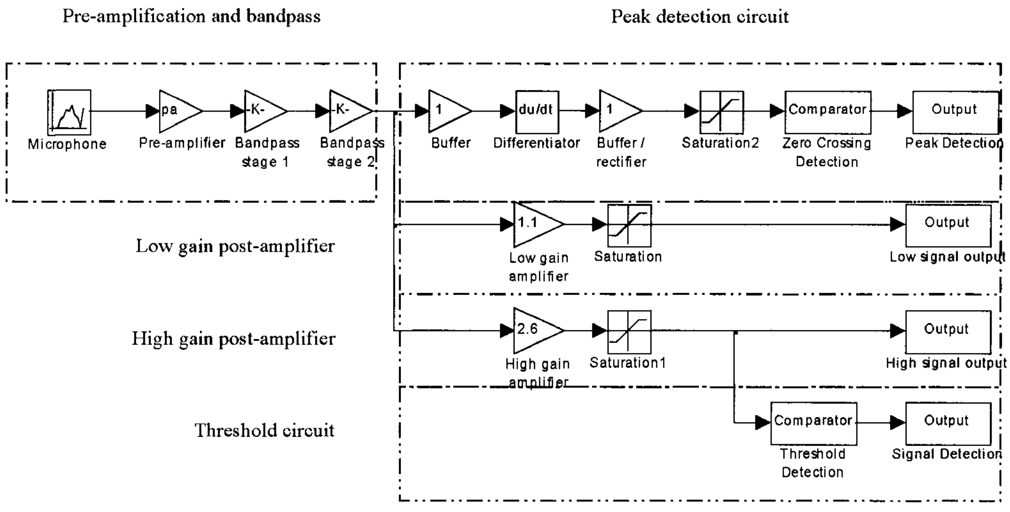

Figure 5.7 Ranging Module Electrical Schematic

5.3.2 Theory of Operation

The signal sent to the piezo transducer is a square wave consisting of 16 pulses. Before reaching the microcontroller ATD input, the signal will have been through the piezo transducer, air, the microphone, the pre-amplification and bandpass stage, and the post-amplification stage. All those modules have non-infinite bandwidth. The input signal, as a square wave, can be express in the frequency domain as a sum of signals each with a single frequency. A square wave can be expressed as a Fourier series:

$$f(t) = \frac{4}{\pi} \cdot \sum_{k=1}^{\infty} \frac{\sin((2 \cdot k - 1) \cdot t)}{(2 \cdot k - 1)} \qquad (18)$$

Where

f(t) is the signal amplitude at time *t*

In the frequency domain, a square wave will be composed of a component at the fundamental frequency, and other harmonics at *3f*, *5f*, ... The higher harmonics will be attenuated by the different parts in the signal part (piezo transducer, air, microphone, amplifier and bandpass filter), so the signal sampled by the MCU will be quite different from the initial square wave. An example of the signal, taken with a digital storage oscilloscope, is shown in Figure 5.8.

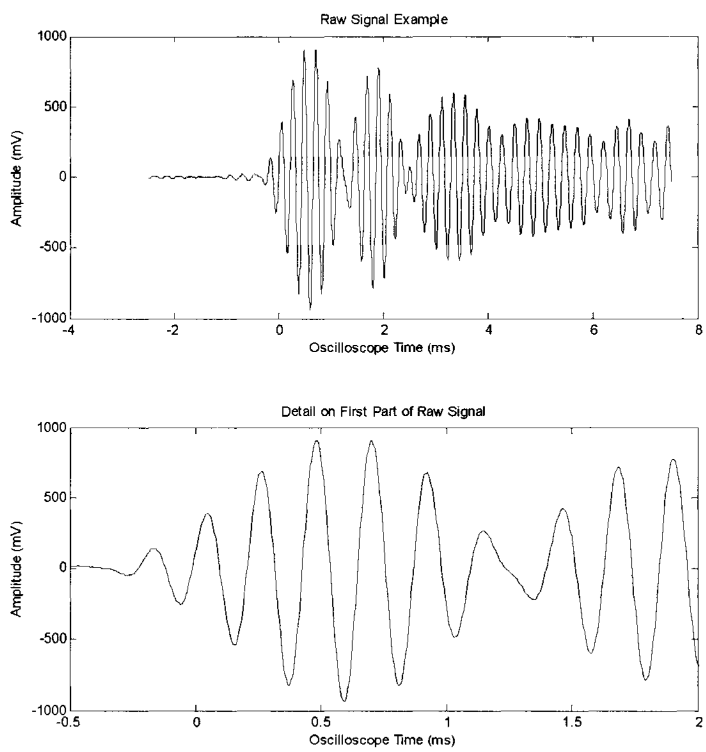

Figure 5.8 Raw Signal Example

The output of the pre-amplification and bandpass stages has three characteristics. The signal amplitude changes mainly with distance, but can be affected by other factors such as the emission amplitude. The shape of the signal, at least for the first portion (0 to 1 ms in Figure 5.8) is essentially unaffected. The third characteristic concerns the time scale. Recording of the signal by the oscilloscope starts at a time when the amplitude passes the programmed level of 100 mV. If the time counter is started the moment the signal is emitted, the received signal will be shifted in time proportionally to the distance separating the emitter and the receiver.

The following steps are taken to calculate time:

1. Emission of a signal (16 pulses at 5 kHz) and start of elapsed time calculation
2. Signal travels through air, speed is mainly dependent on temperature
3. Receiver detects an incoming signal, samples it
4. Correlation of incoming signal with a reference signal
5. Calculation of distance based on elapsed time when correlation is maximum

It is supposed that the signal treated received by the receiver came by a direct path from the emitter. This assumption is true if there are no objects between the emitter and the receiver. Even if there are walls or other objects around the system, the signal that will reach first the receiver will always be the direct signal, with the reflected signals travelling a longer path, thus arriving at the receiver afterwards. This poses a limitation on the system, as there can be vegetation present between the robots during a demining operation. It therefore limits the system where the vegetation will not cause interference with the SRPS.

The implementation of those steps is detailed in the following Section.

5.3.3 Implementation of Short Range Positioning System

Signal Emission

The signal emission device is a piezo transducer driven by a square wave at 5 kHz. Battery voltage is supplied to a L298 dual full-bridge driver. It permits supplying the piezo transducer with positive and negative amplitude signal from a single positive signal, thus doubling the possible amplitude from a single supply.

The piezo transducer is mounted facing upward, and an aluminium cone is mounted pointing at the piezo transducer. This permits 360° horizontal emission from a single transducer.

Signal Reception and Filtering

A physical setup similar to the one of the burst emission unit is used for the receiving unit. An electret condenser microphone is mounted facing upward with an inverted aluminium cone facing it to allow sound reception over 360°. The signal is then pre-amplified and fed through two cascaded bandpass filters. The output of the bandpass filters presents a good signal to noise ratio, as shown in Figure 5.8. It filters out acceptably well the undesired frequencies coming from ambient noise.

The section labeled "Peak detection circuit" in Figure 5.7 is a differentiator with a very high gain. The derivative of the signal is amplified sufficiently so that the output of the amplifier will saturate to either positive or negative supply voltage. Thus, the circuit generates a signal that can be used by the digital inputs of the Microcontroller Unit (MCU). A rising edge occurs at each positive peak of the signal.

The low and high gain post-amplifiers generate a signal amplified by gains of 1.1 and 2.6 respectively. The negative portion of the signal is removed and the signal is clipped to 5 V in order to avoid damage to the inputs of the MCU.

A comparator, connected to the high gain post-amplifier, is used to detect the presence of a signal high enough to start the sampling process.

Signal Sampling

To minimize the sampling necessary to the detection of the ranging signal and reduce necessary processing power, sampling is done only when three conditions are present:

1. Ranging in progress
2. Signal crossed above threshold value
3. A positive peak of the signal is recognized

When a ranging command is sent to all robots, each of them processes the instruction. Only one of them will be the target of the command. The targeted robot will emit the pulse to the other robots. The robots which are not the target of the command will start counting elapsed time and begin analyzing an incoming signal. This is the first condition called "Ranging in Process".

The second condition is set by a comparator that will generate a digital signal. The signal is set to logic 1 if the filtered signal is above a certain level. For the prototype robot, this level is set by a potentiometer.

The third condition is the presence of a signal peak that is recognized by analyzing the incoming burst.

The MCU will only sample the first peaks of the incoming wave. Figure 5.9 shows the global signal after filtering, amplification and removal of the negative portion. The bottom plot shows the detail of the initial part of the incoming signal. The output of the peak detection circuit is added to the bottom plot together with the values sampled by the Analog-To-Digital converter (ATD) of the MCU. Those values do not perfectly match the value of the peak, both in time and in amplitude, but they provide sufficient information about the shape of the signal to permit calculating distance information. The time scale on this plot begins when the signal is emitted.

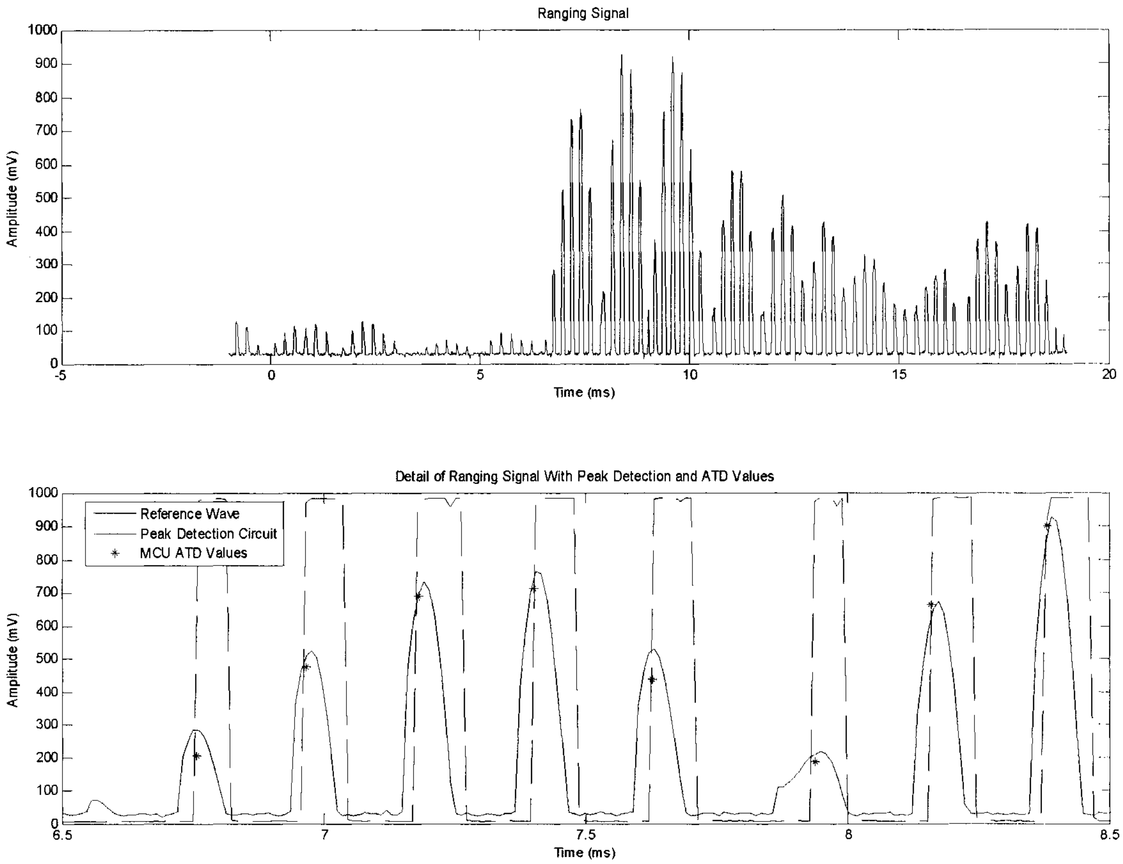

Figure 5.9 Incoming Signal with Peak Detection Circuit and Resulting ATD Values

Correlation of Incoming Signal

After all that hardware processing, when digitized, the signal consists of 8 pairs of 16-bit values for amplitude and elapsed time of each detected peak. This data is sent by wireless communication to the base station for processing. The first peak of the signal is searched using a simple differentiator. The data is then normalized with respect to this peak (all values of amplitude divided by the amplitude of first peak). The data obtained is then compared to a reference wave for different temporal overlaps. The correlation is computed for each overlap value by summing the square of difference between each wave, as shown by Equation (19).

$$correlation = \sum_{i=0}^{7} (S_r[i] - S_m[i])^2 \qquad (19)$$

Where

S_r is the array of reference signal

S_m is the array of measured signal

Once the measured signal is properly matched with the reference signal, the time value corresponding to the 5th value is taken as the elapsed time from emission to detection of the wave. The 5th value was chosen because it is the first to occur after the first peak. It was chosen arbitrarily, but what is important is that the same value is always chosen.

That time value is proportional to the distance separating the emitter and the receiver. An offset is present in the data, due to software and hardware delays, but they are repeatable. Software delays include time elapsed after the time counter is started and the wave is actually generated. Code has to be executed, and that takes a certain amount of time. Hardware delays include the delay inherent to the design of the bandpass filter, the peak detection circuit and the ATD circuitry inside the MCU.

Temperature Correction

A temperature sensor is installed on the ranging system module. It is a National Semiconductor model LM335 in a TO-92 package. It outputs a voltage directly proportional to the temperature 10 mV/K. Since the input of the ATD of the MCU used has 10-bit resolution, and the full-span voltage is 5 V, a temperature resolution of 0.49 K is possible. Automatic temperature correction for the SRPS module has not been implemented.

6 Design and Construction of Robots

6.1 Vehicle Platform

6.1.1 General

In order to be able to navigate through a minefield without detonating the landmines, the vehicle must exert minimal ground pressure. This can be accomplished in two ways: minimizing the vehicle weight and maximizing ground contact area. The chosen structure is a frame made with rigid foam insulation board serving as a platform, with four wheels and differential steer architecture. Those choices are detailed in the two subsequent Sections.

6.1.2 Frame

Rigid foam insulation board offers good stiffness to weight ratio, and permits different construction techniques. The technique used is to cut a panel of insulation board, bond a thin acrylic sheet on each side to improve stiffness, and attach the components afterwards (wheels, motors, transmissions, electronics, etc). Another suggested technique would be to place each component in a mold, and fill the cavity with expanding rigid urethane foam. It would improve shipping of components to many regions of the world, as all parts can be transported separately to the site, and the robots could be assembled on-site.

This construction technique can also be used as a part of a blast protection system against detonation of landmines. If each component attached to the robot can easily be detached and propelled away in the case of an explosion, less force will be exerted on the individual components. If a certain part was rigidly fixed to a sturdy frame, the part would have more chances to be destroyed.

It has to be noted that this frame construction technique was not tested. The author does not pretend to have any knowledge in explosives, nor in blast resistance. This is outside the scope of this work.

6.1.3 Propulsion and Steering

As simplicity was an important factor in the design, construction and operation of the robot, differential steer architecture was chosen. Two motors power the robot, one for left front and rear wheels, and one for right front and rear wheels. If both motors turn at the same speed, the robot will go in a strait line. If there is a difference, the robot will turn in the direction of the slower motor. Skid will necessarily take place with this architecture. The wheels are made of Ø100 mm plastic tube 180 mm wide. This is done with the objective of minimizing ground pressure. To further aid this objective, tracks can easily be installed.

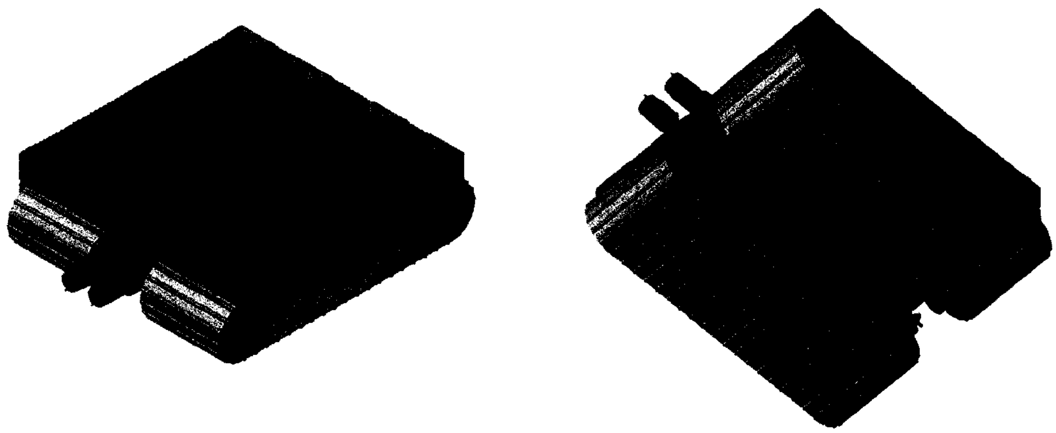

Figure 6.1 Robot Top and Bottom Views

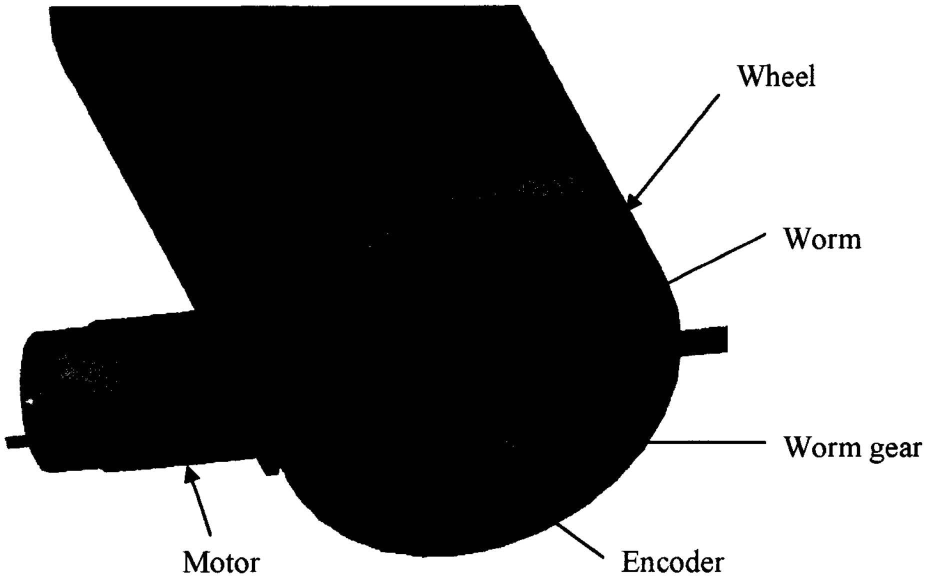

Figure 6.2 Detail of Motor with Encoder, Transmission and Wheel

6.2 Movement Control

DC motors control the speed of the wheels, two wheels at a time. Therefore, by controlling the motor's rotational speed, it is possible to control both the robot speed and direction. A DC motor speed is proportional to the voltage and torque applied. There is little control over the torque applied to the motors, as it is dependent on the friction in the transmissions, the payload present on the robot, and the terrain load (slope, soil properties). Therefore, the only variable left to control the motors speed is the applied voltage. This voltage is generated by an H-Bridge driver, described in Section 6.3.2, and a closed loop is formed in software to compensate for factors affecting the motors speed (battery voltage, varying external loads). The software part of the speed control is described in Section 7.7. Optical encoders, described in Section 6.3.4, are used as a sensor to detect the wheel rotational speed.

The position resolution that can be achieved is dependent on wheel diameter, ratio between worm and worm gear, and the number of pulses per rotation of the optical encoder. The wheel has 101.6 mm diameter (4 in.), the ratio between the worm and worm gear is 1:50, and the encoder generates 3 pulses per rotation. Thus, each pulse of the encoder indicates a linear distance of 2.13 mm at the circumference of the wheels.

6.3 Electronics Modules

To facilitate development, several electronic modules were constructed, each fulfilling a specific task. This approach also has the advantage of producing re-usable modules that can be of interest in other projects. Moreover, the development is much easier, as each module can be updated without having to reconstruct each other. However, it has the inconvenience of taking more space, as integration between each module is not the prime consideration.

Figure 6.3 shows the modules with their interconnections. The arrows show the direction of the signals going to and/or from the modules.

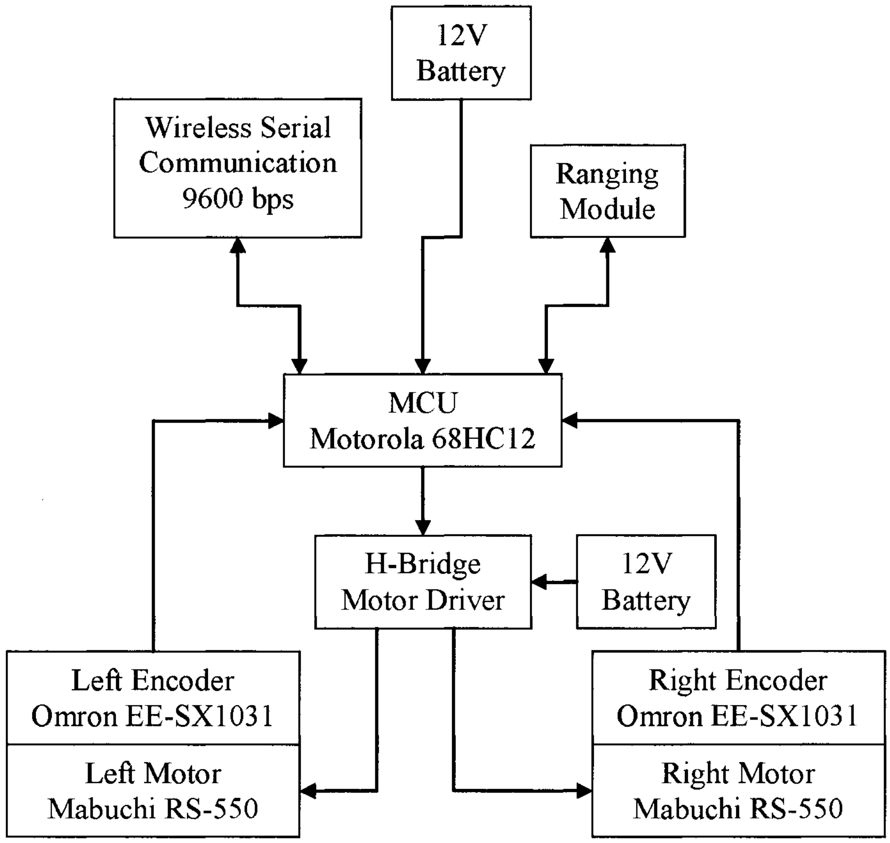

Figure 6.3 Block Diagram for Robot Electronic Modules

All the Printed Circuit Boards (PCB) were done using MG Chemicals PCB prototyping system [27]. The PCBs are made from a fibreglass-epoxy layer, coated with a layer of copper, an etch-resistant layer, and a photoresist layer. By exposing the PCB to ultraviolet light and with further manipulations, copper traces can be obtained. Once a proper copper circuit is etched on the PCB, it can then be drilled to accommodate through-hole or surface-mount components, and then assembled.

6.3.1 MCU

The MCU module is the central piece all the electronics installed on the robot. It is based on a Motorola 68HC12 micro-controller unit. It should be noted that the MCU module was designed and fabricated in-house in the course of this work

The MCU module receives its power from a 12V nickel-cadmium battery pack. The voltage is regulated to 5V by a voltage regulator, and then distributed to the other modules. Only one battery pack is necessary to operate all the modules, except for the H-bridge motor driver, which requires its own battery pack to power the motors.

Three Light-Emitting Diodes (LED) are installed for diagnostic purposes during development, and to ensure the software is executing properly during normal operation. One of the LEDs (red) flashes at 5 Hz to indicate that the code executes properly.

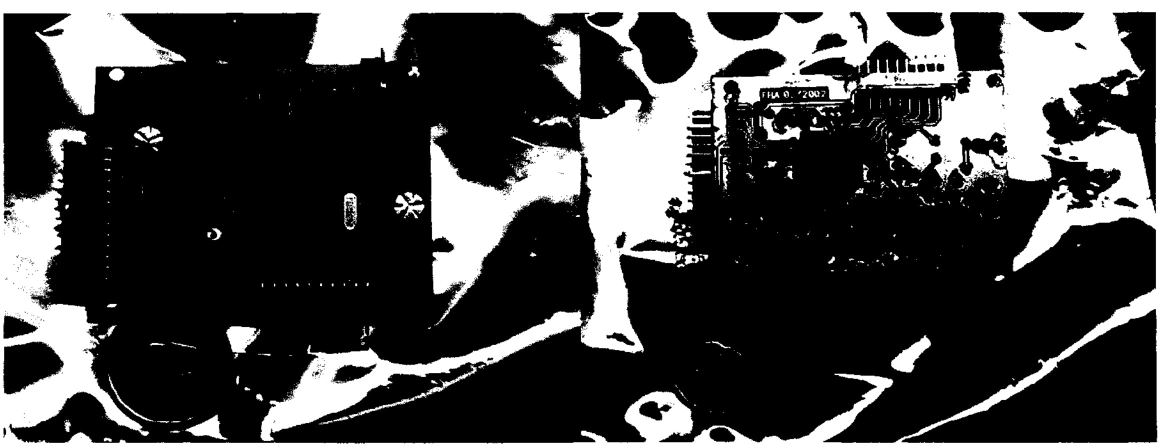

Figure 6.4 MCU Module, Top and Bottom View

A Schmitt trigger is also present on the module to filter the signal coming from the encoders. Since the encoder modules need to be very small to be fitted near the encoder wheels, some of the signal conditioning had to be placed on the MCU module. Its function is described in Section 6.3.4. Figure 6.4 shows photographs of the top and bottom sides of the MCU module.

The components are all through-hole devices, except for the MCU itself, which is in a TQFP-80 package, a surface mount device. It is mounted under the PCB.

The electrical schematics for the MCU module are shown in Appendix B. On the first sheet is shown the MCU itself, with some of the associated hardware required to sustain its operation. The second sheet depicts the power supply system. The third sheet shows the connectors used to connect the MCU module to each other module.

6.3.2 Driver

The H-Bridge module purpose is to amplify the signal coming from the MCU to the motors. An H-Bridge is a way of arranging switches (MOSFET transistors in this case) to reverse the voltage polarity to a device from a single supply so as to achieve bi-directional rotation. The descriptive schematic of an H-Bridge is shown in Figure 6.5.

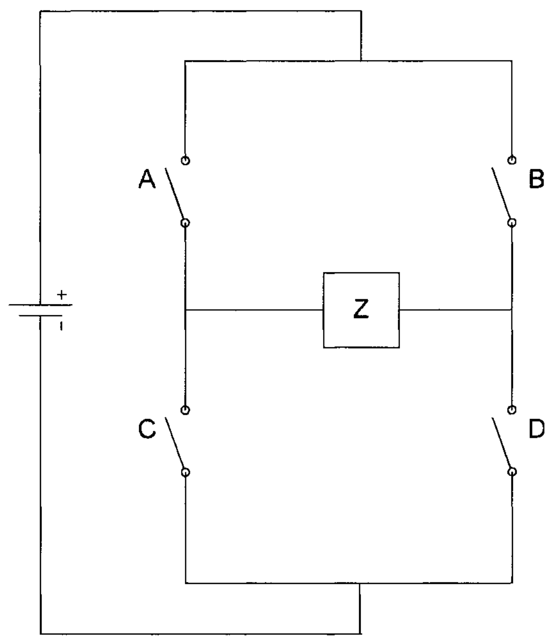

Figure 6.5 H-Bridge Schematic Description

A device (Z in the picture) is connected via two switches to positive supply, and via two switches to negative supply. If switches A and D are closed, current will flow in the device Z from left to right on the picture. If switches B and C are closed, current will flow in the device Z from right to left on the picture.

Additionally, by using the PWM (Pulse Width Modulation) technique, the power supplied to a system can be modulated. Using this technique, the switches are opened and closed at a fixed frequency, but using a variable duty cycle. The duty cycle is defined as the ratio of switch closed time over the total period of the PWM. Therefore, as an example, if the switches are closed for 25% of the duty cycle, then the effect load Z will be supplied with 25% of the full voltage capacity. Mathematically, this is equivalent to supplying the system with 0.25 of the supply voltage without having to actually reduce or throttle the supply voltage. On the robot, the supply voltage is 12 V, so a 25% duty cycle would yield 3V at the motor.

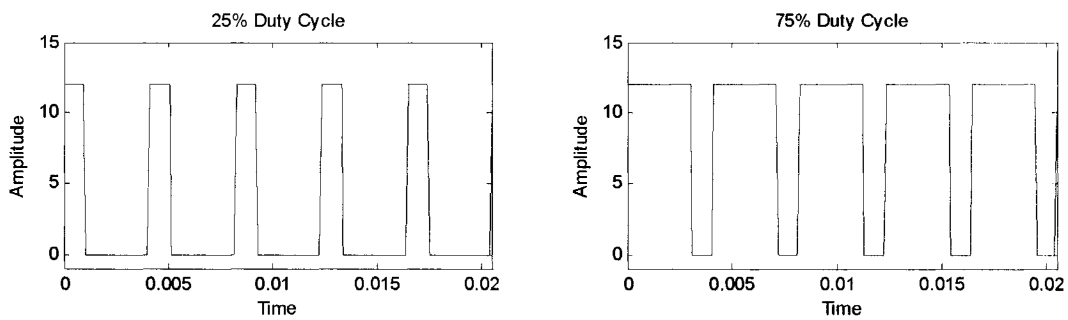

Figure 6.6 Duty Cycle Example

If the switches are replaced by transistors, the power to a device like a motor can therefore be controlled continuously by using the digital outputs of a microcontroller, without the need for D/A converters or analog circuits. In the designed H-Bridge, Metal-Oxide-Semiconductor Field-Effect Transistor (MOSFET) devices are used: model IRFIZ44N for switches C and D, and IRF5305 for switches A and B, in Figure 6.5. Those were chosen for their current capacity, and their low internal resistance.

Some logic chips are also used to decrease the necessary number of connection between the MCU and the driver module. Instead of using four PWM signal lines to drive the four MOSFETs on a H-Bridge, only one PWM signal line and a direction signal line are used. This is because the robot has a total of four PWM signal lines with 8-bit precision each. Those four outputs can be combined into two 16-bit precision PWM outputs. The later option was chosen to have finer control over the electrical motors.

Equivalence Between PWM-Controlled Voltage and Variable DC Voltage

The equivalence between a PWM-controlled voltage and a variable Direct Current (DC) voltage supply is dependent on the load applied. A DC motor is a device that converts electrical current to mechanical torque, as given by the following relationship:

$$T = K_T \cdot I \tag{20}$$

Where
T is the output torque
K_T is the motor torque constant
I is the motor current

An electric DC motor can be modelled as an inductance in series with a resistance powered by a DC voltage source. The motor angular velocity for a given load is proportional to the voltage supplied, if the motor windage and frictional losses are neglected. While the rotor spins within the stator magnetic field, it generates a voltage that tends to oppose the supply voltage. This generated voltage is called the back electromotive force voltage (V_{bemf}).

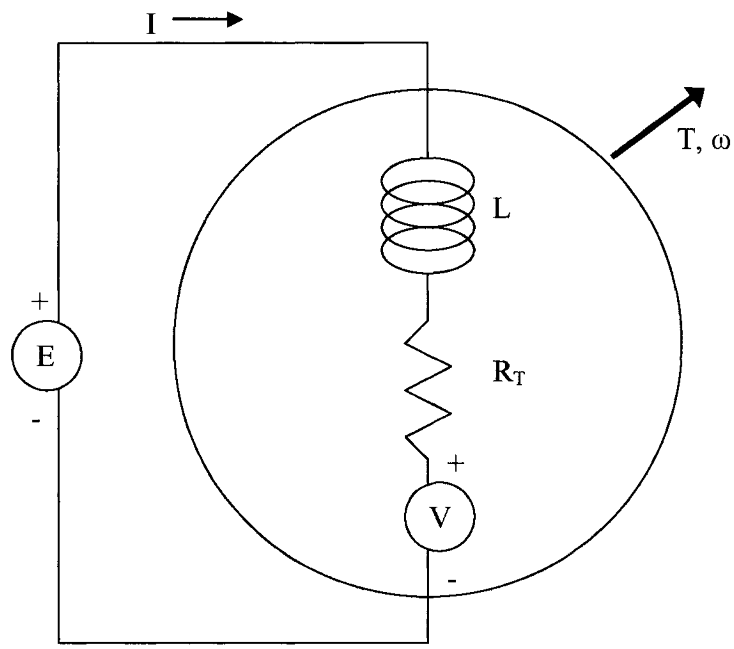

Figure 6.7 DC Motor Model

The current flowing in the motor can be calculated as follows:

$$I(s) = \frac{E - V_{bemf}}{Ls + R_T} \tag{21}$$

Where

E is the applied voltage

L is the motor inductance

R_T is the motor resistance

Thus, for a constant speed, V_{bemf} remains constant and R_T is also a constant. The current is therefore only dependent on the applied voltage.

A periodic signal can be represented by a Fourier series, which decomposes a signal into a sum of sine and cosine functions [20] as follows:

$$E(t) = a_0 + \sum_{n=1}^{\infty}\left(a_n \cdot \cos\left(\frac{2 \cdot n \cdot \pi}{T} \cdot t\right) + b_n \cdot \sin\left(\frac{2 \cdot n \cdot \pi}{T} \cdot t\right)\right) \tag{22}$$

Where

E(t) is the applied voltage as a function of time

a_0, a_n, b_n are the Fourier series coefficients

T is the PWM period

The terms a_0, a_n, b_n can be found using:

$$a_0 = \frac{1}{T} \cdot \int_{-T/2}^{T/2} E(t)dt \tag{23}$$

$$a_n = \frac{2}{T} \cdot \int_{-T/2}^{T/2} E(t) \cdot \cos\left(\frac{2 \cdot n \cdot \pi \cdot t}{T}\right)dt$$

$$b_n = \frac{2}{T} \cdot \int_{-T/2}^{T/2} E(t) \cdot \sin\left(\frac{2 \cdot n \cdot \pi \cdot t}{T}\right)dt$$

With the coefficients expressed by:

$$a_n = \frac{2 \cdot A}{T}\left[\sin\left(\frac{\pi \cdot n \cdot \tau}{T}\right) - \sin\left(\frac{-\pi \cdot n \cdot \tau}{T}\right)\right] \tag{24}$$

$$b_n = \frac{2 \cdot A}{T}\left[-\cos\left(\frac{\pi \cdot n \cdot \tau}{T}\right) + \cos\left(\frac{-\pi \cdot n \cdot \tau}{T}\right)\right]$$

Where

A is the signal amplitude

τ is the pulse width

Thus, for the PWM signal of interest, the coefficient a_0 is:

$$a_0 = A \cdot \frac{\tau}{T} \tag{25}$$

Since all other terms of the Fourier series are sinusoidal, their average is 0, and the total signal average is a_0. At high PWM frequencies, the inductance impedance will be high, so it will filter out the a_n and b_n terms of the Fourier series, and the resulting current in the motor will approximate a DC current, albeit with a small ripple if the higher frequency terms are not perfectly filtered out. This phenomenon can be observed in the following Figure 6.8 to Figure 6.11. In Figure 6.8, a 3 V DC input was applied to the DC motor model (PWM frequency is 0 Hz). As expected the voltage and current are steady at the prescribed levels. Subsequently, the PWM frequency was increased to 25 Hz in Figure 6.9. Since the frequency is low enough, the motor inductance does not offer substantial impedance. The only noticeable change in the output is a rounding off of the peak of the leading edge and the trough of the trailing edge as the current is being established and cut-off from the motor winding. The current peaks at about 18 A. It should be noted that the average of the current pulses is almost identical to that in Figure 6.8. At this frequency, the motor torque will be pulsed and will be averaged by the motor and load inertia via the flywheel effect. The average torque will still be proportional to the PWM amplitude times the duty cycle. Finally in Figure 6.10, the PWM frequency is ramped up to 5000 Hz. At 5000 Hz, the winding impedance is high enough that it diminishes the output current to a level similar to that when the motor was subjected to 3 V DC. A ripple though can be observed in the signal. Figure 6.11 expands the time scale of Figure 6.10 so as to observe the ripple effect.

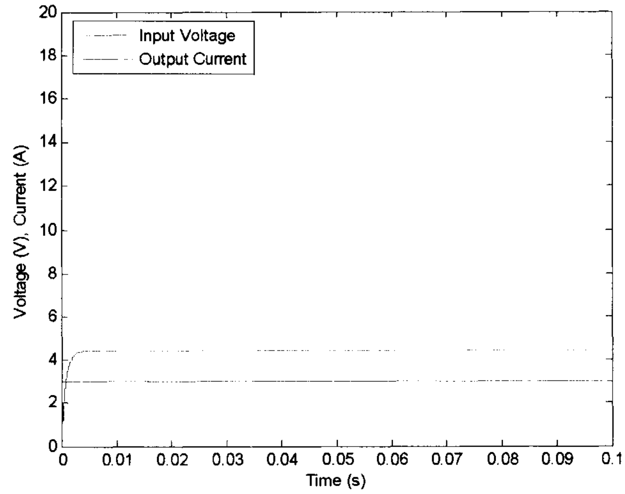

Figure 6.8 Output Current for a 3 V DC Voltage

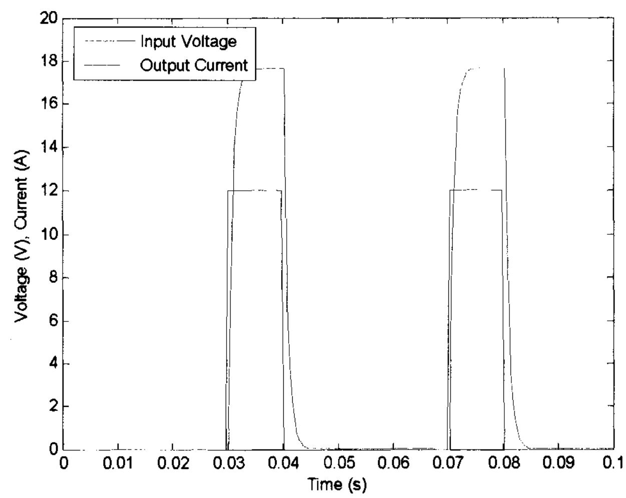

Figure 6.9 Output Current for a 12 V 25% 25 Hz PWM Voltage

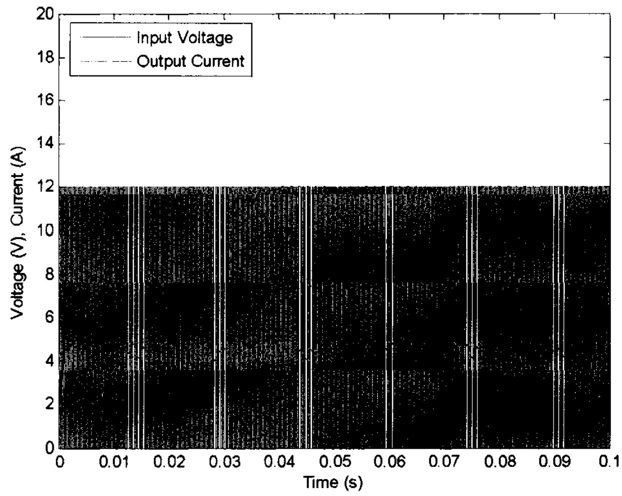

Figure 6.10 Output Current for a 12 V 25% 5000 Hz PWM Voltage

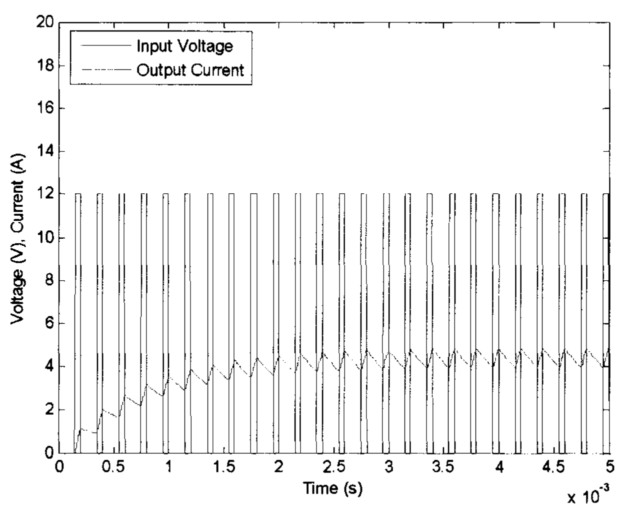

Figure 6.11 Detail of the Output Current for a 12 V 25% 5000 Hz PWM Voltage

The electrical schematics for the driver module are shown in Appendix C. In this schematic, two H-Bridges are shown. Each H-Bridge is composed of 4 MOSFET transistors that are controlled via logic gates and transistors. The logic gates are used to allow the control of four MOSFET transistors with one PWM signal and one logic signal. The PWM signal controls the amplitude of the voltage supplied by the H-Bridge, while the logic signal controls its polarity.

6.3.3 Robot Communications

To effectively work as a team, the robots need to communicate between them, and also with the base station. The communication system is used for SRPS, LRPS, and other general communications, such as speed commands. Linx TR-916-SC transceivers are used. They are ready-made modules that can be used to transmit data at up to 33.6 Kbps. Since they are half-duplex, transmit and receive functions cannot be used simultaneously. The manufacturer claims they can be used outside for distances up to 152 m (500 ft). Although this is under the maximum 200 m range stated in Section 3.4, those modules were readily available at a reasonable cost. Further research is expected if the robot system is to be implemented later to full expected range.

The communications module used on the robot is very simple. Since the Linx module is electrically compatible with the MCU, only a connector and an antenna are added to this module to implement robot communication. The communication module that interfaces with the base station is intended to connect to a Personal Computer (PC) serial port, with different voltage levels. An interface chip must be used between the PC and the PC communication module. Some components are also added to connect to a power supply because power for the Linx module cannot be derived from the PC serial port.

The electrical schematics for the PC serial communication module are shown in Appendix D, and for the robot serial communication module in Appendix E. On each of those schematics a Linx module is depicted. In Appendix E, the module interface to the robot MCU directly via a connector on the case of the robot serial communication module. In Appendix D, the PC serial communication module requires signal conditioning components to convert the signal of the PC serial port into a signal compatible with the Linx module. Some components are also used to form a power supply section, since the PC serial communication module cannot derive its power from the PC serial port.

6.3.4 Encoders

In order to measure speed and position of the wheels, encoders were installed. They are comprised of a slotted wheel mounted in-line with each motor shaft, and a dual optical sensor. The optical sensor (Omron EE-SX1031) is a slot-type sensor. A LED emitting an infrared light (~940 nm) is placed in front of a phototransistor sensitive to infrared light. When an opaque object is placed in the slot between the LED and the phototransistor, it blocks the light coming to the phototransistor. The resulting output from the phototransistor is converted by a Schmitt trigger to a signal suitable for a MCU digital input.

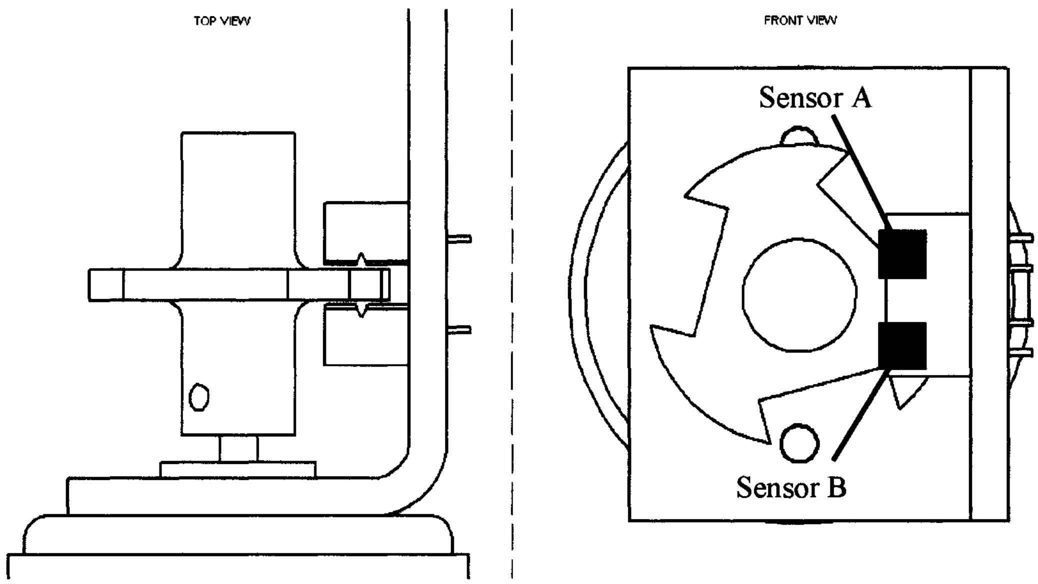

Figure 6.12 Encoder Layout

This type of sensor produces a quadrature signal, which gives information on both the number of turns and the direction of rotation. As seen in the front view of Figure 6.12, if the sensor is turning clockwise and the sensor gives a high signal when it is in front of a slot, the sensor A will give a rising edge before the sensor B, and both signals will be between 0° and 180° out of phase. Note that these are extreme values. An ideal signal would be 90° out of phase.

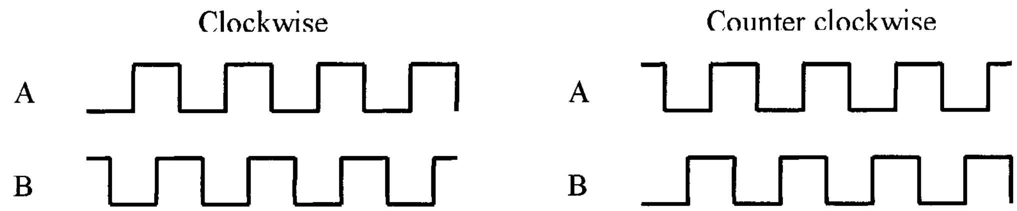

Figure 6.13 Quadrature Signal Explanation

Therefore, by sampling input B when a rising edge is detected on input A, it is possible to compute both rotational speed and direction.

The electrical schematic for the encoder module is shown in Appendix F. It consists in a simple encoder disk with slots, and a pair of LED and phototransistor embedded in a plastic case that can be installed on a PCB.

6.3.5 Ranging

The ranging system electrical circuit comprises different sections, and the block diagram of the circuit is depicted in Figure 5.7.

Bandpass Filter

The first part of the circuit is the bandpass filter section. The requirements for the design of the bandpass filter is to only pass the desired frequency, in this case the 5 kHz band, while filtering out or attenuating considerably all other frequencies that are considered noise. This is accomplished by an active filter made of an operational amplifier and discrete components (resistors, capacitors). The general arrangement for an inverting filter is shown in Figure 6.14.

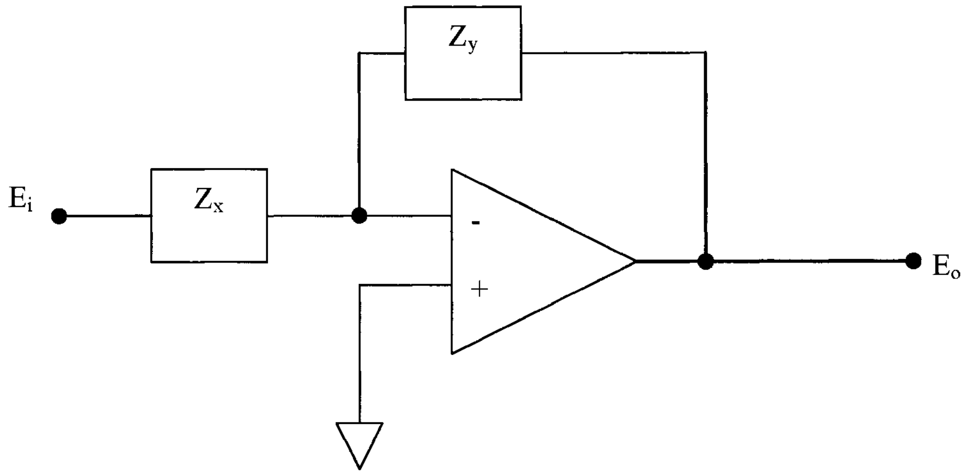

Figure 6.14 Negative Feedback Operational Amplifier Filter Schematic

Where

Z_x, Z_y are the impedance

E_i is the input voltage (function of time)

E_o is the output voltage (function of time)

For an inverting op-amp filter, the transfer function is:

$$\frac{E_o}{E_i} = -\frac{Z_y}{Z_x} \tag{26}$$

Z_x and Z_y are impedances that can be made of a combination of resistors and capacitors. The transfer function can be such that the filter acts as an all-pass (simple gain), low-pass, bandpass or high-pass filter. In this application, only one specific frequency is needed, and all the other frequencies must be attenuated, so that the frequency of interest can be detected with sufficient certainty. A bandpass filter is therefore needed. A second order bandpass filter is used in the SRPS, and is shown in Figure 6.15.

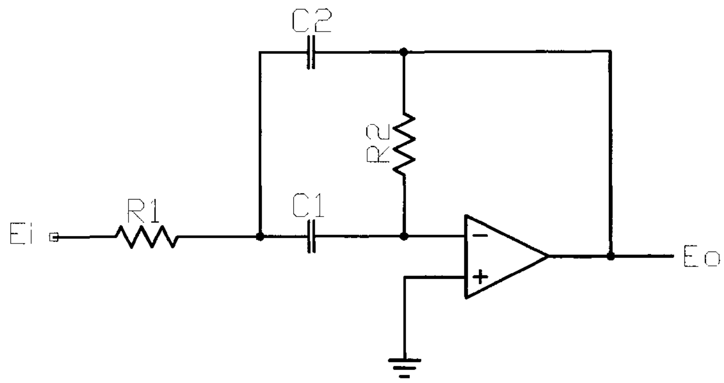

Figure 6.15 Bandpass Filter Circuit

To extract the transfer function of the filter, the circuit must be simplified to the one shown in Figure 6.14. The components C_1, C_2 and R_2 form a Δ pattern, and can be modeled by a Y pattern. Those arrangements are shown in Figure 6.16.

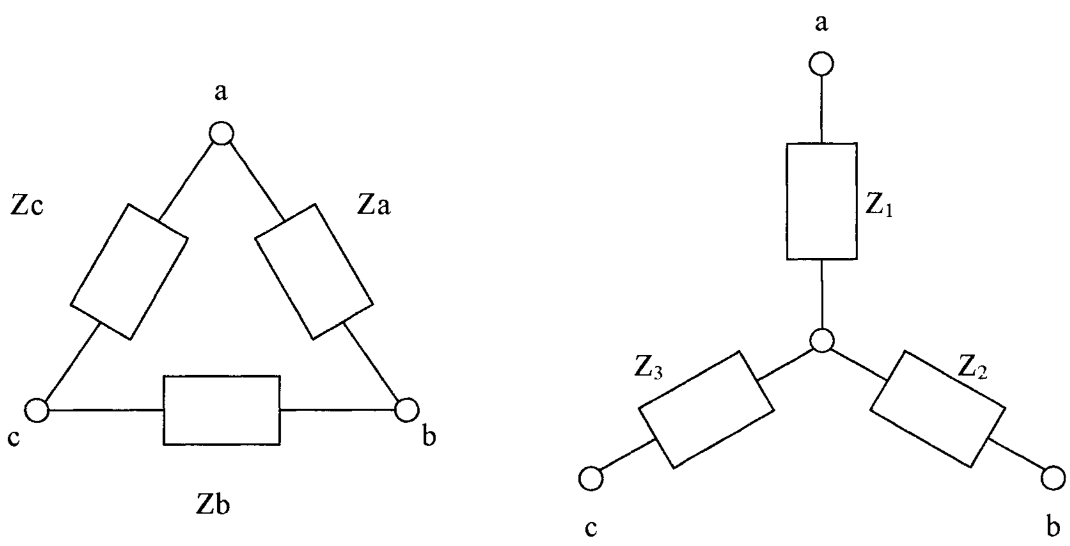

Figure 6.16 Delta and Y Impedance Arrangements

The impedances Z_1, Z_2 and Z_3 in the Y arrangement (right in Figure 6.16) can have a value so that the impedance between points a and b, a and c, and b and c would be the same as for the Δ arrangement (left in Figure 6.16) [3].

$$Z_1 = \frac{Z_a \cdot Z_c}{Z_a + Z_b + Z_c} \tag{27}$$

$$Z_2 = \frac{Z_a \cdot Z_b}{Z_a + Z_b + Z_c} \tag{28}$$

$$Z_3 = \frac{Z_b \cdot Z_c}{Z_a + Z_b + Z_c} \tag{29}$$

Thus, the circuit in Figure 6.15 can be converted to the circuit shown in Figure 6.17, where parts C_1, C_2 and R_2 have been replaced by the complex impedances Z_1, Z_2 and Z_3.

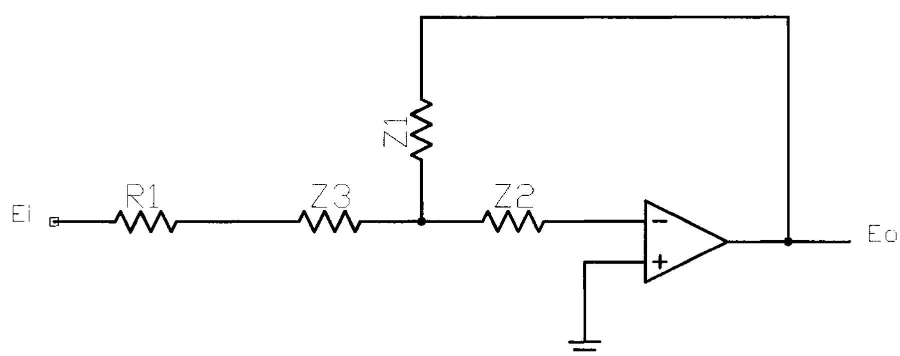

Figure 6.17 Simplified Bandpass Filter

Using Equations (27), (28), and (29), the value of Z_1, Z_2 and Z_3 can be found.

$$Z_1 = \frac{Z(R_2) \cdot Z(C_2)}{Z(R_2) + Z(C_1) + Z(C_2)} \tag{30}$$

$$Z_2 = \frac{Z(R_2) \cdot Z(C_1)}{Z(R_2) + Z(C_1) + Z(C_2)} \tag{31}$$

$$Z_3 = \frac{Z(C_1) \cdot Z(C_2)}{Z(R_2) + Z(C_1) + Z(C_2)} \tag{32}$$

Where

Z(x) is the complex impedance of component x

$Z(R) = R$

$Z(C) = \frac{1}{Cs}$

To obtain the equivalent of the circuit shown in Figure 6.14, R_1 can be arranged in series with Z_3 to form Z_x, and Z_2 replace Z_y.

The input current (I_{in}) flows through R_1, Z_3 and Z_2. No current flows through Z_2 (ideal operational amplifier assumption), since the input impedance of the operational amplifier is considered to be infinite. Therefore, if no current flows through Z_2, and the voltage at the input of the operational amplifier is assumed to be 0, then, the voltage across Z_2 is also 0, and the voltage at the junction between Z_1, Z_2 and Z_3 is also 0. The voltage drop across R_1+Z_3 is proportional to the current flowing in R_1+Z_3 (ohm's law):

$$I_{in} = \frac{E_{in}}{Z_x} = \frac{E_{in}}{R_1 + Z_3} \tag{33}$$

The current flowing through Z_2 can be calculated in a similar manner and gives:

$$I_{Z2} = \frac{-E_{out}}{Z_2} \tag{34}$$

Since no current flows through Z_1, $I_{in} = I_{Z2}$, hence Equations (33) and (34) are equal, hence:

$$\frac{E_{in}}{R_1 + Z_3} = \frac{-E_{out}}{Z_2} \tag{35}$$

Rearranging the terms in Equation (35) to take the form of Equation (26):

$$\frac{E_{out}}{E_{in}} = \frac{-Z_2}{R_1 + Z_3} \qquad (36)$$

The transfer function of this bandpass filter is as follows [33]:

$$H(s) = \frac{V_o(s)}{V_i(s)} = \frac{Ks}{s^2 + \frac{\omega_0}{Q} \cdot s + \omega_0^2} \qquad (37)$$

By choosing the components C_1, C_2, R_1 and R_2 used in this filter, one can design this filter to achieve the desired center frequency and filter sharpness using the following equations:

$$\omega_0^2 = \frac{1}{R_1 \cdot R_2 \cdot C_1 \cdot C_2} \qquad (38)$$

$$\frac{\omega_0}{Q} = \frac{C_1 + C_2}{R_2 \cdot C_1 \cdot C_2} \qquad (39)$$

$$K = \frac{-1}{R_1 \cdot C_2} \qquad (40)$$

Where

ω_0 is the center frequency

Q is the quality factor of a bandpass filter

ω_0 is the first parameter to be determined, and it is by necessity set to 5 kHz. Q is the sharpness of the filter, defined as the ratio of the center frequency to the filter bandwidth. The bandwidth is defined by the lower and upper cutoff frequencies, which are the points where the filter response is 3 dB below the filter peak response. The center frequency is the geometric mean of those two frequencies:

$$\omega_c = \sqrt{\omega_u \cdot \omega_l} \tag{41}$$

$$Q = \frac{\omega_c}{\omega_u - \omega_l} \tag{42}$$

Where

ω_u is the upper cutoff frequency

ω_l is the lower cutoff frequency

Therefore, the higher the quality factor, the more acute the filtration, that is to say the sharper the slope of attenuation as the input frequency deviates from the center frequency.

To choose component values, the value of ω_0 and Q had to be fixed. After trial and error, it was found that increasing Q too much tends to produce instability in the filter, so two filters, each which a $Q = 5$, were cascaded. The following frequency response was obtained for the two cascaded filters:

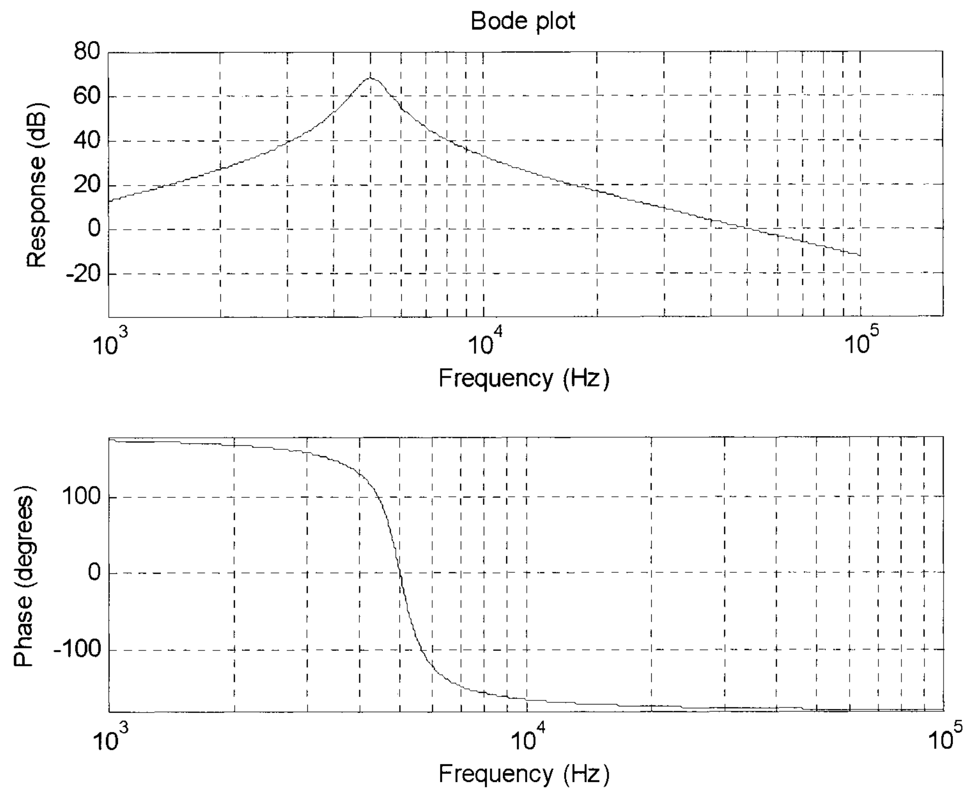

Figure 6.18 Frequency Response of Cascaded Filters

Such a filter has transient response characteristics when subjected to an input wave. Figure 6.19 shows the response of the filter when subjected to a series of square waves at 5 kHz. One characteristic of this filter is its amplification of 68 dB at 5 kHz. This is desirable because the output of the microphone is very weak. The filter performs both a frequency filtering and amplification for further processing.

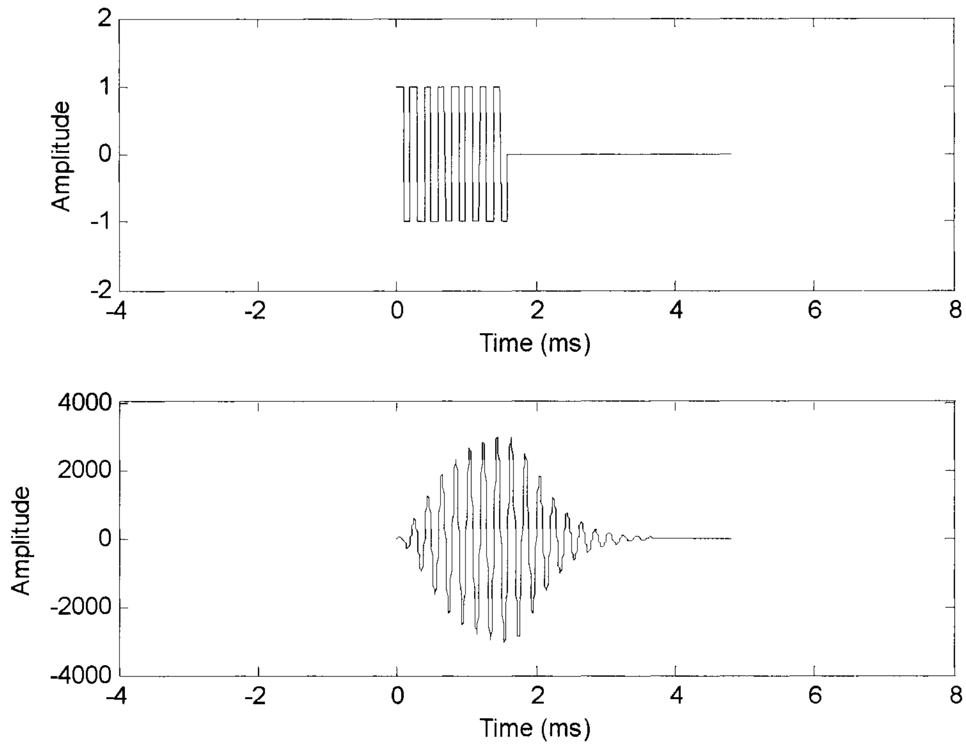

Figure 6.19 Transient Response of Filter to Square Wave Input

Peak Detection Circuit

As explained in Section 5.3.2, a peak detection circuit is needed to sample the signal at the correct moment. The peak detection circuit is composed of a differentiator built around a LF-442 operational amplifier. When the signal is rising, the output of the differentiator is positive, and when the signal is falling, the output is negative. The output of the differentiator is supplied to a comparator, with a reference value of 0 V. Therefore, when the signal is positive (higher than the reference signal), the comparator will output 5 V, and when the signal is negative (lower than the reference signal), the comparator will output 0 V. The output of the comparator is used as a digital input by the microcontroller. When a falling edge is detected, it indicates that a peak has occurred in the signal.

The electrical schematics for the ranging module are shown in Appendix G. It is composed of numerous sections. The first sheet shows the microphone input circuit, with the pre-amplifier, bandpass section, and a buffer for subsequent sections. The second sheet presents a low gain and a high gain amplification stages, with a threshold detection stage. On the third sheet is the power supply section for the ranging module. The fourth sheet shows the temperature sensor arrangement and the output connector for the module. The fifth sheet is the section used for the signal emission via the piezo transducer, and the sixth sheet contains the details of the peak detection circuit.

Speaker Driver

When the ranging system is used in emit mode, a pulse is emitted by a piezo transducer. The power supplied to this device is too large for the microcontroller. A H-Bridge is used to interface the piezo transducer to the microcontroller. The H-Bridge principle is explained in Section 6.3.2. Contrary to using a custom H-Bridge, the speaker driver uses a one piece H-Bridge. The H-Bridge used in this case is the L298 dual full-bridge driver.

Temperature Sensor

A temperature sensor is implemented. A National LM335 is used. It is housed in a TO-92 package, and outputs a voltage signal proportional to the temperature. The quoted accuracy is 1°C, and the sensor is able to operate from -40°C to +100°C.

7 Robot Software

The processor chosen for the purposes of this project is the Motorola MC68HC912B32CFU8, a variant of the 68HC12 family. It is a 16-bit microcontroller, and it uses a similar instruction set and architecture as the widely known 68HC11 family. Programs written for the 68HC11 can usually be recompiled with minor modifications for the 68HC12. The characteristics of this microcontroller are presented in Table 7.1. All the information related to the chosen microcontroller in this Chapter 7 is taken from [28].

Table 7.1 Characteristics of Motorola MC68HC912B32 Microcontroller

Clock speed	8 MHz
Flash EEPROM memory	32 Kbytes
EEPROM memory	768 Bytes
RAM memory	1 Kbytes
Analog to Digital Converter	1, 8 channels, 10-bit precision
Total number of I/O	63
Package	80-QFP (surface mount, 80-pin)

7.1 Microcontroller Memory

On the 68HC12 series of microcontrollers, the memory addresses are 16-bit wide. Hence, as each memory location contains 1 byte, it provides an address space of 64 Kbytes. The different types of memory, like Random Access Memory (RAM), Electrically-Erasable Programmable Read-Only Memory (EEPROM), Flash EEPROM, are all mapped to specific ranges of addresses in this 64 Kbytes address space. Figure 7.1 shows the basic memory arrangement for the MC68HC912B32.

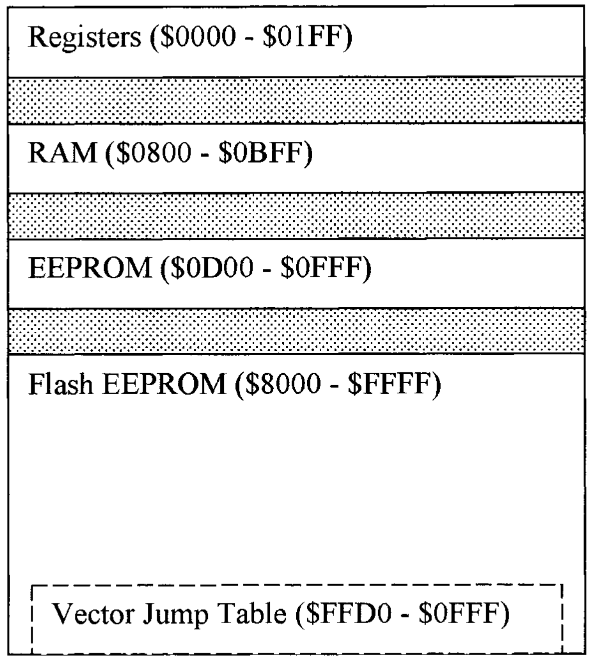

Figure 7.1 MC68HC912B32 Memory Map

7.1.1 Flash EEPROM Memory

The Flash EEPROM is a type of non-volatile memory that can be electrically erased. There is 32 Kbytes of Flash EEPROM on the MC68HC912B32. This type of memory can be used to store software and data that needs to be accessible when the microcontroller is powered up. The Flash EEPROM is not designed to be erased and written a large number of times. Motorola states that the Flash EEPROM on this microcontroller has an erase and program minimum life of 100 cycles. Also, the Flash EEPROM only support bulk erase, meaning that the whole 32 KB has to be erased before reprogramming it.

The very last part of the Flash EEPROM memory contains the Vector Jump Table (VJT). These are specific addresses that contain pointers for the Interrupt Service Routines (ISR). It permits the microcontroller to execute the proper ISR when a hardware interrupt is generated.

7.1.2 EEPROM Memory

Similar to the Flash EEPROM, the EEPROM memory is non-volatile, and its content is not affected by powering down or powering up the microcontroller. At 768 bytes, its size is much smaller than the Flash EEPROM. The EEPROM is byte erasable, so it is possible to reprogram only sections of it if needed. It also supports a much larger number of erase and program cycles. Motorola states that it can be erased and programmed a minimum of 10,000 times.

7.1.3 RAM Memory

The RAM memory is used to store temporary data, and its contents are lost whenever the power is removed from the microcontroller. RAM memory is usually used to store variables during program execution, and to hold the stack. The stack is a last in, first out (LIFO) data structure which is mainly used to store the processor state when interrupted to execute an ISR. When the ISR execution is finished, the can be restored to its state before the execution of the ISR. The stack can also be used to store variables in certain cases.

7.1.4 Hardware Registers

Hardware registers are memory locations in which writing has a direct effect on microcontroller hardware. Those locations can also be read to inquire about the state of different parts of the microcontroller.

For example, to control the electrical state of a microcontroller output pin, a logical 0 or 1 can be written to the proper register. In the same manner, for an input pin, the proper memory location can be read to know the input pin state.

Hardware registers are also used to configure the various hardware modules present on the microcontroller, such as hardware timers, Flash EEPROM, EEPROM, RAM, serial communication modules, etc.

7.2 Interrupt Service Routines (ISR)

An ISR is a software function written to handle hardware interrupts. A hardware interrupt is generated under certain conditions by the microcontroller. When a hardware interrupt is generated, the currently running function is paused, the state of the microcontroller is placed on the stack, and the proper ISR is executed. When the ISR execution is completed, the state of the microcontroller is restored from the stack, and the paused function execution is resumed.

7.3 Vector Jump Table

The VJT is a table located at the end of the Flash EEPROM. It contains the addresses of the ISRs. A part of the VJT is shown in Table 7.2.

Table 7.2 Example of Vector Jump Table for Motorola M68HC12B Family Microcontroller

Vector Address	Interrupt Source
$FFFE, $FFFF	Reset
$FFFC, $FFFD	COP clock monitor fail reset
$FFFA, $FFFB	COP failure reset
$FFF8, $FFF9	Unimplemented instruction trap
$FFF6, $FFF7	SWI
$FFF4, $FFF5	XIRQ
$FFF2, $FFF3	IRQ
$FFF0, $FFF1	Real-time interrupt
$FFEE, $FFEF	Timer channel 0
$FFEC, $FFED	Timer channel 1
...	...

Since each memory location in the M68HC912B microcontroller contains 8-bit, two of those locations are required to form an address, which is 16-bit. Starting from the end address of the Flash EEPROM, pairs of memory locations form the VJT. At each entry in the VJT, the address of an ISR is placed. Therefore, the contents of the memory locations $FFFE:$FFFF contains the address of the routine to be executed when the microcontroller is reset. Following the same scheme, the memory locations $FFEE:$FFEF points to the routine to be executed when an interrupt is generated by Timer channel 0.

7.4 Hardware Timers

Throughout the software, hardware timers are used. On the chosen microcontroller, there are 8 of them, each with 16-bit precision. A timer can be used to know the time of arrival of a certain pulse on a digital input (input capture mode), or to produce an event at fixed intervals, without intervention from the main processing unit (output compare mode).

In the case of the chosen microcontroller, the timer section is composed of a free running 16-bit counter, with a clock which is derived from the system clock, at 8 MHz. The system clock frequency can be divided by 1, 2, 4, 8, 16, or 32 to produce the timer clock. At each clock, the Timer Count Register (TCNT) in incremented by 1, up to the maximum value of the accumulator, which is 65,535. In this implementation, the prescaler is set at 16, so the timer clock is 500 kHz. Therefore, each 2 μs, the Timer Count Register is incremented by 1.

Each channel of the timer can be configured as an input capture channel, or an output compare channel. If the timer channel is configured in input capture mode, when an input is detected on the corresponding processor pin, the content of the TCNT is saved in a register, and an interrupt can be generated. The input can be a rising edge, a falling edge, or any of the two on a corresponding external pin. The input capture can be used to measure an input waveform. When the timer is configured in output compare mode, a value is put in the proper register for the selected channel, and when that value matches the value of the TCNT, an event is produced. That event can be an action on the corresponding output pin (set, clear, toggle), or an interrupt is generated. The output compare mode can therefore serve to execute a certain function at fixed intervals.

7.5 Software Structure and Development

As for the case of the hardware development, a modular approach is adopted for developing the software. The software is divided into more or less separate modules to ease the development and debugging of the system.

7.5.1 Memory Utilization

Since the Flash EEPROM can only support a limited number of erase-write cycles, the modules under development were placed in EEPROM, as they require frequent modifications. When a certain module did not required further modifications, it was placed in Flash EEPROM.

7.5.2 Vector Jump Table

Another problem is that the VJT is located in the Flash EEPROM. As explained in Section 7.3, each entry in the VJT points to a routine to be executed when an ISR occurs. If the location of the ISR changes, the corresponding entry in the VJT needs to be modified accordingly. To avoid having to modify the contents of the Flash EEPROM each time an ISR is moved, a second VJT was placed at the end of EEPROM. Each entry in this second VJT consists in a jump instruction pointing to the proper ISR. In this way, the VJT placed in the Flash EEPROM does not need to be modified each time an ISR is moved.

7.6 Communications

7.6.1 General Considerations

The general objective of the project is to have a group of Autonomous Guided Vehicles (AGV) interacting together. Therefore, a mean of controlling them must be provided. The distance between the group of AGVs and the base station is likely to be in the hundred meters range, since the possibility of explosion of a landmine must not threaten the security of the operator.

The base station must issue commands to the robots in a wireless manner. A good and simple solution is to use Radio Frequencies (RF) modules. RF modules already made are readily available on the market, and, depending on their functionality and performances, they are affordable and easy to implement.

7.6.2 Communication Protocol

The chosen communication modules communicate in half-duplex, meaning that simultaneous emission and reception are not possible. Moreover, when one module emits a message, all the other modules receive it (broadcast). Therefore, a communication protocol had to be designed and implemented to insure that all communications take place in an orderly manner.

To respect this constraint, only the base station is able to initiate communication. Whenever the robots transmit something, it is in answer to a request from the base station. Each transmission is encapsulated in a packet, to ensure data integrity. This protocol has been inspired from recommendations of the manufacturer, *Linx Technologies*, in [21]. The information is passed via packets. A packet contains a robot identifier, to indicate the intended target of the command, a command, and parameters necessary to the command. The packet construction is as follows:

Table 7.3 Packet Construction

Section	Length (bytes)	Signification
RF Sync	1	RF Synchronization
SOP	1	Start Of Packet
CMD	1	Command
RID	1	Robot Identifier
PARAM	variable	Parameters
CHK	1	Checksum

RF Sync is a byte of value 0xFF (%11111111). It is used to synchronize the RF Modules together by creating a strong mark period to distinguish from random electromagnetic noise.
SOP (start of packet) is a byte of value 0x55 (%01010101). It is used to mark the beginning of a packet.
CMD (command) is a byte used to indicate which command the robot must execute.
RID (robot identification) is a byte used to indicate to which robot the packet is targeted.
PARAM (parameter) is a variable number of bytes used as parameters to the command, if needed.

CHK (checksum) is a checksum of one byte, used to verify the data integrity of the packet. It is the sum of **SOP**, **CMD**, **RID**, and **PARAM** bytes, truncated to one byte.

Currently, there are 9 commands possible, 7 of which are implemented.

1. **LED_ON** – Turn on one of the three LED
2. **LED_OFF** – Turn off one of the three LED
3. **LED_TOGGLE** – Toggle one of the three LED
4. **SET_SPEED** – Set the speed command of the left and right motors
5. **RANGING** – Initiate a ranging sequence (emit if the robot is the target of the command, receive if the robot is not the target of the command)
6. **SET_PID** – Unimplemented, modify the gains of the speed controller
7. **GET_STATUS** – Unimplemented, get information about the robot status
8. **RANGING_ANSWER** – Packet emitted by a robot to the base station about the last ranging command as an answer to the **RANGING** command
9. **STATUS_ANSWER** – Packet emitted by a robot to the base station as an answer to the **GET_STATUS** command

7.6.3 Base Station Side

The base station is responsible for initiating all the communications with the robots. This centralized scheme avoids any confusion over the timing of communications and possible collisions between packets. The base station can emit commands to manipulate the individual LEDs present on the MCU module of each robot, to set the speed (and so, the direction) of the motors of each robot, and initiate ranging sequences. A screenshot of the PC interface in shown in Figure 7.2.

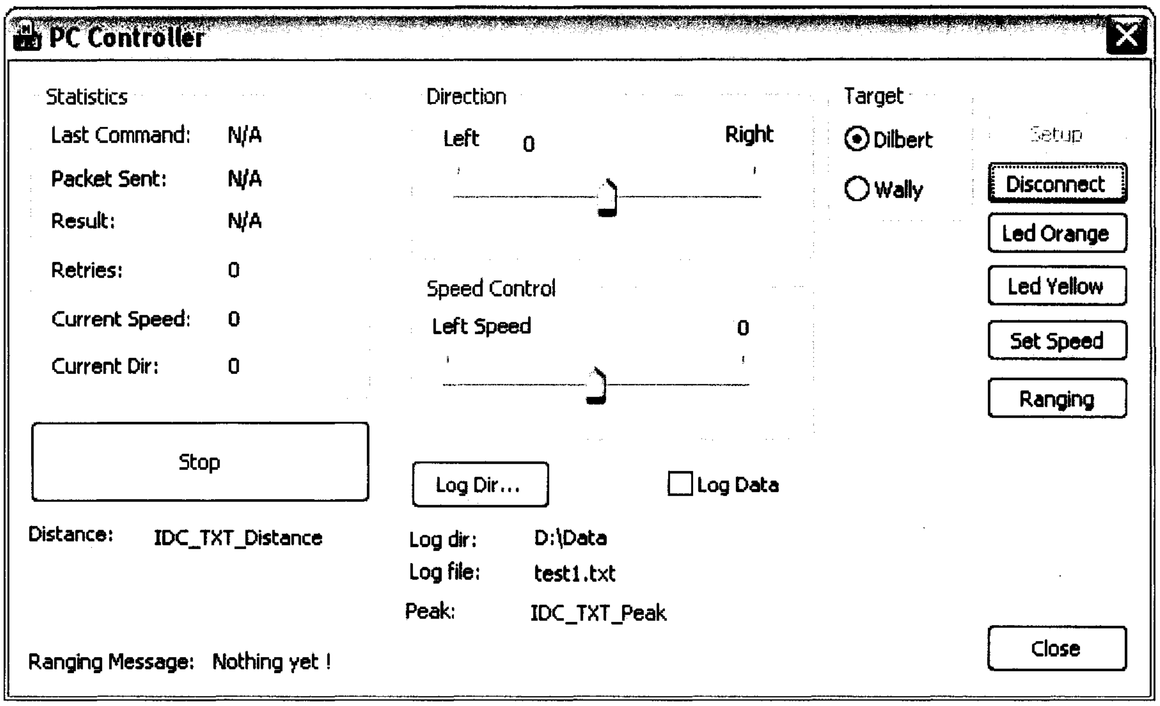

Figure 7.2 Screenshot of PC Interface Communication Software

7.6.4 Robot Side

The individual robots can only communicate back in answer to a command from the base station. Currently, out of the two answer-back commands that the robot can issue, only that reporting the results of a ranging sequence is implemented.

7.7 Speed Control

The speed control part of the software is divided in two parts. The first part deals with speed information. It has to detect whether the wheels are moving or not. If they do so, the module will measure the elapsed time between two rising edges coming from the optical encoder. The speed is then calculated as the inverse of the period.

The second part is the control part. It will look at actual speed and desired speed, and will set the power of left and right motors accordingly.

7.7.1 Speed Calculation

As stated earlier, the speed of the vehicle is proportional to the inverse of the period measured by the optical encoders.

The tangential speed of the wheels, which is also the vehicle speed if both wheel speeds are identical, is given by:

$$V_s = W_d \cdot \pi \cdot N_1 \quad (43)$$

Where

V_s is the vehicle speed

W_d is the wheel diameter

N_1 is the wheel rotational speed (rotation/s)

Since the motors are driving the wheels through a worm gear reducer, the relation between the motor and the wheel speed is given by:

$$R_w = \frac{N_2}{N_1} \quad (44)$$

Where

N_2 is the encoder rotational speed (rotation/s)

R_w is the speed ratio and is equal to the number of teeth in the worm gear, 50 in this case

The encoder frequency is proportional to its speed and number of slots, and is given by:

$$E_f = N_s \cdot N_2 \quad (45)$$

Where

N_s is the number of slots in encoder

E_f is the encoder frequency

Solving Equations (43) to (45) simultaneously, it is possible to relate encoder frequency to wheel tangential speed as follows:

$$V_s = W_d \cdot \pi \cdot \frac{E_f}{N_s \cdot R_w} \tag{46}$$

In this equation, all the terms except E_f are constants, so deducing the vehicle speed from the encoder frequency is straightforward.

As explained earlier, each encoder generates a quadrature signal, which is composed of two digital signals, out of phase by ideally 90°. The signal A is connected to a timer channel, configured as input capture. When the signal A presents a rising edge, an interrupt is triggered, and the direction is known from the level of the signal B. The value of the Timer Count Register is stored, and compared against the last stored value of the Timer Count Register to calculate the elapsed time since the last rising edge on signal A. From this difference, the period of the signal is known, and stored for further calculations as a 16-bit unsigned integer. The direction information is stored in another variable.

A special case is the detection of the zero-speed condition. When the wheels do not turn, no signal is present to trigger the interrupt that calculates the period. The period information stored in memory is from the last time the interrupt was trigger by a rising edge in signal A. When a certain amount of time (sufficiently long) has elapsed since the last interrupt, the speed is considered to be 0.

The actual speed command is calculated in the control low routine, which executes every 200 ms. The role of the control low routine is to calculate the actual speed based on the period of the encoders, and calculate the speed command from the actual speed and the desired speed. To calculate the speed information, the inverse of the period is first calculated. At the microcontroller level, in assembler language, the speed information is obtained by dividing $7FFF (32,767) (largest positive signed 16-bit integer) by the period divided by 2. The period must be divided by 2 (shifted right) because the largest value of an unsigned 16-bit integer is $FFFF (65,535), but if interpreted as a signed 16-bit integer, becomes -1 in decimal value. The resulting speed is always positive, and the result must therefore be converted to a negative value if the direction was determined negative from the quadrature signal. The calculations executed in the control low routine are explained in Section 7.7.2.

7.7.2 Speed Control

In order to control the vehicle speed, a controller is necessary. A speed command is issued to the robot, and the controller has to adapt the voltage supplied to the motors to attain the desired speed. For the purposes of the controller design, the robot was modelled. The motor is an electric device converting current into torque. This torque is directly proportional to current. Re-arranging Equation (20) gives:

$$t_m = K_t \cdot i_a \tag{47}$$

Where

t_m is the output torque of the motor

K_t is the motor torque constant

i_a is the armature current circulating in the motor

The motor will act as a generator. It will produce a voltage proportional to its rotational speed as follows:

$$e_b = K_b \cdot N_2 \tag{48}$$

Where

e_b is the back electromotive force (BEMF) voltage

K_b is the motor BEMF constant

The motor speed, N_2, is proportional to the vehicle speed, as shown by Equations (43) and (44). The current circulating in the motor armature is therefore related to the applied voltage and the motor rotational speed:

$$e_i - e_b = R_a \cdot i_a \tag{49}$$

Where

e_i is the motor applied voltage

The output torque of the motor will be used to accelerate the motor rotational speed, accelerate the vehicle and counter the resistive torque from the vehicle drag. Considering the drag as a disturbance, the output torque of the motor can be related to the vehicle acceleration:

$$T_m = \left(\frac{J_m \cdot R_w}{W_d \cdot \pi} + \frac{W_d \cdot M_v}{2 \cdot R_w} \right) \cdot \dot{v}_s \tag{50}$$

The motor input voltage can then be related to the vehicle speed:

$$e_i = \frac{R_a}{K_t} \cdot \left(\frac{J_m \cdot R_w}{W_d \cdot \pi} + \frac{W_d \cdot M_v}{2 \cdot R_w} \right) \cdot \dot{v}_s + \frac{K_b \cdot R_w}{W_d \cdot \pi} \cdot v_s \tag{51}$$

Where

J_m is the motor's rotor polar moment of inertia

M_v is the vehicle mass

The input to the system is the duty cycle commanded to the H-Bridge via the PWM module of the MCU. The duty cycle is 100% when the command is 65,535, and the H-Bridge voltage is 12 V.

$$e_i = e_h \cdot \frac{D_{PWM}}{65{,}535} \tag{52}$$

Where

e_h is the H-Bridge supply voltage

D_{PWM} is the PWM duty cycle command to the MCU (65,535 is 100%)

The speed, as measured by the MCU, is the reciprocal of the encoder period. The reciprocal is multiplied by 32,767 to avoid dealing with fractional numbers in the MCU. Modifying Equation (46):

$$v_s = \frac{speed \cdot MCUClock \cdot W_d \cdot \pi}{32{,}767 \cdot 2 \cdot N_s \cdot R_w \cdot timer\Pr escaler} \tag{53}$$

Where

speed is the speed, as measured by the MCU

MCUClock is the clock speed of the MCU (8 MHz)

timerPrescaler is the prescaler value by which the Timer Module clock is derived from the clock of the MCU

The constants of Equation (53) can be combined as follows:

$$K_{MCU} = \frac{MCUClock \cdot W_d \cdot \pi}{32{,}767 \cdot 2 \cdot N_s \cdot R_w \cdot timer\Pr escaler} \tag{54}$$

Combining Equations (51), (53), and (54) and applying the Laplace transform results in the following:

$$\frac{SPEED(s)}{D_{PWM}(s)} = \frac{1}{(A+B) \cdot s + C} \tag{55}$$

Where:

$$A = \frac{65{,}535 \cdot K_{MCU} \cdot R_a \cdot J_m \cdot R_w}{e_h \cdot K_t \cdot W_d \cdot \pi}$$

$$B = \frac{65{,}535 \cdot K_{MCU} \cdot R_a \cdot W_d \cdot M_v}{e_h \cdot K_t \cdot 2 \cdot R_w}$$

$$C = \frac{65{,}535 \cdot K_{MCU} \cdot K_b \cdot R_w}{e_h \cdot \pi \cdot W_d}$$

Equation (55) represents the transfer function of the vehicle. It is a first order system. It has a pole along the real axis, given by $-C / (A+B)$, at -2.39. This indicates that the time constant of the system is 0.38 seconds. Such time constant is considered large and would result in a slow system response.

In order to properly control the speed of the vehicle, a compensator has been added, within the negative feedback loop. Without closed loop control, the vehicle would not react to changes in vehicle drag (due to terrain, slopes, added weight), or battery charge level. A proportional controller alone is the simplest on that can be implemented. It consists of multiplying the error (desired speed – actual speed) by a proportional gain. This will have the effect of moving the pole toward negative infinity, thus decreasing the time constant of the system. It will make it react faster. The proportional controller will however always produce a steady state error between the desired speed and the actual speed. To counter that, an integrator has to be added to the controller. The controller takes the form of:

$$C(s) = K_P + \frac{K_I}{s} \tag{56}$$

Where

$C(s)$ is the controller transfer function

K_P is the controller proportional gain

K_I is the controller integral gain

A root locus plot of different options is shown in Figure 7.3.

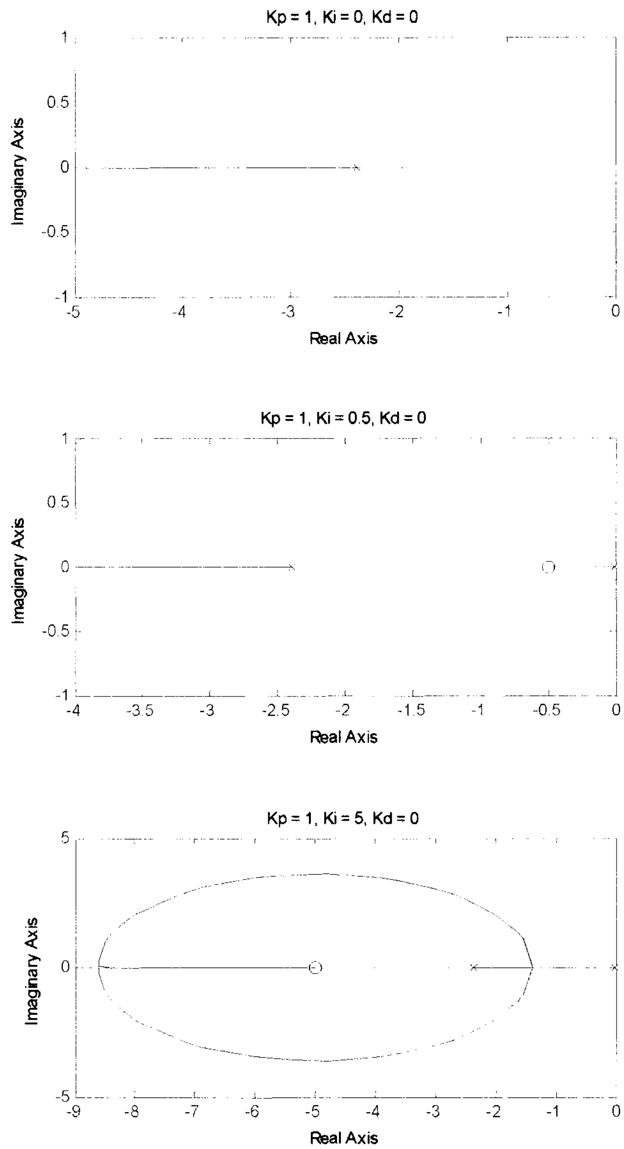

Figure 7.3 Root Locus Plot of Closed Loop System with a PI controller

As it can be seen, a system with a proportional controller alone will have an acceptable response time, however, it will exhibit a steady state error. The steady state error [32] in response to a step input of the proportionally controlled closed loop first order system shown in Equation (55) is given below:

$$e(\infty) = \frac{1}{1 + {K_P}/{C}} \tag{57}$$

Where

$e(\infty)$ is the error between desired and actual output

C is the combination of constants shown in Equation (55)

Thus, for the particular system shown here, the steady state error for a proportional only controller as a function of the proportional gain is shown in Figure 7.4.

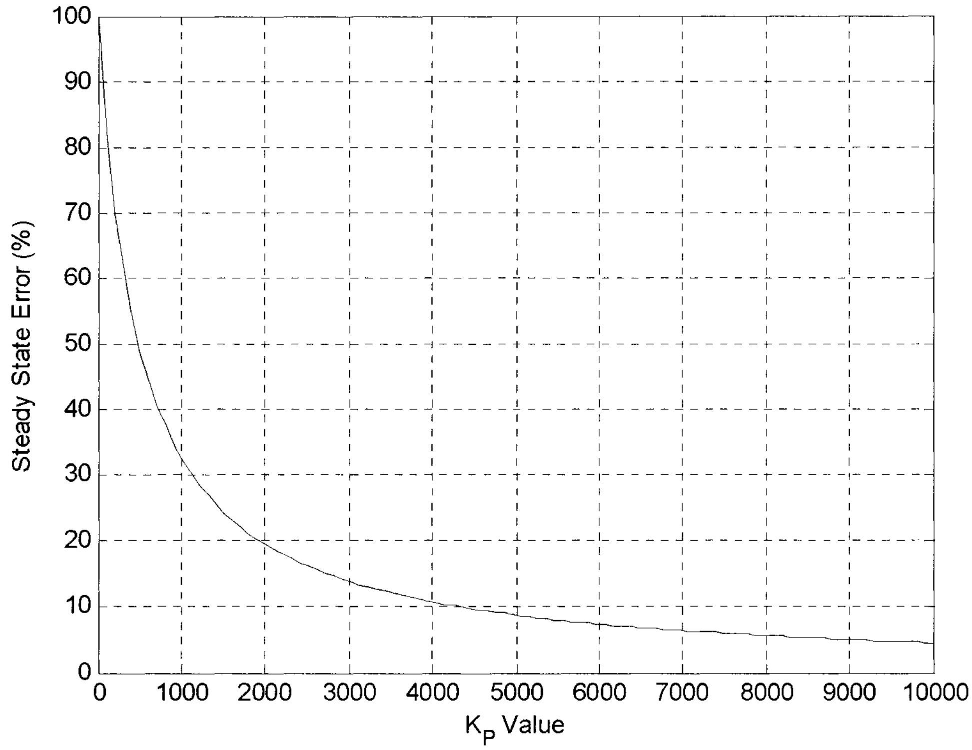

Figure 7.4 Steady State Error as a Function of Proportional Gain

If an integral action is added, with a small integral gain, say 50% of the proportional gain, it will results in a pole coincident with the origin of the root locus in the Laplace domain, and a zero between the first order system pole and the origin as shown in Figure 7.3. Such a pole-zero distribution will decrease the system response time. However, due to the integral action, the steady state error will be eliminated given adequate time. Increasing the integral controller gain will cause the zero to move towards the system pole. Eventually, the zero will coincide with the first order system pole. Further increase in the integral gain will cause the zero to move to the left of the system pole as shown in Figure 7.3. As the proportional gain of the system is increased, keeping the ratio K_I/K_P constant will cause the closed loop system characteristic equation root to migrate along the real axis in between the two adjacent poles and then leave the real axis to become complex conjugate. When that happens, the system will experience oscillations, will be fast in response, and will have zero steady state error. Further increase in the proportional gain, again keeping the ratio K_I/K_P constant, will cause the two roots of the characteristic equation to migrate back onto the real axis. At that point the system will have the fastest response and no steady state error. The root locus in Figure 7.3 depicts all these cases. It should be noted however, that very high proportional gains may not be always practical or desirable from a physical implementation stand point.

As the PI controller is coded in 68HC12 assembler, some precautions had to be taken. The first one is about precision. The 68HC12 deals mainly with integers of 8-bit, 16-bit and exceptionally 32-bit size. Thus, the calculations had to be constructed in consequence to avoid imprecision due to number representation.

7.8 Short Range Positioning System

7.8.1 Robot Software

The SRPS algorithm is mainly implemented in hardware, within the ranging module. The output signals of the ranging module are as follows:

Table 7.4 List of Hardware Signals Used for Ranging

Signal Name	Input / Output	Description	Type
SPKR_SIG	Output	Speaker signal output	Square wave
RX_IN	Input	Input signal over threshold	Digital
PK_IN	Input	Peak detected	Digital
TEMP	Input	Temperature	Analog
HIGH_SIG	Input	High gain signal	Analog
LOW_SIG	Input	Low gain signal	Analog
SPKR_EN	Output	Speaker amplifier enable	Digital

In receiver mode, the microcontroller receives signals from the ranging module that indicate when does a peak is occurring, together with the analog signal itself, at two different amplification levels. At the start of the ranging process in receive mode, the value of the TCNT register (see Section 7.4) is saved and considered the initial time. The PK_IN signal is channelled to a timer input pin of the microcontroller. The associated timer channel is configured in input capture mode, and generates an interrupt each time a rising edge is detected on the PK_IN signal. When this interrupt occurs, it samples and stores in memory the analog signal present at that moment on the inputs HIGH_SIG and LOW_SIG. Those signals are the amplified and filtered ranging signal. The elapsed time since the initial time is also stored in memory. After the ISR is finished executing, the microcontroller waits for another rising edge on the PK_IN signal. When 8 samples have been taken, or when too much time has elapsed, the values of the elapsed time, HIGH_SIG and LOW_SIG signals are returned to the base station for further processing. If a timeout occurred, a ranging error message is returned to the base station instead.

In emitter mode, the microcontroller will simply enable the speaker amplifier and generate a 5 kHz signal on the SPKR_SIG pin to emit the ranging signal.

7.8.2 Base Station Software

The ranging process is always initiated by the base station, by sending a ranging command to one of the robots. When the ranging sequence is done, the robots return their unprocessed results to the base station, where the actual distances are calculated. As explained in Section 7.8.1, three series of 8 values each are returned by the robots. They consist of the elapsed time at which the peaks of the signal occurred and the signal level from the low gain amplification stage and the high gain amplification stage at those precise moments.

The signal from the high gain amplification stage is normalized to the highest value of the array. The signal is then correlated using Equation (19). This correlation is verified for different overlaps of the normalized signal to a reference mask, and the overlap with the maximum correlation is considered correctly matching the reference mask. The elapsed time associated with a particular peak then becomes the output of the SRPS.

8 Results

8.1 Testing Objectives

At this stage of development of the SRPS, the objective of the tests was to determine the viability of the concept. To be usable, the system has to produce an output that is highly correlated with the input, in that case, the distance separating two ranging modules. The correlation can be linear or non-linear. By design, the SRPS presented in this thesis has a linear correlation between the output and the input variables, provided that the temperature does not change significantly in the course of a test.

The primary output of the SRPS is a 16-bit value expressing the time elapsed between the start of the ranging command and the reception of the first peaks of the signal. By pattern matching, the same peak needs to be consistently identified. This value is affected by distance separating the two SRPS modules, the air temperature, air turbulence, air speed, signal reflection, acoustic and electrical noise.

8.2 Methodology

To verify the linearity of the output of SRPS, it was necessary to measure a range of distances under different conditions. The modules were placed at different separation distances, and their location was measured with a measuring tape, with a precision of ±0.25 cm. One of the SRPS modules was placed at a fixed location, and another module was gradually moved away, in 10 cm increments. At each position, 10 or more distance measurements were taken and recorded. The temperature was measured with a glass thermometer, having a precision of ±1°C. This experiment was conducted in several locations, each having different environmental conditions, such as temperature, floor, walls, other reflecting objects, wind speed, and ambient noise.

8.3 Data Processing

Measurement data from the sets of measurements taken at each distance exhibited either of three characteristic patterns. In the first pattern, all readings were grouped around a central value, corresponded to the measured distance within the tolerance limits of the SRPS.

In the second pattern, one or two of the readings exhibited an error. Such errors are easily identifiable, as they are outside the normal repeating values in the set.

Table 8.1 Partial Data Set Example for Distance Experiment

Data point	Distance (cm)	Timer Value (clock units)
1	220	3827
2	220	3824
3	220	3823
4	220	3827
5	220	3929
6	220	3825
7	220	3827
8	220	3825
9	220	3824
10	220	3823

In Table 8.1, one raw data set is presented. This set was taken at University of Ottawa, in Colonel By building, room B210 and shows the clock count for a distance of 220 cm. All the resulting timer values are closely grouped between 3823 and 3827 with the exception of one value at 3929. This value is clearly an outlier, and could be easily eliminated with proper software filtering, and by taking multiple values at the same distance. When processing the data, all the raw data was cleaned from such obvious outliers.

In the third pattern, data in a set were grouped around 2 or 3 values, such as in the partial data set shown in Table 8.2. The timer values for the distance 110 cm oscillates between two distinct values, around 2160 and 2275, but with very few variations around each of those values, ranging from 2157 to 2162 and from 2271 to 2277.

Table 8.2 Partial Data Set Showing Wavelength Error

Data point	Distance (cm)	Timer Value (clock units)
1	110	2160
2	110	2271
3	110	2157
4	110	2158
5	110	2275
6	110	2275
7	110	2160
8	110	2274
9	110	2277
10	110	2161
11	110	2274
12	110	2160
13	110	2162
14	110	2275
15	110	2276

Considering the operating parameters of the microcontroller, the timer values correspond to a clock frequency of 500 kHz. Each unit corresponds to 2 μs. The difference between 2160 and 2275 counts being 115, this translates to 230 μs. Using Equation (5) and for a sound speed of 340 m/s (refer to Section 4.3), the 115 clock units correspond to a distance value of 7.82 cm. This is close to the 6.8 cm wavelength used by the SRPS. This indicates that in some instances the system may have an error of one wavelength in its peak identification.

8.4 Experimental Results

Four comprehensive tests where conducted to evaluate the efficacy of the SRPS. Details of these tests follow.

8.4.1 First Test

The first test was done in a closed lab room. Room temperature was 24°C. Distance was varied from 100 cm to 240 cm. The ranging modules were laid directly on the floor, which is smooth concrete. Acoustic panels were arranged around the test area to reduce sound wave reflections and stray noise. Figure 8.1 shows the results for the test.

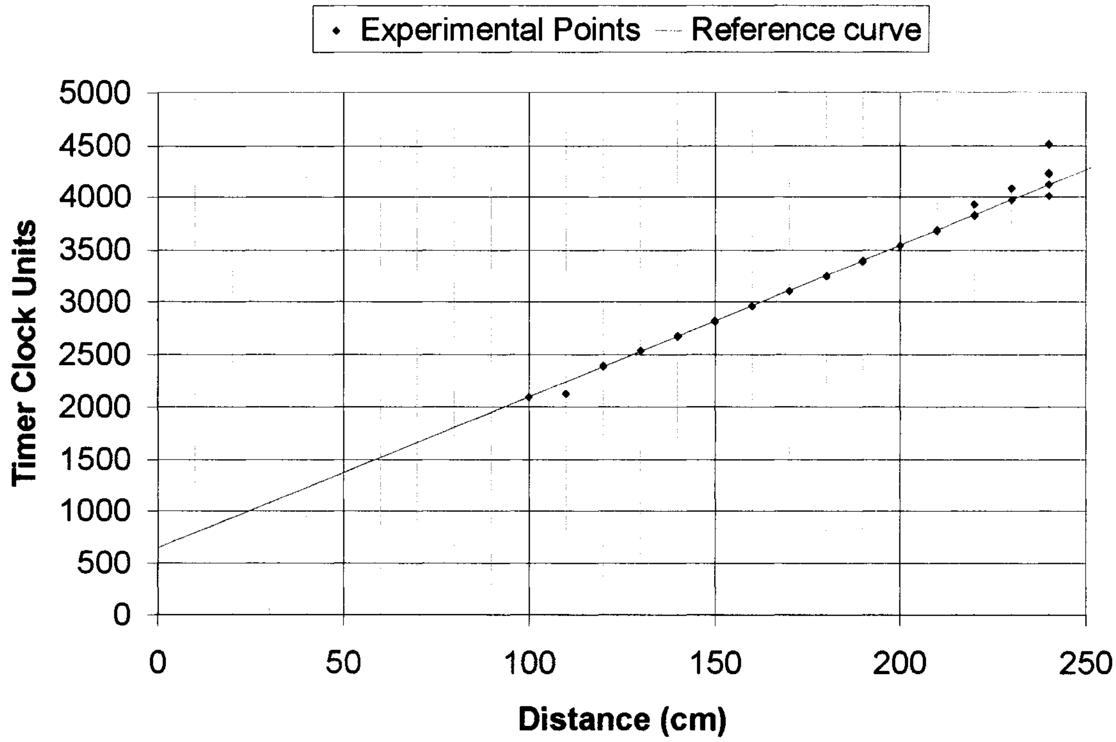

Figure 8.1 Experimental Results for First Test

A theoretical curve was plotted over the experimental results. The curve is a first order equation, with the slope being proportional to the speed of sound. The offset was adjusted to obtain an average error of 0 when removing the evident outliers. In the case of the first test, the offset was found to be 644 timer clock units. The speed of sound has been calculated using the ambient temperature at the time of the test, and then converted to match the time scale of the MCU timer module, which is running at 500 kHz.

At 220 cm, over a group of 10 samples, 1 outlier can be observed, having around 100 timer clock units more than the rest of the group, which is equivalent to one wavelength. The same phenomenon can be observed at 230 cm.

At 240 cm, the values are grouped into 4 distinct groups. According to the reference curve, the second group, around 4120, seems to be the right value, although this is difficult to deduce from the time value information alone.

It can be seen in Figure 8.1 that no point lies on the reference curve at 110 cm, which could be caused by an anomaly in room conditions, such as ventilation or a particular standing wave.

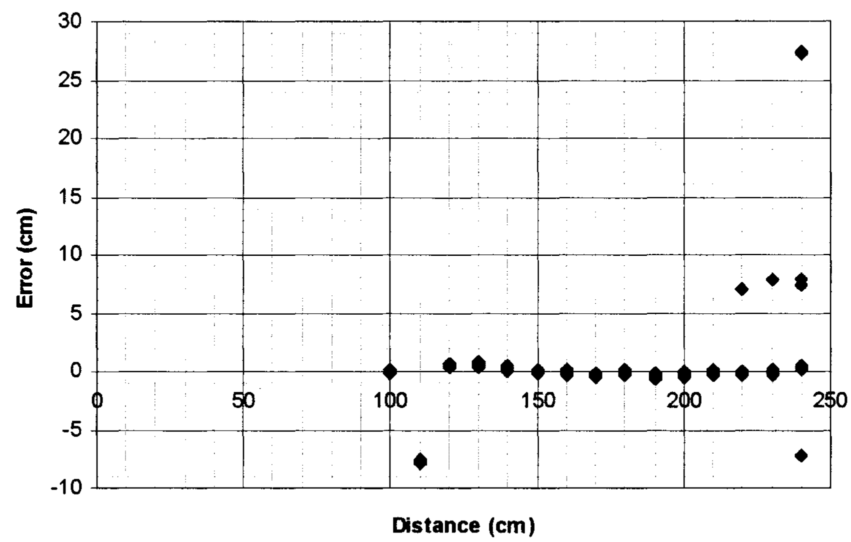

Figure 8.2 Error in Position Estimation for First Test (Raw Results)

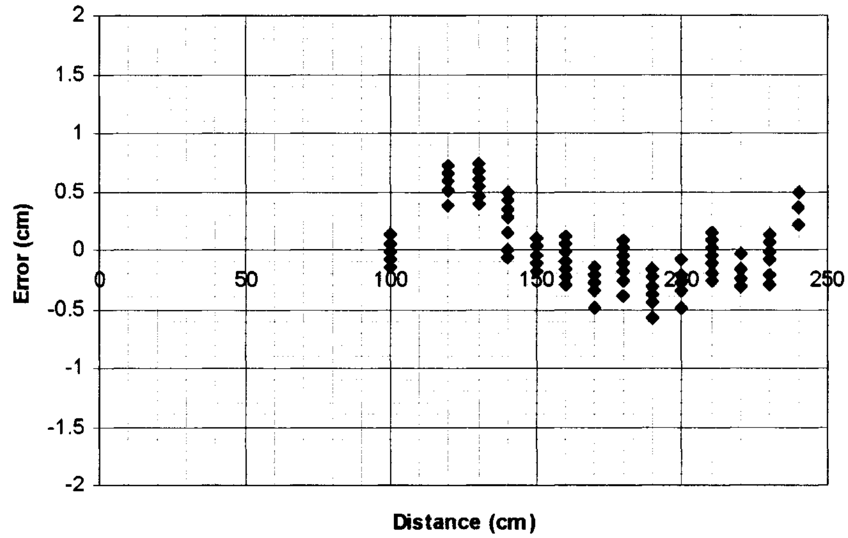

Figure 8.3 Error in Position Estimation for First Test (Cleaned Results)

As the experimental offset has been found, the resulting constants were used to compute the distance from the obtained timer values. For purposes of calibration and analysis, results away from the reference curve by 1 wavelength or more were removed from the dataset for this graph. The resulting error in the measurement of the distances is presented in Figure 8.2 and Figure 8.3. The errors shown in Figure 8.2 include outliers, while those shown in Figure 8.3 exclude them. The error does not seem to be correlated with the distance. The relative error is also very low, ranging from 0.6% at 100 cm to 0.3% at 230 cm. This data has also to be viewed in light of the ±0.25 cm precision to which the distance separating the SRPS is being measured.

In Figure 8.2, the error in the raw data results increases somewhat beyond a certain distance. This will also be observed in subsequent tests. This effect may be due to the peak detection algorithm and hardware being not robust enough to a decreasing signal level. A variable gain amplifier controlled by a constant amplitude circuit may solve this problem.

8.4.2 Second Test

The second test was carried out under the same conditions as for the first test but at ambient temperature of 23°C. The distance was varied from 90 cm to 250 cm.

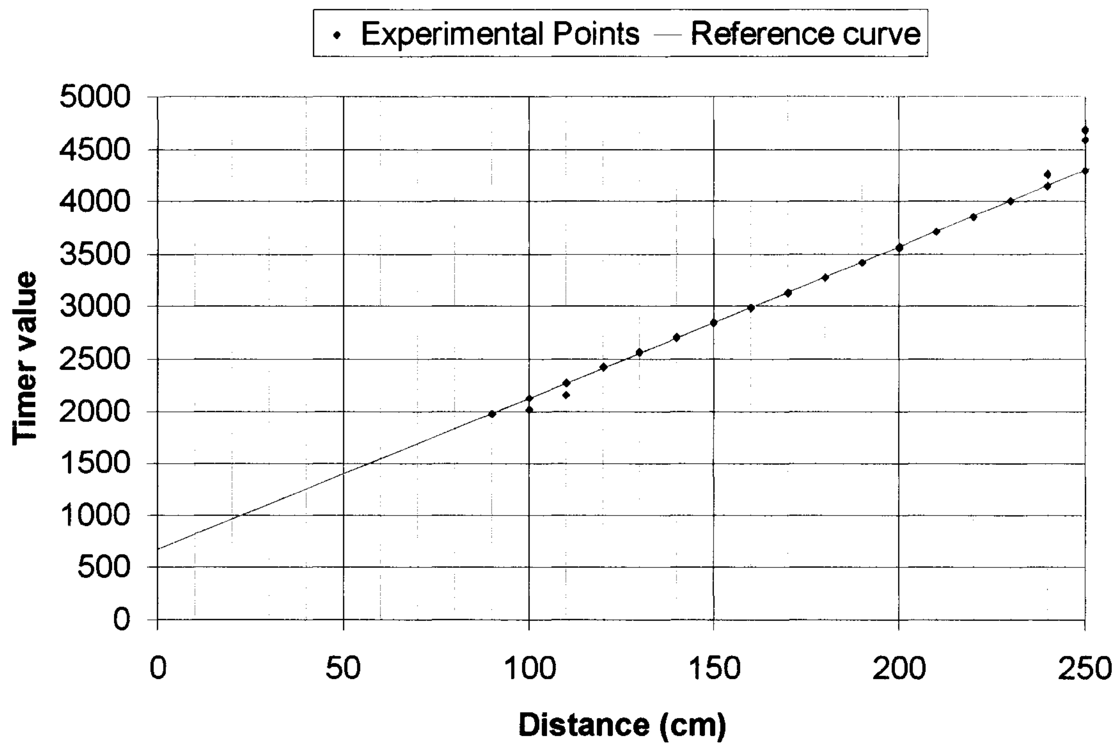

Figure 8.4 Experimental Results for Second Test

A theoretical curve was plotted over experimental points. The slope of the curve was computed based on speed of sound at the recorded temperature during the test, and the offset was adjusted to obtain an average error of 0 cm once the outliers are removed. The resulting offset using this technique is 671 timer clock units, which is slightly higher than the offset found in first test by about 4%. Nearly all the results fall on the reference curve. At 100 cm, 2 points out of 12 are below the reference curve by the equivalent of about 1 wavelength. At 110 cm, over 15 readings, 8 of the points coincided with the reference curve, while the remaining ones were under it by about 1 wavelength. At 240 cm, out of the 10 readings, only 4 appear to be correct, while the remaining 6 were above the reference curve by one wavelength. At 250 cm, only 1 reading is correct, while the other 9 are over the reference curve.

The data scattering seems to be similar to that from the first test. After removal of easily identified outliers, the distance was computed using the timer value results, and was compared against the actual distances measured. The results are shown in Figure 8.5 and Figure 8.6.

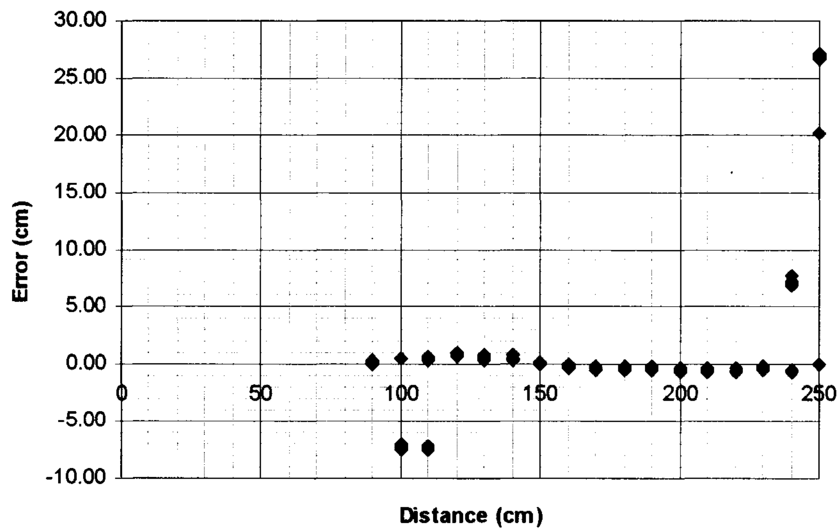

Figure 8.5 Error in Position Estimation for Second Test (Raw Results)

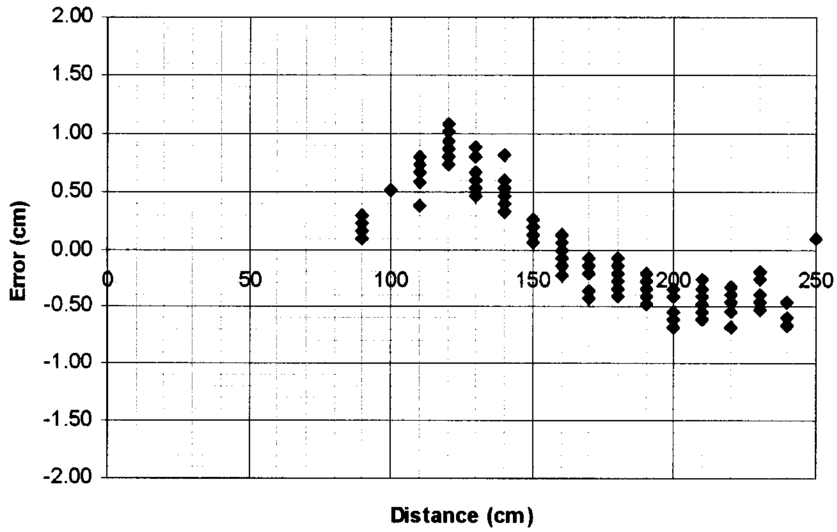

Figure 8.6 Error in Position Estimation for Second Test (Cleaned Results)

The figures show that the error increases with distance. This can possibly be explained by the fact that the signal level is decreasing with increasing distance. Both the threshold detection and the peak detection circuits experience functional difficulties due to the decreasing Signal-to-Noise Ratio (SNR), with ambient noise level remaining constant while the signal level decreases.

8.4.3 Third Test

The third test was conducted outside, and the temperature was decreasing during the test. At the beginning of the test, the temperature was +2°C and it dropped to -1°C by the end of the test. The ranging modules were installed on a wheeled transport table, about 1 m above an asphalt ground. The test was conducted between two buildings, spaced about 25 m apart.

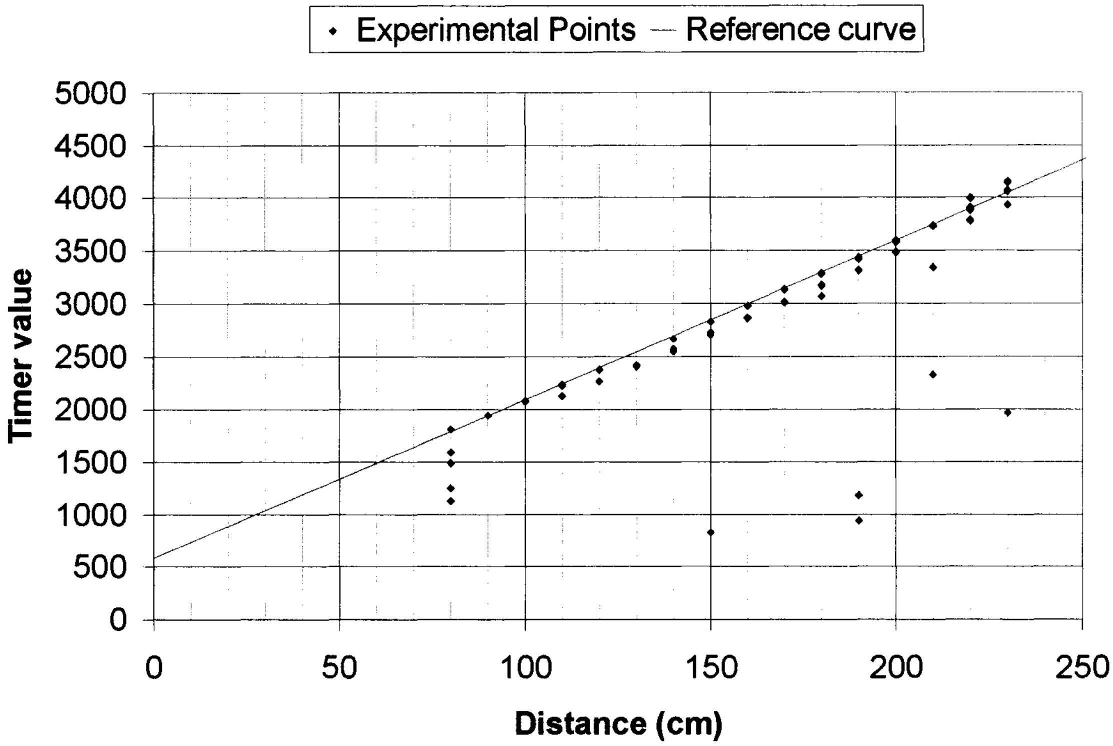

Figure 8.7 Experimental Results for Third Test

The data obtained during the third test presents more outliers than in other test, presumably because the test was conducted outdoor, with a passing street at proximity, generating more random noise near the 5 kHz working frequency.

Data points that have considerably lower timer values to those expected can be seen throughout the test. The discrepancy is believed to be caused by ambient noise. Due to the design of the ranging algorithm, when the microcontroller receives a ranging command as a receiver, it waits for a signal. If the ambient noise contains the ranging wave frequency and happens to impact the receiver shortly after the ranging command was issued, but before the ranging wave it is waiting for, microcontroller will sample it under the assumption that it is part of the ranging signal, thus yielding a shorter value for the measured distance.

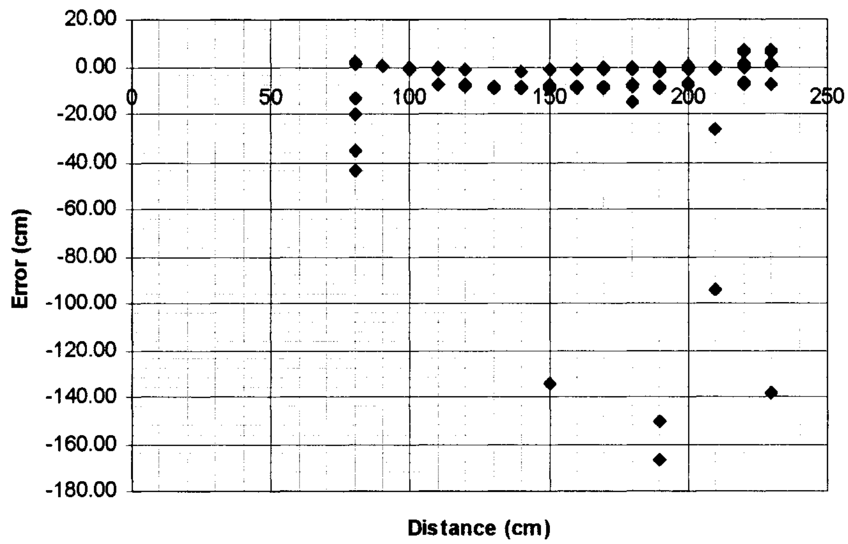

Figure 8.8 Error in Position Estimation for Third Test (Raw Results)

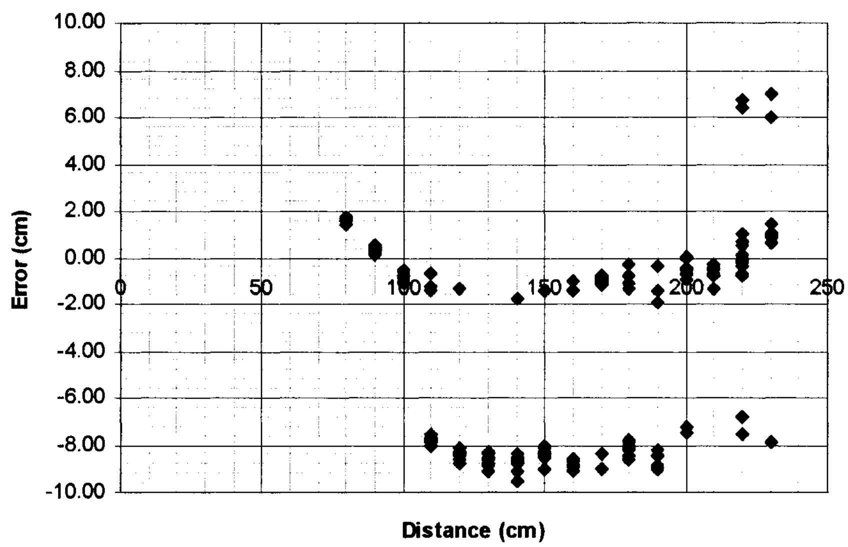

Figure 8.9 Error in Position Estimation for Third Test (Cleaned Results)

Again, the error is not correlated to distance. However, a greater number of results are off by one wavelength. A possible cause for this behaviour is the lower signal-to-noise ratio cause by the conditions of ambient noise caused by passing cars and wind. The signal might not be as clearly defined as in the indoor conditions, and the algorithm might have some difficulties identifying the proper peaks of the signal.

8.4.4 Fourth Test

The fourth test was conducted in a large area situated in a basement. The temperature was 23°C. The ranging modules were installed on a wheeled transport table, about 1 m above a smooth concrete ground. The area has walls made of concrete blocks, and has dimensions of about 25 m by 25 m.

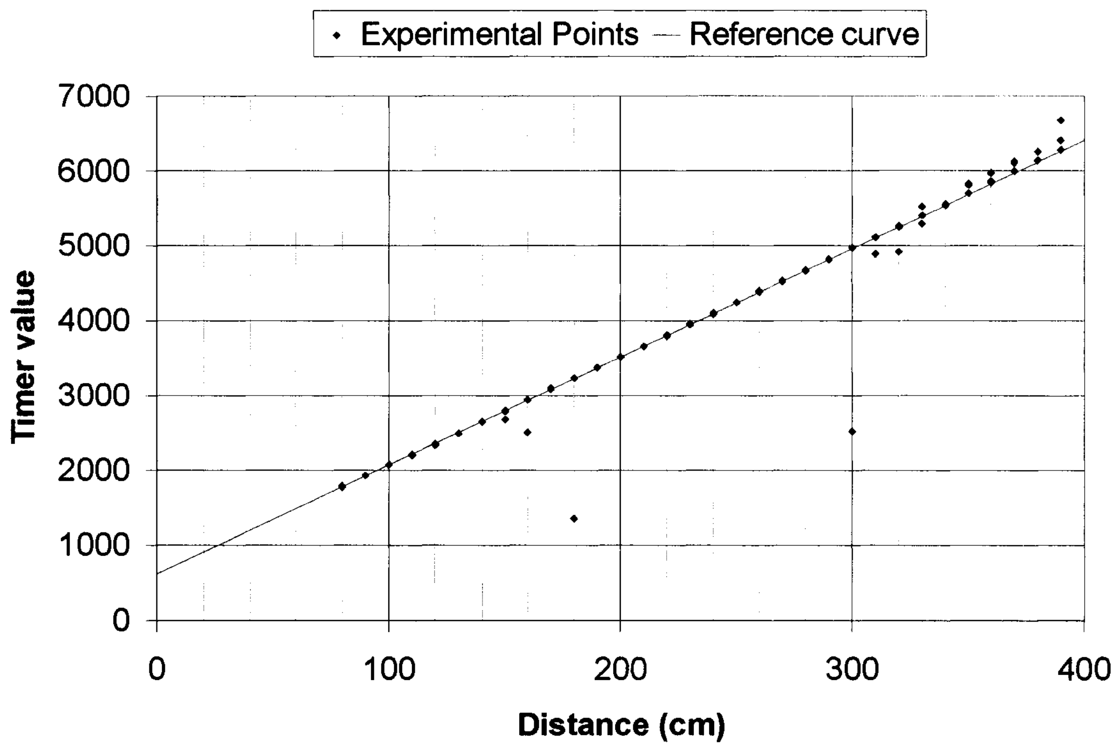

Figure 8.10 Experimental Results for Fourth Test

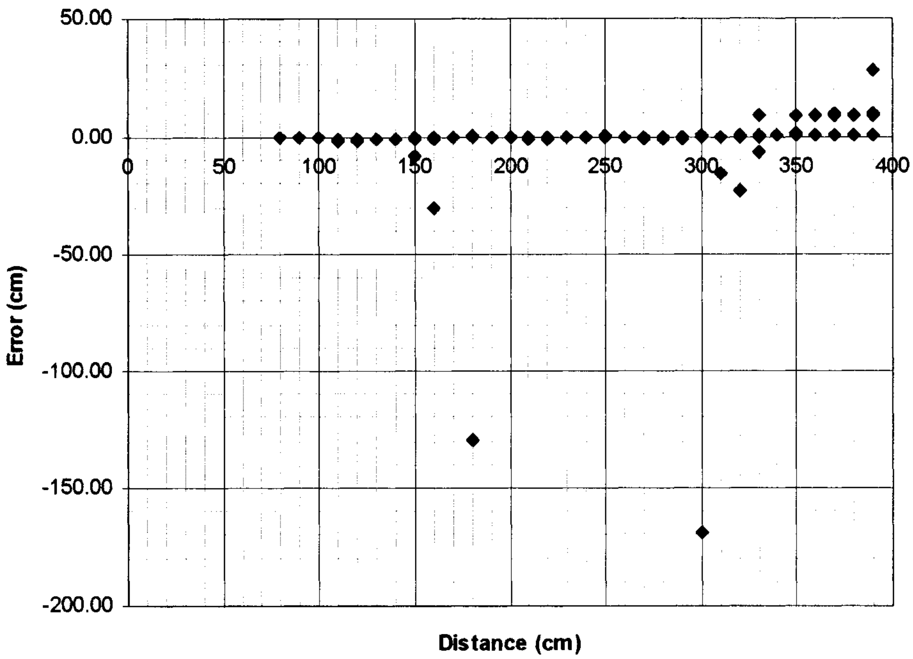

Figure 8.11 Error in Position Estimation for Fourth Test (Raw Results)

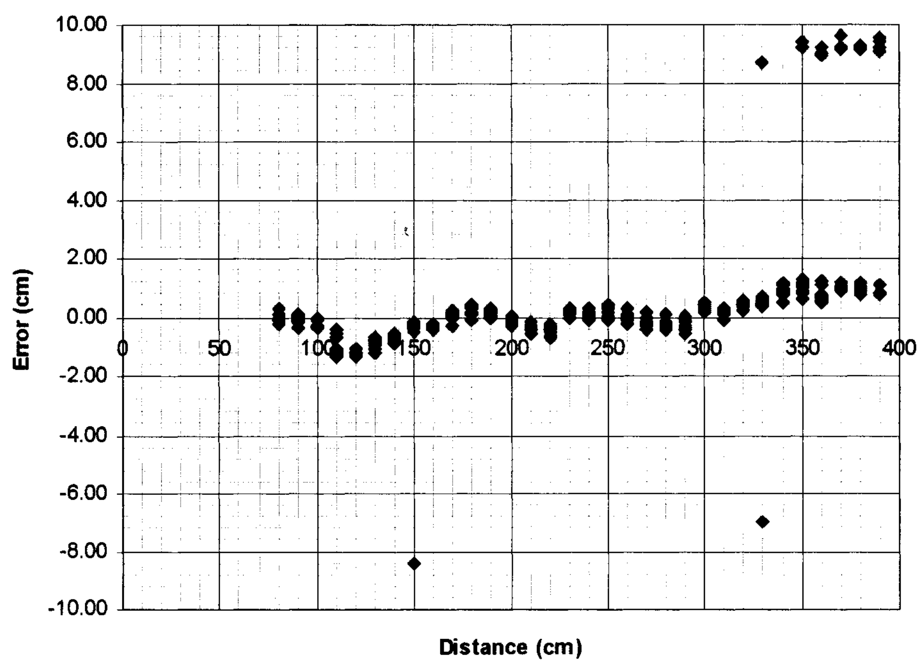

Figure 8.12 Error in Position Estimation for Fourth Test (Cleaned Results)

The experimental error shown for the SPRS for the fourth test is still within ±2 cm of the expected values, except for the outliers and a group of values at one wavelength over the correct values. In this test, the distance was increased to see the point where the signal-to-noise ratio becomes too low for the SRPS to operate correctly. At 380 cm and 390 cm, there were more incorrect values than correct ones. It shows that the SRPS has difficulties applying the algorithm to identify the proper peak in the signal. However, this could be easily overcome with a variable gain amplifier.

9 Discussion and Conclusion

9.1 Summary of the Thesis

The aim of this work was to select and develop the concepts of a system that would be suitable for demining effort in Third World landmine affected countries. The system has to be able to identify the location of landmines in a field. Since the system is to be used in countries where money, expertise and replacement parts are not easily available, it needs to be simple, yet robust.

The chosen concept consists in a group of small autonomous mobile robots that can work in team, moving in formation in a minefield to detect landmines, while exerting small enough ground pressure to avoid detonating landmines. The robot group needs to have a certain level of autonomy, and is controlled by a base station located at a safe distance from the potentially dangerous accidental detonation of a landmine.

The mobile robots consist of a vehicle than can transport a payload while minimizing ground pressure, the associated electronics to control it, a wireless communication system and the associated software were designed and developed. While the payload is beyond the scope of this work, it is expected to be an arm that can sweep a circular path centered at the vehicle and carries a metal detector sensor and a spray paint can. When a suspicious object is detected by the metal detector, a color marker is deposited on the ground. This robot can receive commands from a base station, via a wireless communication channel, to move, to communicate back information, or to do other actions needed by the base station.

Advances in distance measuring devices suitable for mobile robotics were achieved during the course of this work. It consists of a long range positioning system using a consumer grade camera with a variable focal length to deduce the distance separating it from the group of robots. The distance separating the robots from each other must also be known, so a short range positioning system was also designed and developed. The system developed is simple, portable, and is based on the time of flight of audible sonic waves. The precision attained is around 2 cm for distances of 1 m to 4 m under controlled conditions. A comprehensive positioning system is described in this thesis.

While the systems described in this thesis are aimed at humanitarian demining, they can be used for a multitude of other applications, either as a whole system or individually.

9.2 Discussion

9.2.1 Vehicle

The robot platform mechanical design was conceived with three main objectives in mind: minimize weight, maximize surface contact area with the ground, and provide payload capacity and space. The platform was designed and constructed as a foam sandwich structure with the assumption that it would break apart in case of an explosion, hence minimizing the damage done to the other parts by letting them be dispersed away under the force of the explosion. The platform is easy and inexpensive to reconstruct, while the smaller but more expensive parts such as the electronic circuits and the electric motors can be recovered and re-used if not damaged. The sacrificial platform concept has not been tested since it was deemed to be outside the scope of this thesis. Differential steer was chosen for its simplicity. It is functional, yet requires a mechanically simple system to provide the propulsion and steering functions.

9.2.2 Electronic

While developing the robot, many electronic modules were designed and constructed. To ease development, the electronic design was split in different functions, so more or less independent modules could be realized. The total volume taken by the electronic modules could be reduced by combining many of them (if not all) together on 1 or 2 bigger modules. The integration could save many connectors and redundant devices, such as power decoupling capacitors.

9.2.3 Software

The main part of the software resides in the microcontroller. All this software was written in 68HC12 assembly language. While being compact and efficient, it is fairly intensive to develop, debug and maintain. A transition to a higher level language, such as C/C++, would definitely reduce those problems. Also, the intelligence level of the robots is currently quite low. They only take commands from the base station and execute them. The only higher level task they perform is the PI loop for motor speed control. Trajectory control and formation control within the robot group would be a welcomed addition.

9.2.4 Positioning System

A long and a short range positioning systems are described in this thesis. Only the short range positioning system was fully developed. It presents a very linear output with respect to distance. However, its electronic circuitry is quite complex, involving many amplifier modules, analog filters, and signal strength detectors. The development and tuning of this system was carried out to a successful first prototype. The prototype circuitry is far from being optimally designed. The current precision is around ±2 cm with little post-processing of the data. The main error sources come from air movement, precision of the peak detection in the analog circuits and electrical noise affecting the circuit. The timer clock being 500 kHz, its time resolution is 2 μs, equivalent to a distance of 0.68 mm, which is around 30 times less than the currently observed precision.

9.3 Further Work

While substantial progress has been realized during the course of this thesis, a number of areas still need to be addressed to make this system practical and gain acceptability. Among these are the following.

The sacrificial platform concept constructed as a foam sandwich structure was inexpensive and proved to be a viable light weight and amply rigid structure. However, it was never subjected to an explosion to verify its ability to disintegrate and protect valuable components mounted on it. Analysis, simulation, and experimental work still need to be carried out to prove this concept.

The principle of operation and preliminary studies on the long range positioning system has been conducted and are reported in the thesis. However, the system has not been implemented yet. While industrial systems can be easily purchased off the shelf and used immediately to fulfill the requirements of the long range positioning system, their cost would render the low cost demining system impractical.

Many of the filtering and signal detection functionalities required for the operation of the short range positioning system have been implemented in hardware. These functionalities can be implemented in software and delegated to the MCU to simplify the associated electronics. Furthermore, the SRPS can be rendered more robust in functionality if a variable gain amplifier is used to restore the amplitude of the microphone signal as the distance measured increase. The decay of the microphone signal with distance has proven to be a problem as outlined in Chapter 8.

The mobile robot was built as a first prototype to prove the concept. A more rugged machine suitable for rough terrain should be designed and fabricated.

Proper base station software has to be developed to control the robot group, using information from the LRPS, the user, and the individual robots. It has to be realized while keeping in mind that the system is likely to be used in developing countries, where operators trained in computers could be difficult to find.

Finally, the ultimate goal of this platform is to carry some form of a landmine detection device. This is an area of active research and many technologies are promising. The reader can consult Table 2.1 for some of the current technologies being researched.

10 References

[1] Adams, M. D., *"Coaxial Range Measurement – Current Trends for Mobile Robotic Applications"*, IEEE Sensors Journal, Vol. 2, No. 1, February 2002, pp. 2-13

[2] Borenstein, J., Everett, H.R., and Feng, L., *"Where am I? Sensors and Methods for Mobile Robot Positioning"* Technical report, The University of Michigan, 1996

[3] Boutin, N., Clavet, A., *"Signaux et Circuits"*, André Noël, Éditeur, 1989

[4] Brooker, G., *"Time of Flight Measurement"*, Lecture notes for Sensor Systems Course, Australian Center for Field Robotics, University of Sydney, 2002

[5] Bruschini, C., Gros, B., *"A Survey of Current Sensor Technology Research for the Detection of Landmines"*, Proceedings of the International Workshop on Sustainable Humanitarian Demining (SusDem'97), 29 Sept.-1 Oct. 1997, Zagreb, Croatia, pp. 6.18/6.27

[6] Bruschini, C., *et al.*, *"EUDEM: The EU in humanitarian DEMining – Final Report (Study on the State of the Art in the EU related to humanitarian demining technology, products and practice)"*, EPFL-LAMI and VUB-ETRO, July 1999

[7] Canada National Defence / Défense Nationale du Canada, *"Canadian Forces Landmine Database"*, http://ndmic-cidnm.forces.gc.ca/index.asp?lang=e, October 2004

[8] Cepolina, E. E., *"Progetto di un dispositivo per la localizzazione di mine anti-uomo"* (Design of a mechatronic system for anti-personnel landmines localization, in English), M.Sc Thesis, Universita' Degli Studi Di Genova, Italy, January 20, 2003

[9] Chong, K. S., Kleeman, L., *"Accurate Odometry and Error Modelling for a Mobile Robot"*, Proceedings of the 1997 IEEE International Conference on Robotics and Automation

[10] Figueroa, F., Barbieri, E., *"An Ultrasonic Ranging System for Structural Vibration Measurements"*, IEEE Transactions on Instrumentation and Measurement, Vol. 40, No. 4, August 1991, pp. 764-769

[11] Garmin, GPS receiver manufacturer, www.garmin.com, 2004

[12] Grabowski, R., *et al.*, *"Heterogenous Teams of Modular Robots for Mapping and Exploration"*, Autonomous Robots (special issue on heterogenous and distributed robotics), Vol. 8, No.3, June 2000, pp. 293-308

[13] Gueuning, F. E., *et al.*, *"Accurate Distance Measurement by an Autonomous Ultrasonic System Combining Time-of-Flight and Phase-Shift Methods"*, IEEE Transactions on Instrumentation and Measurement, Vol. 46, No. 6, December 1997, pp. 1236-1240

[14] Habib, M. K., *"Mine Clearance Techniques and Technologies for Effective Humanitarian Demining"*, Journal of Mine Action, , Issue 6.1, April 2002

[15] Heberlein, D. C., *"Progress in Metal-Detection Techniques for Detecting and Identifying Landmines and Unexploded Ordnance"*, Institute for Defense Analysis, March 2000

[16] Howell, B., *"The Use of Mechanical Means for Humanitarian Demining Operations"*, Handicap International, 2000

[17] Hua, H., *et al.*, *"A Low-Cost Dynamic Range-Finding Device Based on Amplitude-Modulated Continuous Ultrasonic Wave"*, IEEE Transactions on Instrumentation and Measurements, Vol. 51, No. 2, April 2002, pp. 362-367

[18] International Campaign to Ban Landmines, *"Landmine Monitor Report 2003: Toward a Mine-Free World"*, New York: Human Rights Watch, August 2003, 826 pages

[19] Kleeman, L., *"Real Time Mobile Robot Sonar with Interference Rejection"*, Sensor Review, Vol 19, No 3, 1999, pp214-221

[20] Kreyszig, E., *"Advanced Engineering Mathematics"*, Seventh Edition, John Wiley & Sons, Inc., 1993

[21] Linx Technologies, *"Consideration For Sending Data With the HP Series"*, Application Note AN-00160, www.linxtechnologies.com, 1998

[22] Mächler, P., *"Detection Technologies for Anti-Personnel Mines"*, Proceedings of Symposium on Automomous Vehicles in Mine Countermeasures, Monterey, April 4-6, 1995

[23] Magellan, GPS receiver manufacturer, www.magellangps.com, 2004

[24] Mahjan, A., Walworth, M., *"3-D Position Sensing Using the Differences in the Time-of-Flights from a Wave Source to Various Receivers"*, Proceedings of the 1997 8th International Conference on Advanced Robotics, July 7-9, 1997, pp. 611-616

[25] Mahjan, A., Walworth, M., *"3-D Position Sensing Using the Differences in the Time-of-Flights from a Wave Source to Various Receivers"*, IEEE Transactions on Robotics and Automation, Vol. 17, No. 1, February 2001, pp. 91-94

[26] McNeff, J. G., *"The Global Positioning System"*, IEEE Transactions on Microwave Theory and Techniques, Vol. 50, No. 3, March 2002, pp 645-652

[27] MG Chemicals, PCB Prototyping products, www.mgchemicals.com, 2004

[28] Motorola, Semiconductors manufacturer, *"M68HC12B Family Advanced Information"*, Motorola reference number M68HC12B/D, 2000. Note: Motorola semiconductor division is now known as Freescale Semiconductor.

[29] Nakahira, K. *et al.*, *"Distance Measurement by an Ultrasonic System Based on a Digital Polarity Correlator"*, IEEE Transactions on Instrumentation and Measurement, Vol. 50, No. 6, December 2001, pp. 1748-1752

[30] Navarro-Serment, L. E., *et al.*, *"A Beacon System for the Localization of Distributed Robotic Teams"*, Proceedings of the International Conference on Field and Service Robotics, Pittsburg, PA, August 29-31, 1999

[31] Nicoud, J-D., *"Mine Clearance: not only a problem for the military any more"*, Proceedings of the 6th International Symposium on Measurement and Control in Robotics, Brussels, May 9-11 1996

[32] Ogata, K., *"Modern Control Engineering"*, Third Edition, Prentice Hall, 1997

[33] Paarmann, L. D., *"Design and Analysis of Analog Filters: A Signal Processing Perspective"*, Kluwer Academic Publishers, 2001

[34] Parrilla, M., Anaya, J. J., Fritsch, F., *"Digital Signal Processing Techniques for High Accuracy Ultrasonic Range Measurements"*, IEEE Transactions on Instrumentation and Measurement, Vol. 40, No. 4, August 1991, pp. 759-763

[35] Schmolke, A., Mallot, H. A., *"Polarization compass for robot navigation"*, Proceedings of the 5th German Workshop on Artifical Life, Lübeck, Germany, 18-20 March 2002

[36] Shapiro, A. H., *"The Dynamics and Thermodynamics of compressible Fluid Flow"*, Vol. 1, The Ronald Press Company, 1953

[37] Tong, C., *et al.*, *"A Method for Short or Long Range Time-of-Flight Measurements Using Phase-Detection With an Analog Circuit"*, IEEE Transactions on Instrumentation and Measurement, Vol. 50, No. 5, October 2001, pp. 1324-1328

[38] Trevelyan, J., *"Landmines Robotic Paper 1: Robotic Landmine Clearance"*, internal report, http://www.mech.uwa.edu.au/jpt/demining/reports/papers1996/wp1.html, May 1995, retrieved April 2, 2005

[39] United States Department of State, Bureau of Politcal-Military Affairs, *"To Walk the Earth in Safety: The United States Commitment to Humanitarian Demining"*, fifth edition, August 2004, 62 pages

[40] Walker, J., *"Minerats: Moore's Law in the Minefield"*, Presentation at the IEEE Asilomar Microprocessor Workshop, April 19th, 1995

[41] Wang, L., *et al.*, *"A 3D Scanning Laser Rangefinder and its Application to an Autonomous Guided Vehicle"*, Proceedings of 2000 IEEE 51st Vehicle Technology Conference 2000, pp. 331-335

[42] Wehn, H. W., Bélanger, P. R., *"Ultrasound-Based Robot Position Estimation"*, IEEE Transactions on Robotics and Automation, Vol. 13, No. 5, October 1997, pp. 682-692

Appendix A Organizations About Demining Operations

Adopt-a-Minefield

Many organizations are dedicated to humanitarian demining. Adopt-a-Minefield (www.landmines.org) is an organization is a program of the United Nations of the USA that works on resolving the global landmine crisis. It raises money for mine clearing and survivor assistance.

Canadian Landmine Foundation

The Canadian Landmine Foundation (CLF) (www.canadianlandmine.org) is a private sector foundation devoted exclusively to the eradication of landmines. Among other things, they are involved in Canine Demine, a program to train dogs to detect landmines.

Handicap International

Handicap International (www.handicap-international.org) is an organization based in Lyon, France, having offices in France, Germany, Belgium, Luxembourg, Denmark, Switzerland, Canada, United-States and United Kingdom. Amongst its activities, there is landmine victim assistance, demining, and one of the six NGO that gave birth to the International Campaign to Ban Landmines.

Norwegian People's Aid

From their website (www.npaid.org)
"Norwegian People's Aid is the humanitarian organization of the Norwegian trade union movement." It is a NGO founded in 1939, and humanitarian mine clearing activities in the 1990's.

Mines Action Canada

Mines Action Canada (www.minesactioncanada.org) is a coalition of about 40 Canadian NGO, and their primary concerns are about human and socio-economic impacts of landmines.

International Campaign to Ban Landmines

The International Campaign to Ban Landmines (www.icbl.org) was founded in 1991 by 6 NGO (Handicap International, Human Rights Watch, Medico International, Mines Advisory Group, Physicians for Human Rights, and Vietnam Veterans of America Foundation). They won the Nobel Peace Prize in 1997, and now, in 2004, are now composed of 13 organizations. Each year, they produce an annual report [18], described in Section 2.1.1.

Appendix B Electrical Schematics for MCU Module

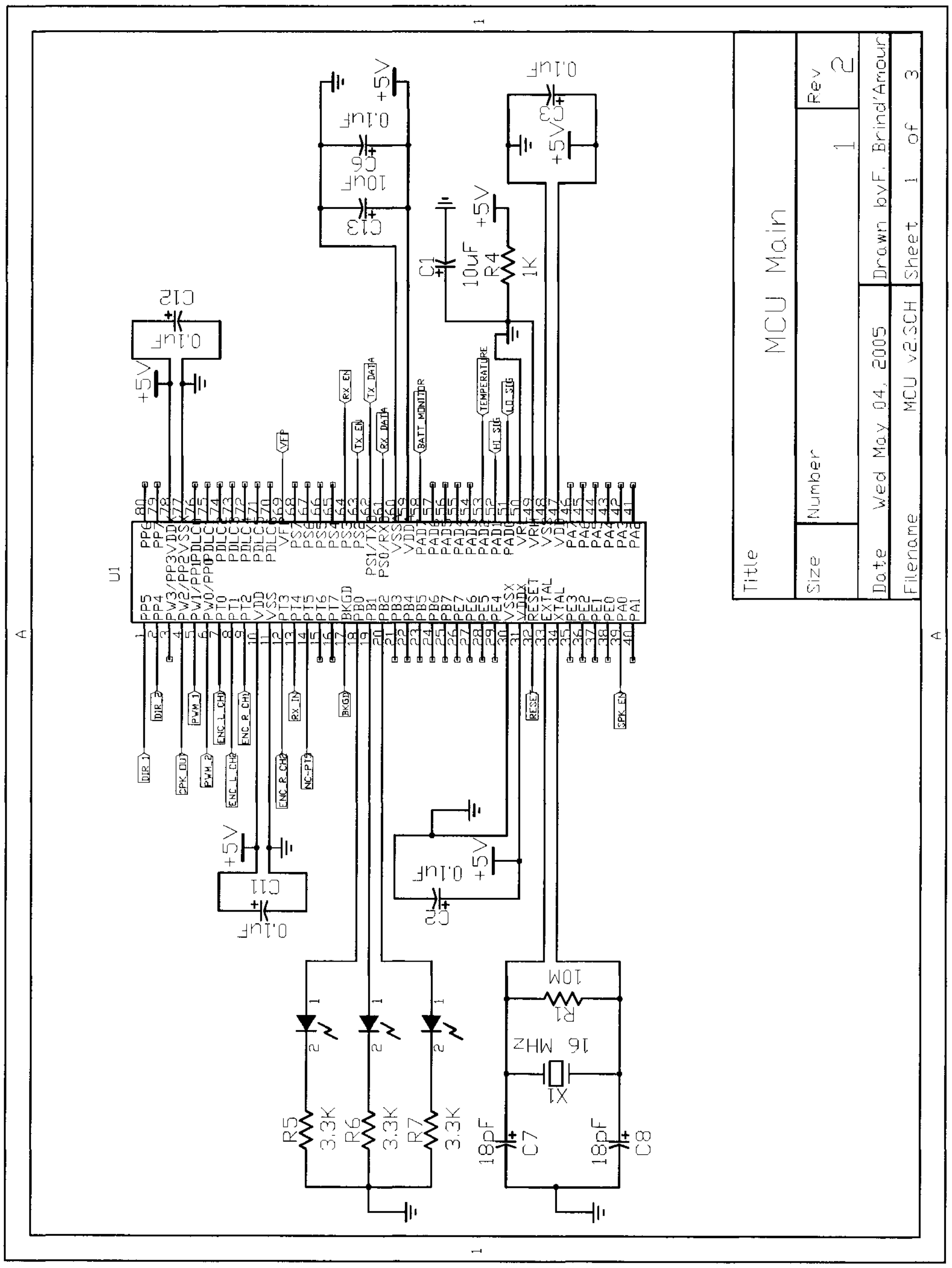

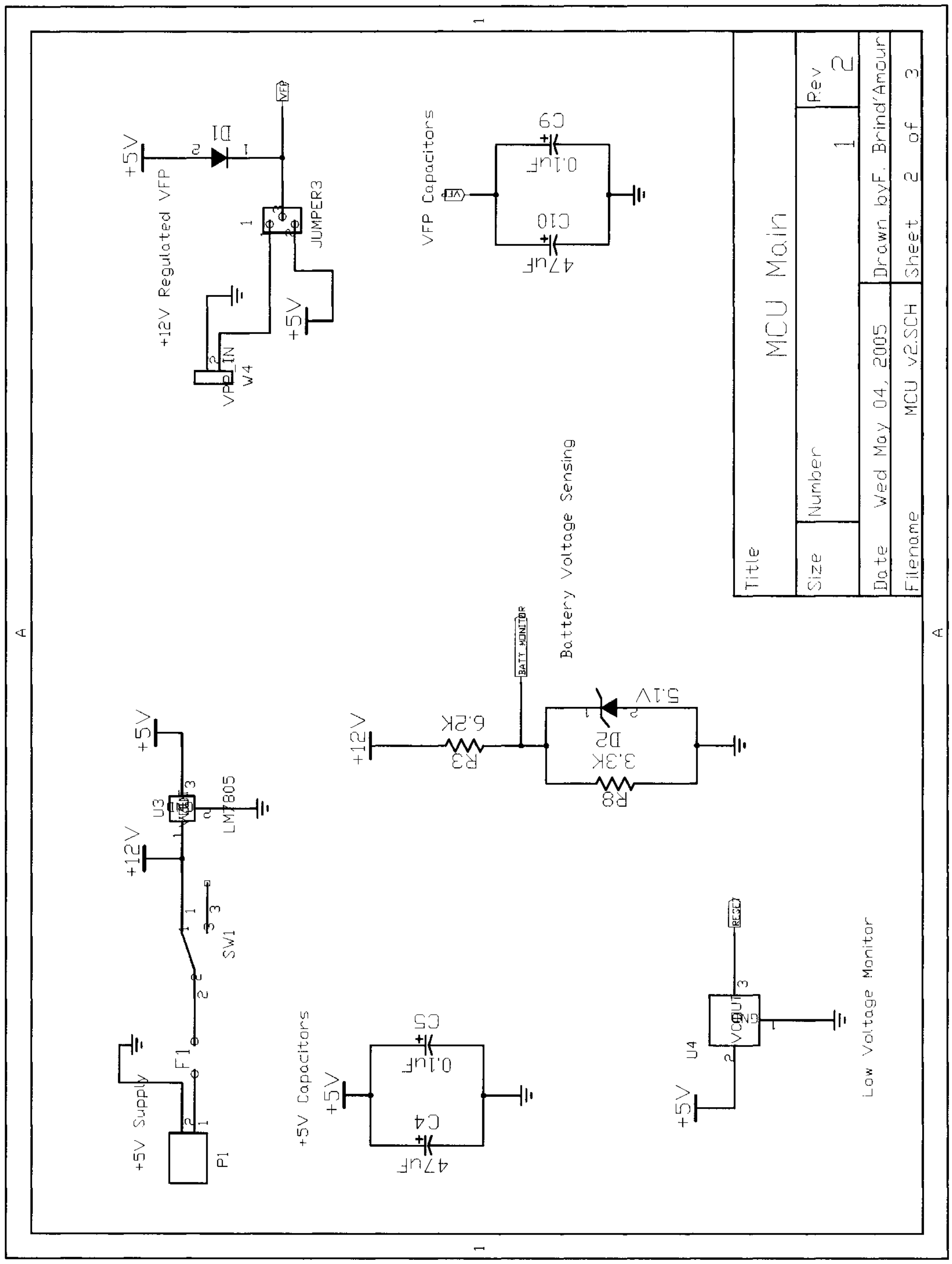
+5V Supply
P1
F1
SW1
+12V
U3
LM7805
+5V
+12V Regulated VFP
VPP_IN
W4
D1
JUMPER3
VFP
+5V Capacitors
47uF
C4
0.1uF
C5
+12V
R3
6.2K
BATT_MONITOR
Battery Voltage Sensing
R8
3.3K
D2
5.1V
VFP Capacitors
47uF
C10
0.1uF
C9
U4
VOUT
GND
RESET
Low Voltage Monitor
Title
MCU Main
Size
Number
1
Rev
2
Date Wed May 04, 2005
Drawn by F. Brind'Amour
Filename MCU v2.SCH
Sheet 2 of 3

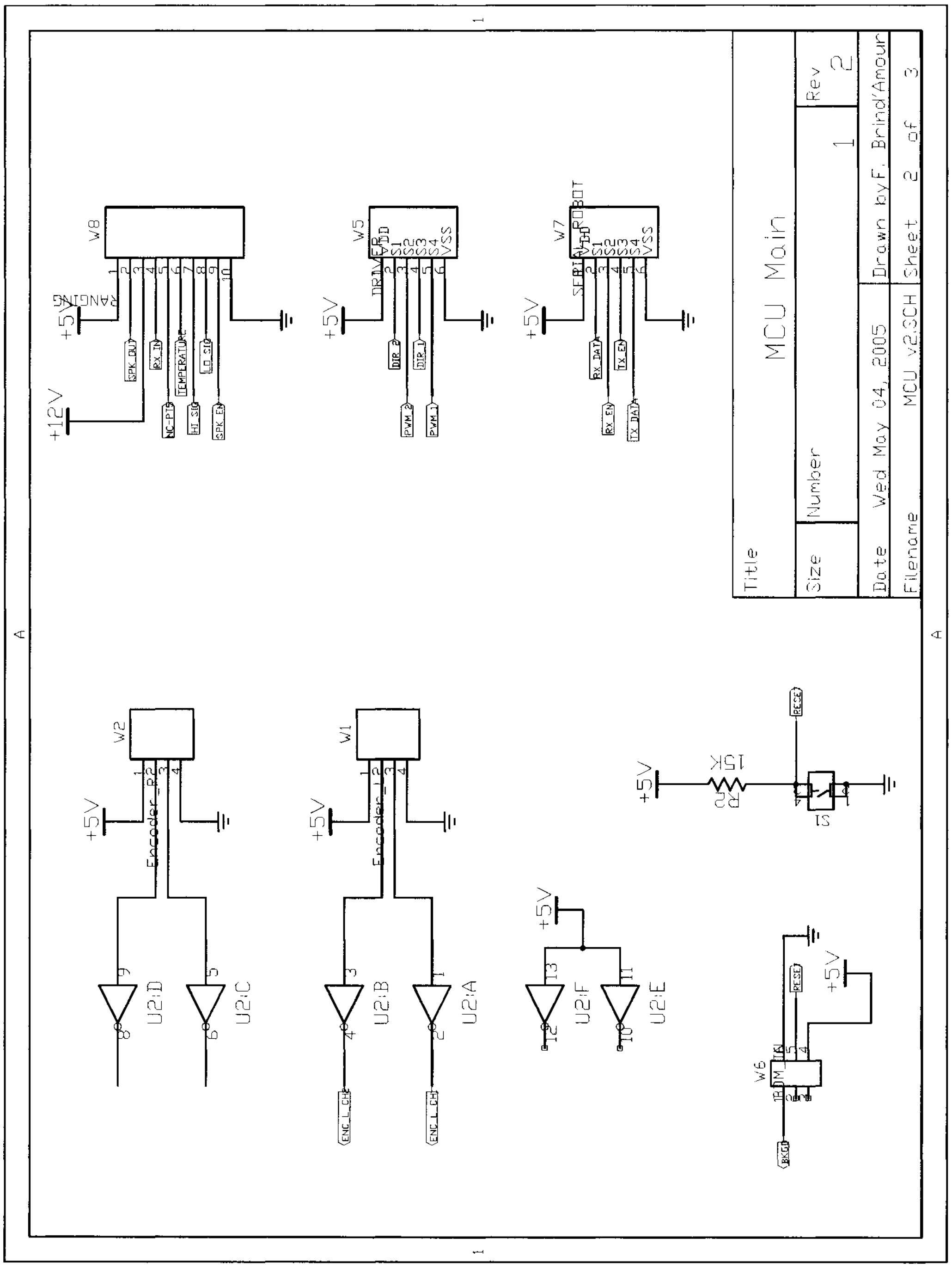
Title
MCU Main
Size
Number
1
Rev
2
Date Wed May 04, 2005
Drawn by F. Brind'Amour
Filename MCU v2.3CH
Sheet 2 of 3

Appendix C Electrical Schematics for Driver Module

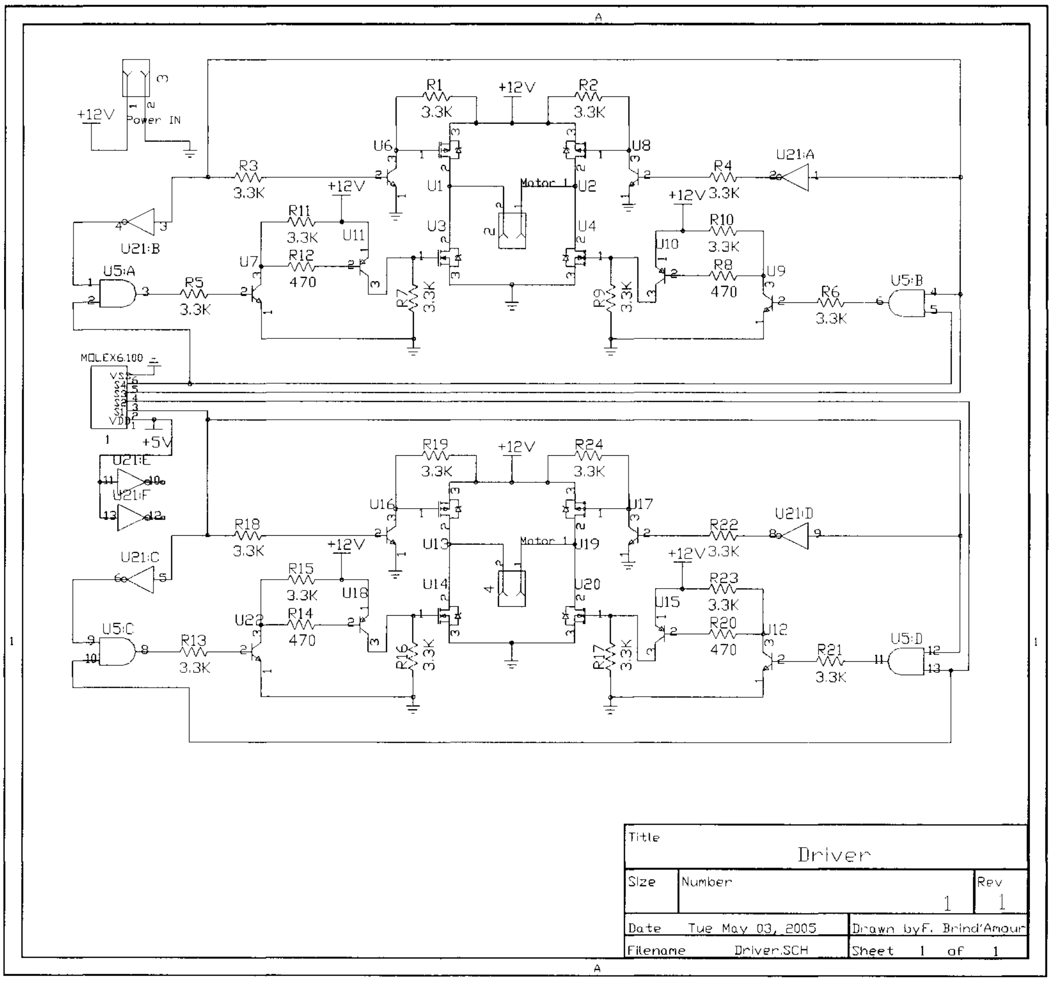

Appendix D Electrical Schematics for Serial Computer Module

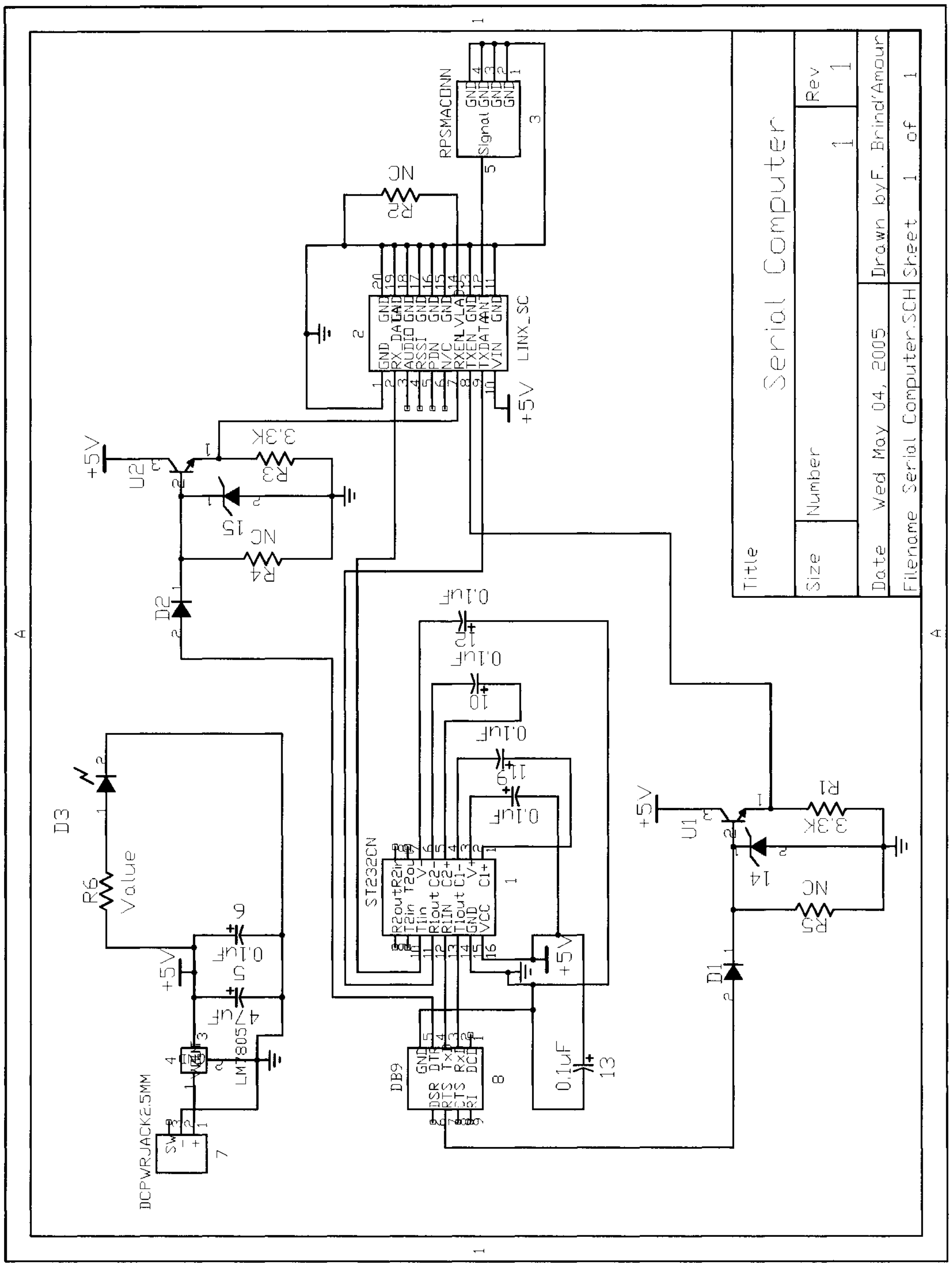

Appendix E Electrical Schematics for Serial Robot Module

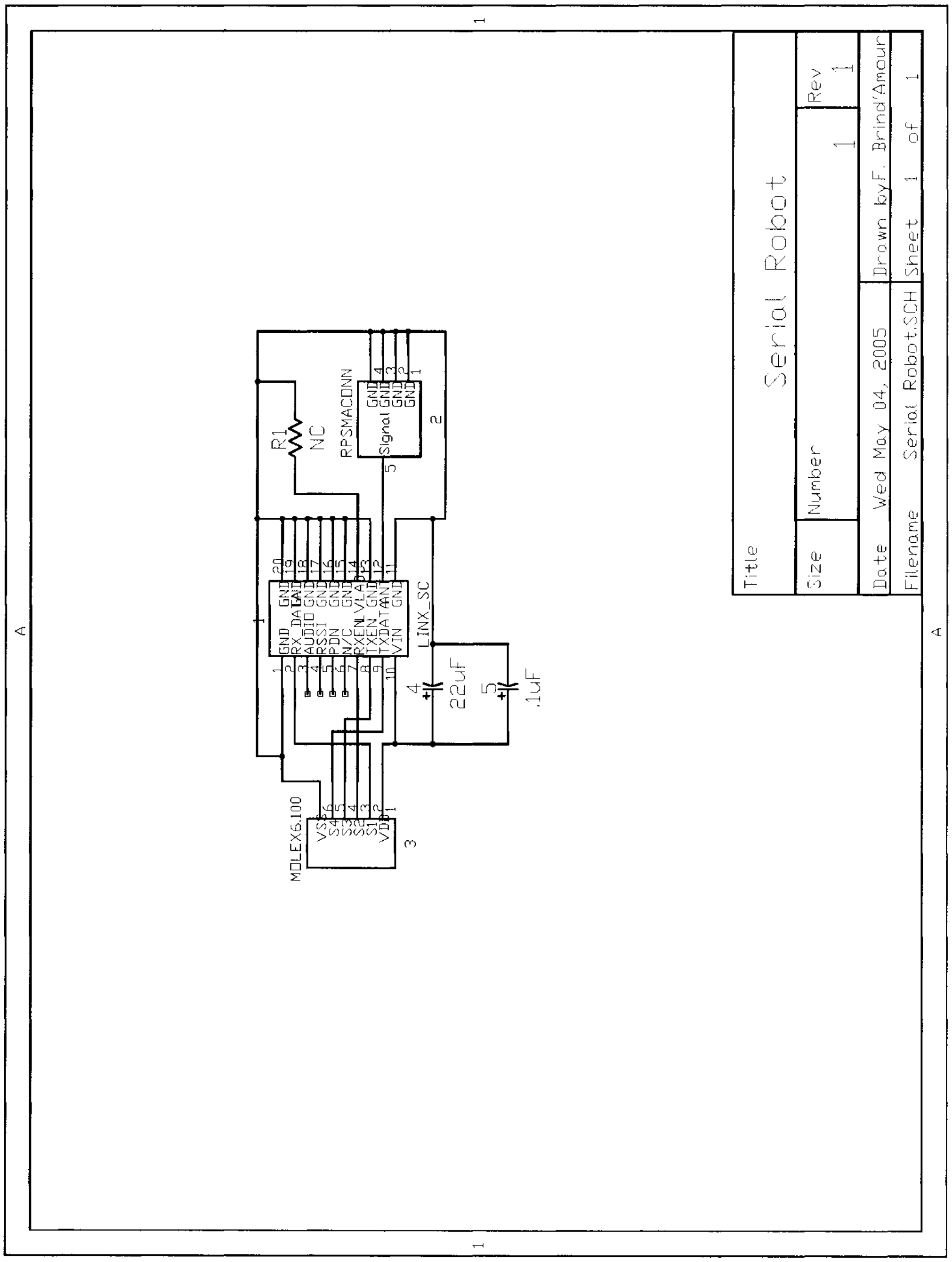

Appendix F Electrical Schematics for Encoder Module

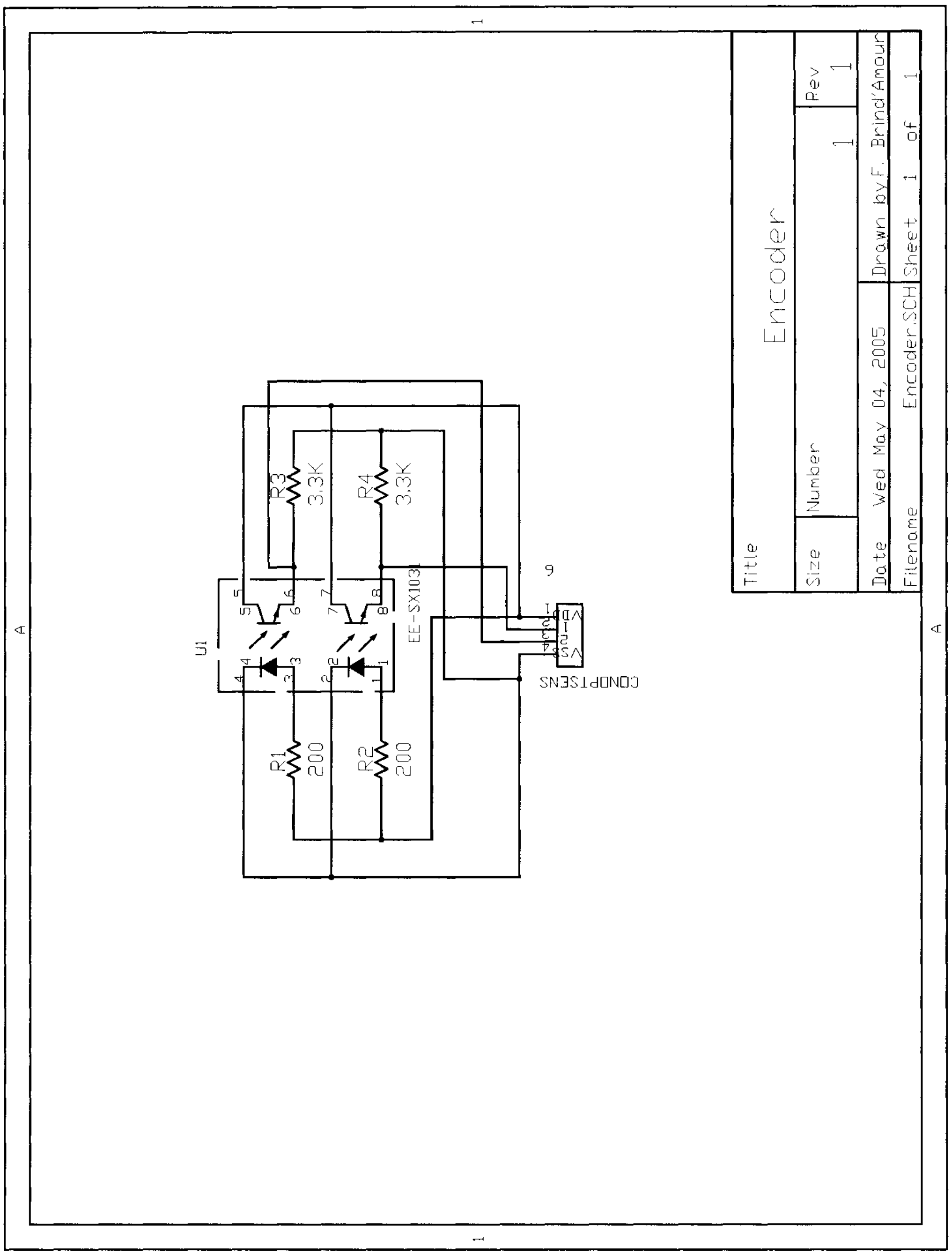

Appendix G Electrical Schematics for Ranging Module

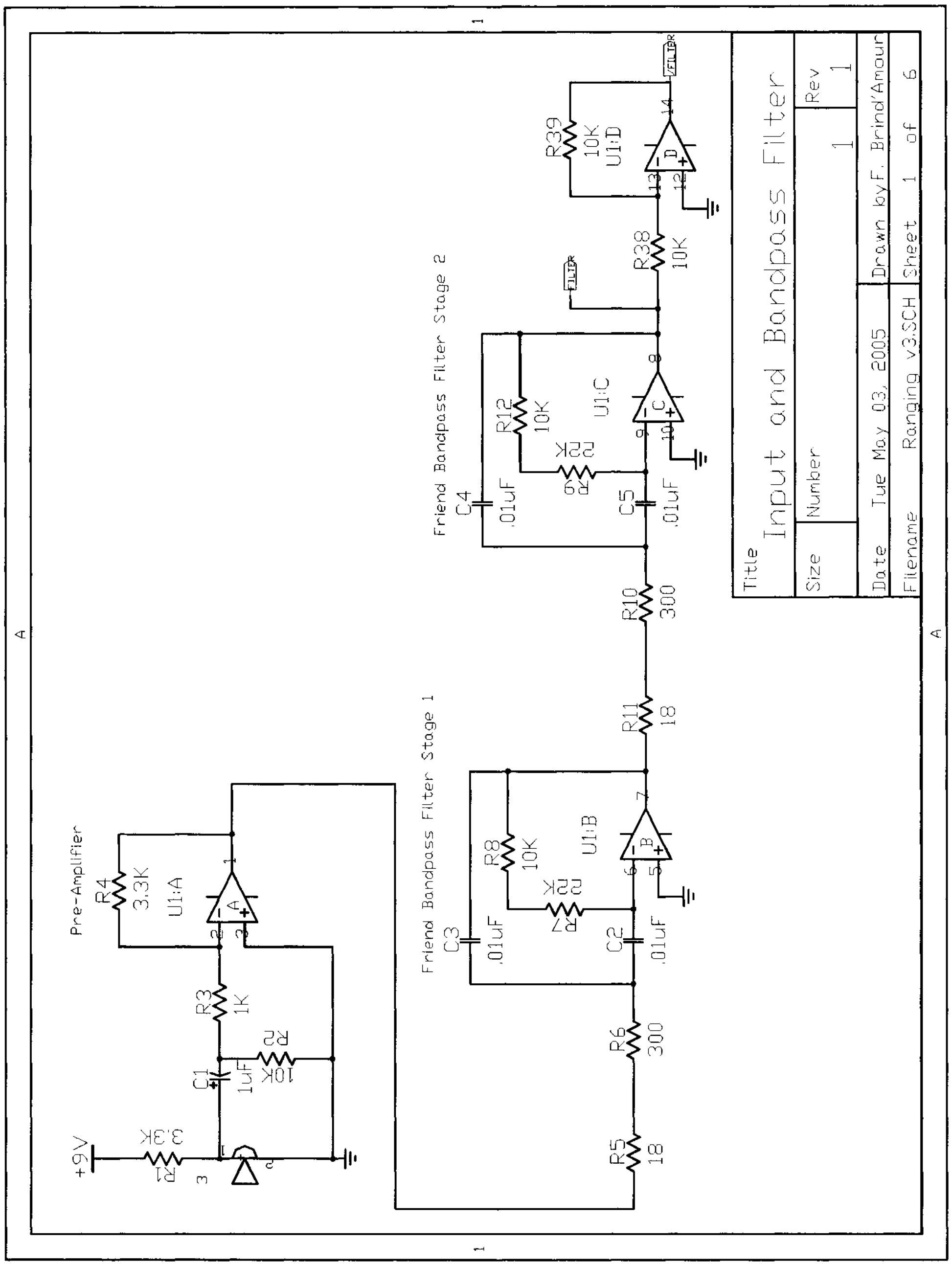

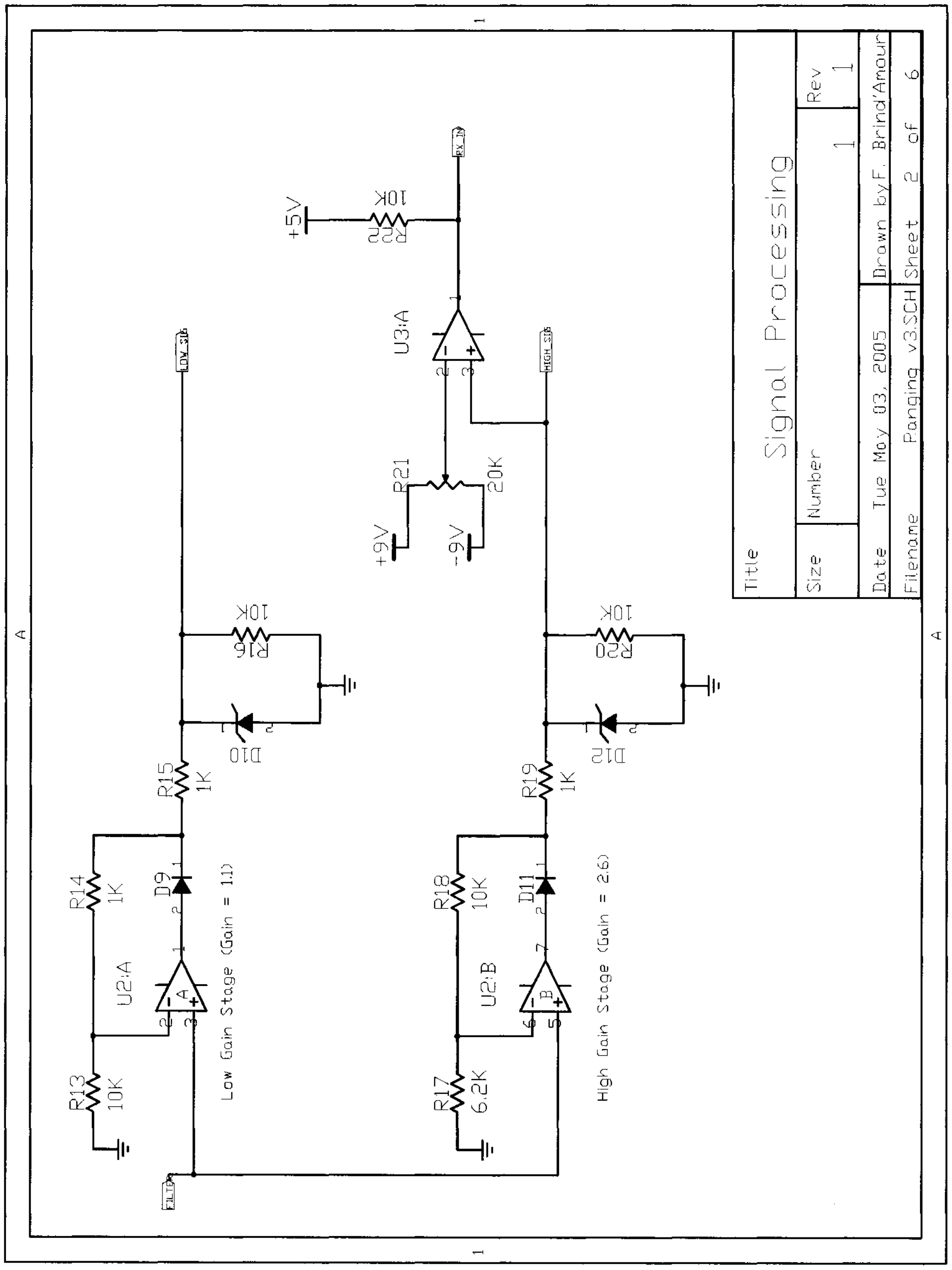

Signal Processing
Title
Size
Number
1
Rev
1
Date Tue May 03, 2005
Drawn by F. Brind'Amour
Filename Ranging v3.SCH
Sheet 2 of 6
Low Gain Stage (Gain = 11)
High Gain Stage (Gain = 2.6)
U2:A
U2:B
U3:A
R13 10K
R14 1K
R15 1K
R16 10K
R17 6.2K
R18 10K
R19 1K
R20 10K
R21 20K
R22 10K
D9
D10
D11
D12
+5V
+9V
-9V
LOW_SIG
HIGH_SIG
RX_IN
FILT

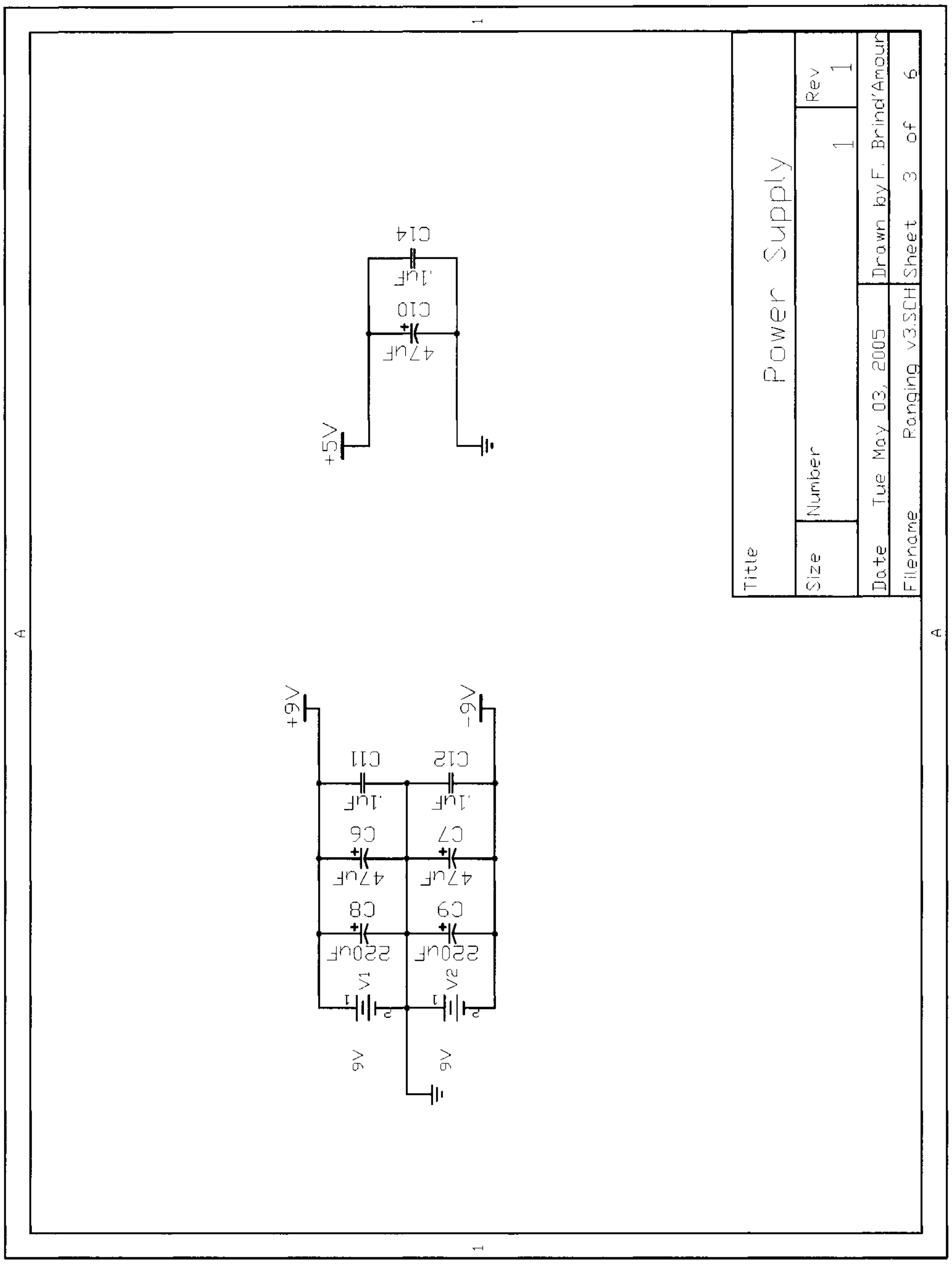

Title
Power Supply
Size
Number
1
Rev
1
Date Tue May 03, 2005
Drawn by F. Brind'Amour
Filename Ranging v3.SCH
Sheet 3 of 6
+5V
47uF
C10
.1uF
C14
+9V
-9V
C11
C12
.1uF
.1uF
C6
C7
47uF
47uF
C8
C9
220uF
220uF
V1
V2
9V
9V

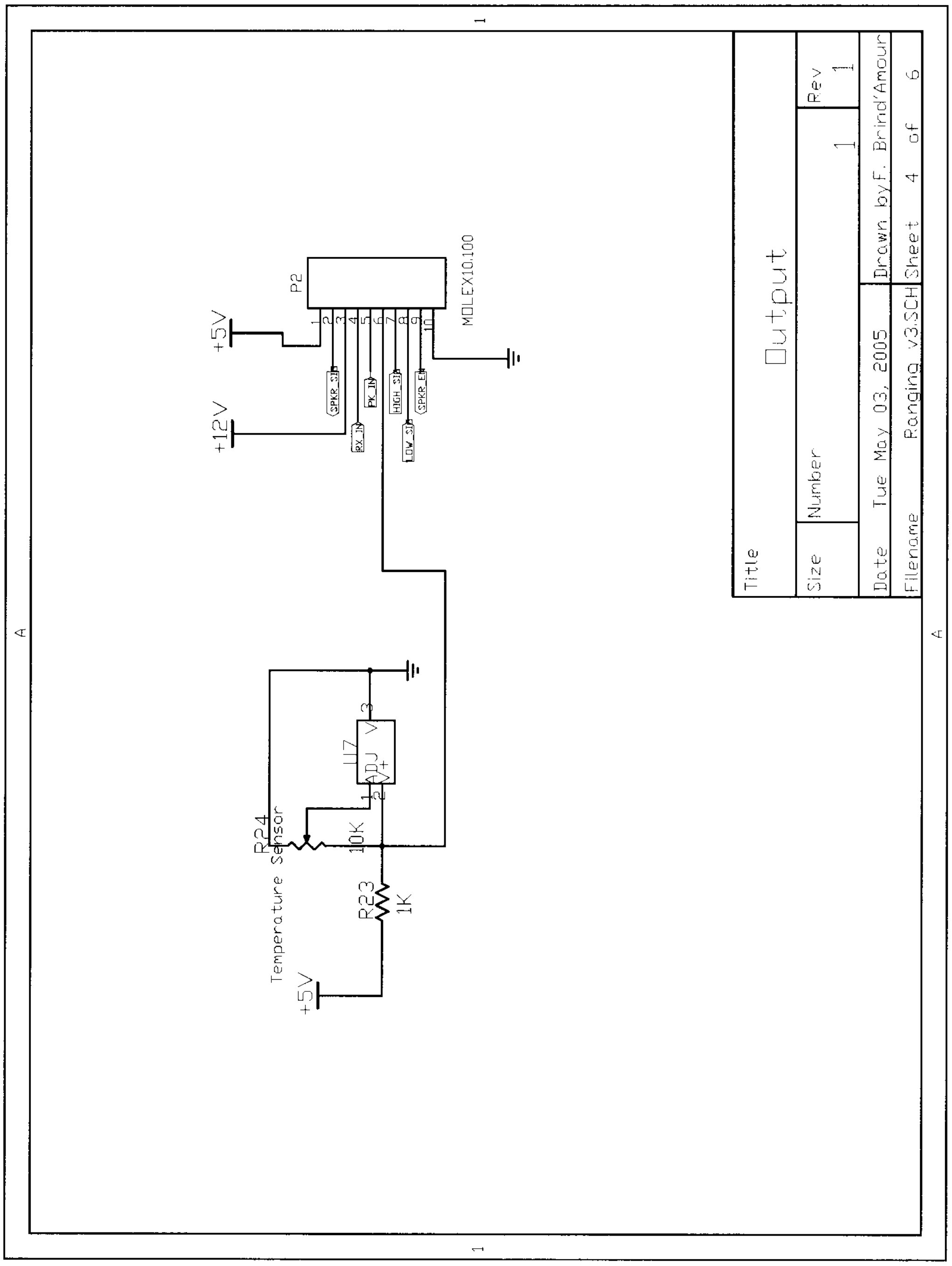
Output
Title
Size
Number
1
Rev
1
Date
Tue May 03, 2005
Drawn by F. Brind'Amour
Filename
Ranging v3.SCH
Sheet 4 of 6
P2
MOLEX10.100
+5V
+12V
U7
ADJ
V+
R24
Temperature Sensor
10K
R23
1K
+5V

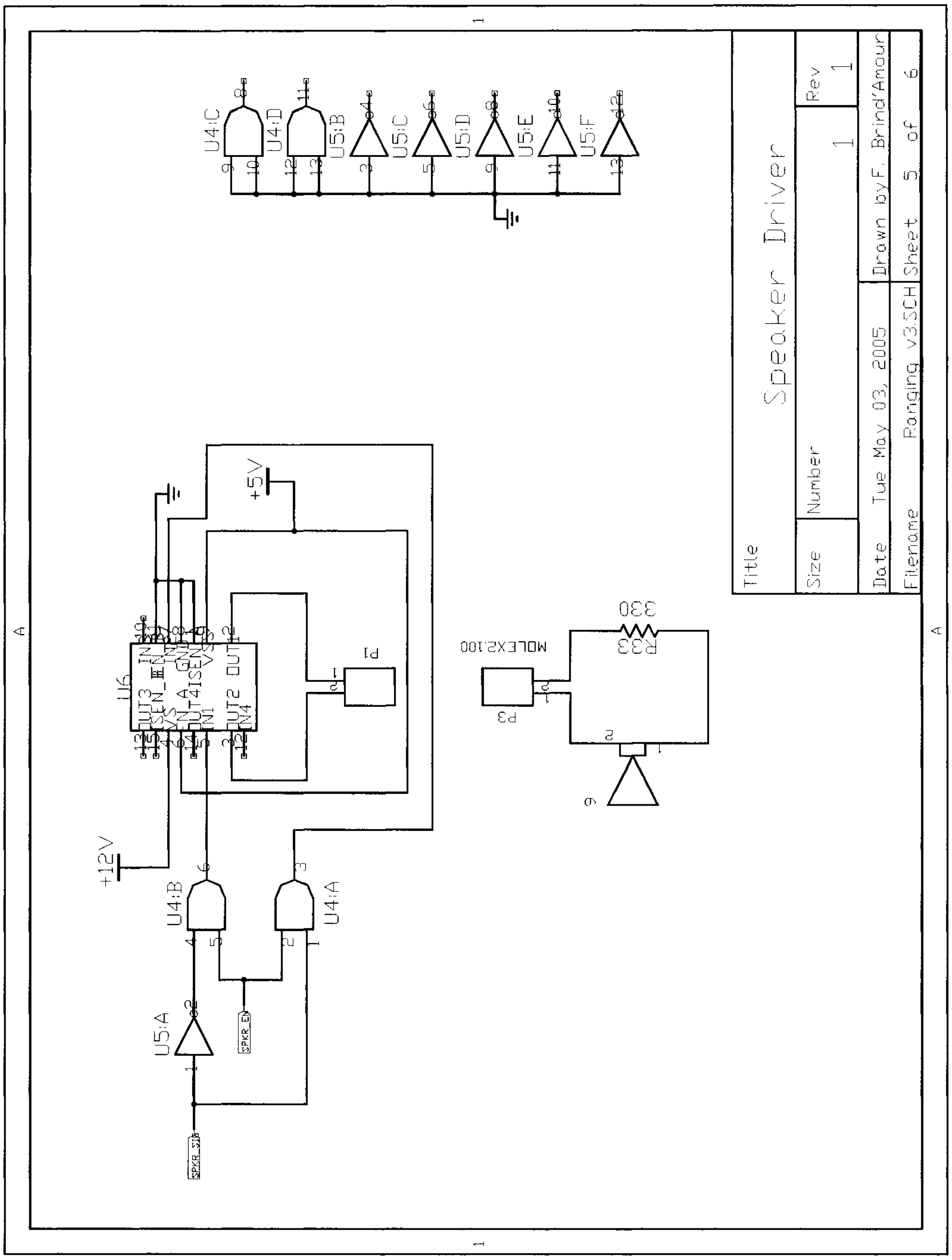
Title
Speaker Driver
Size
Number
Rev
1
Date Tue May 03, 2005
Drawn by F. Brind'Amour
Filename Ranging v3.SCH
Sheet 5 of 6
U6
U4:A
U4:B
U4:C
U4:D
U5:A
U5:B
U5:C
U5:D
U5:E
U5:F
+12V
+5V
P1
P3
R33
330
MOLEX2.100
SPKR_EN
SPKR_SIG

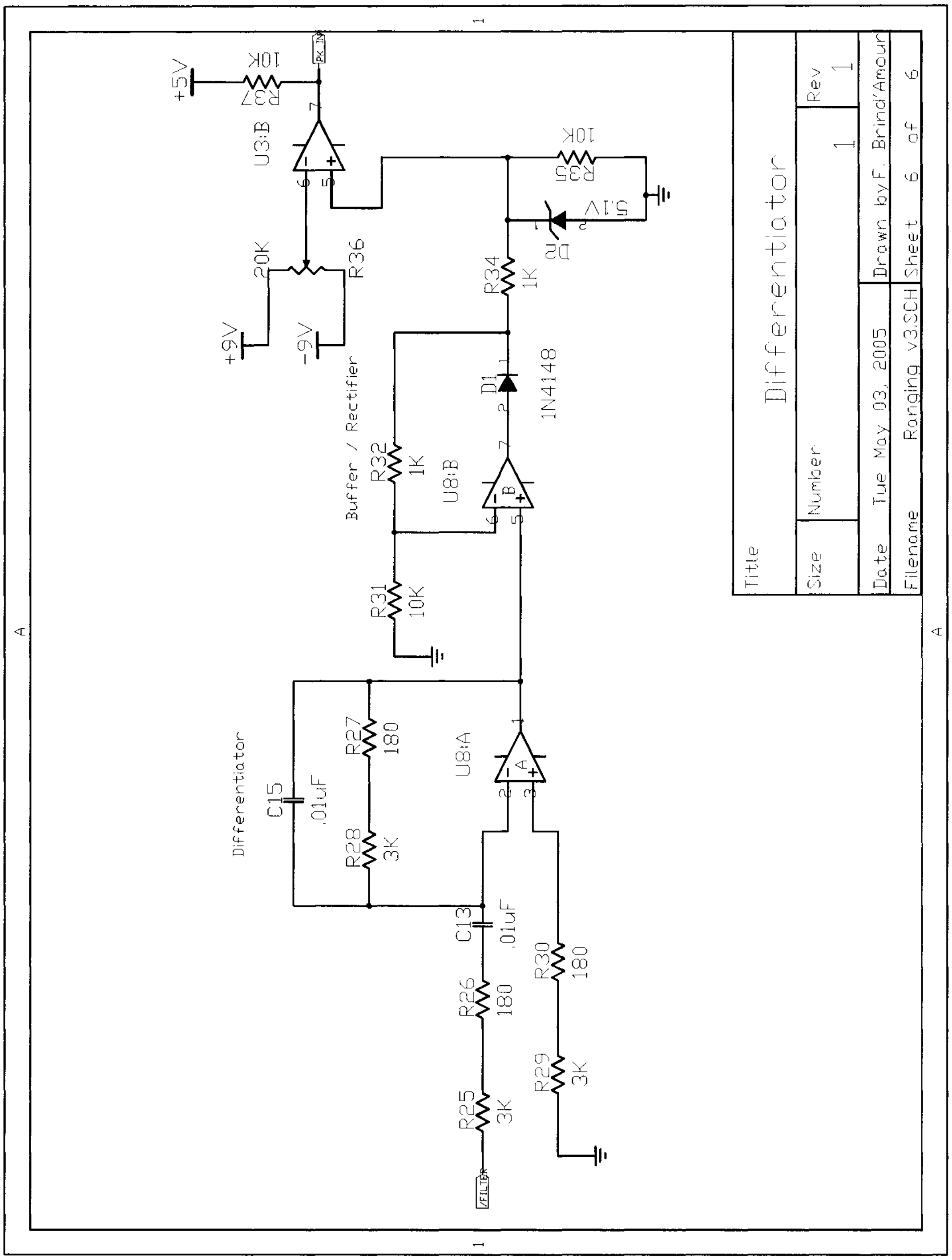
Differentiator
R25 3K
R26 180
C13 .01uF
R29 3K
R30 180
R28 3K
C15 .01uF
R27 180
U8:A
Buffer / Rectifier
R31 10K
R32 1K
U8:B
D1 1N4148
R34 1K
D2 5.1V
R35 10K
+9V
-9V
20K R36
U3:B
R37 10K
+5V
PK IN
FILTER
Title
Differentiator
Size
Number
1
Rev
1
Date Tue May 03, 2005
Drawn by F. Brind'Amour
Filename Ranging v3.SCH
Sheet 6 of 6

Appendix H PID Routine Code (68HC12 Assembler)

```
PIDRoutine:
CheckZDSL:                          ;Check if desired speed left is 0
    ldaa     PIDFlags
    anda     #%00000010
    cmpa     #%00000010
    beq      SetZeroSpeedLeft;If ZDSL flag is set, stop left motor and reset integral
    bra      CheckZeroSpeedLeft   ;Else, check if zero speed left

SetZeroSpeedLeft:
    movb     #$00,PWDTY0
    ldx      #integratorLeft
    movw     #$0000,2,X+
    movw     #$0000,0,X
    lbra     CheckZDSR

CheckZeroSpeedLeft:
    ldaa     encoderFlags
    anda     #%00000010
    cmpa     #%00000010
    beq      ZeroSpeedLeft
    bra      CalcSpeedLeft

ZeroSpeedLeft:
    movw     #$0000,speedLeft
    bra      CalcErrorLeft

CalcSpeedLeft:
    ldd      deltaTLeft
    lsrd                            ;Divide deltaTLeft by 2
    xgdx
    ldd      #$7FFF
    idivs
    stx      speedLeft

CheckNegSpeedLeft:                  ;Check if speed is negative or positive
    ldaa     encoderFlags
    anda     #%0000001
    cmpa     #%0000001
    bne      SetNegSpeedLeft
    bra      CalcErrorLeft

SetNegSpeedLeft:
    clra
    clrb
    subd     speedLeft
    std      speedLeft
    bra      CalcErrorLeft

CalcErrorLeft:                              ;error = speedD - speed
    ldd      speedLeftD
```

```
    subd     speedLeft
    bvs      SaturateErrorLeft    ;If two's complement overflow, handle exception
    std      speedLeftE
    bra      CalcPIDLeft

SaturateErrorLeft:
    bmi      SaturateErrorPositiveLeft
    bra      SaturateErrorNegativeLeft

SaturateErrorNegativeLeft:
    movw     #$8000,speedLeftE
    bra      CalcPIDLeft

SaturateErrorPositiveLeft:
    movw     #$7FFF,speedLeftE
    bra      CalcPIDLeft

CalcPIDLeft:
CalcIntegralLeft:
    ldx      #kI
    ldy      #speedLeftE
    emacs    integratorLeft

CheckSatIntegralLeft:
    ldd      integratorLeft
    cpd      #$0000               ;If high word is greater than 0, saturate positive
    bgt      SaturatePosIntegralLeft
    cpd      #$FFFF                       ;If low word is lower than -1, saturate negative
    blt      SaturateNegIntegralLeft
    bra      CalcProportionnalLeft

SaturatePosIntegralLeft:
    movw     #$0000,integratorLeft
    movw     #$FFFF,integratorLeft+2
    bra      CalcProportionnalLeft

SaturateNegIntegralLeft:
    movw     #$FFFF,integratorLeft
    movw     #$0000,integratorLeft+2
    bra      CalcProportionnalLeft

CalcProportionnalLeft:
    ldx      #integratorLeft
    ldy      #outputPIDLeft
    movw     2,X+,2,Y+            ;Transfer integratorLeft to outputPIDLeft
    movw     0,X,0,Y                      ;Transfer integratorLeft to outputPIDLeft
    ldx      #kP
    ldy      #speedLeftE
    emacs    outputPIDLeft
    bmi      SetNegOutputLeft     ;If result is negative, direction will be negative also
    bra      SetPosOutputLeft

SetNegOutputLeft:
    ldaa     PORTP
```

```
    anda      #%11101111           ;Set negative direction
    staa      PORTP
    ldd       outputPIDLeft
    cpd       #$FFFF
    blt       SatNegOutputLeft     ;If high word of outputPIDLeft is lower than -1,
saturate negative
    ldaa      outputPIDLeft+2      ;Else, high byte of low word is the output, but it must
be converted to positive
    coma
    cmpa      #$FF
    bne       UpdateNegOutputLeft
    ldaa      #$FE
    bra       UpdateNegOutputLeft  ;If output is $FF, set it to $FE (special case of HC12
PWM)

SatNegOutputLeft:
    ldaa      #$FE

UpdateNegOutputLeft:
    staa      PWDTY0
    bra       CheckZDSR

SetPosOutputLeft:
    ldaa      PORTP
    oraa      #%00010000           ;Set positive direction
    staa      PORTP
    ldd       outputPIDLeft
    cpd       #$0000
    bgt       SaturatePositiveOutputPIDLeft
    bra       UpdatePosOutputLeft

SaturatePositiveOutputPIDLeft:
    movw      #$FEFF,outputPIDLeft+2

UpdatePosOutputLeft:
    movb      outputPIDLeft+2,PWDTY0

CheckZDSR:                         ;Check if desired speed right is 0
    ldaa      PIDFlags
    anda      #%00001000
    cmpa      #%00001000
    beq       SetZeroSpeedRight    ;If ZDSL flag is set, stop left motor
    bra       CheckZeroSpeedRight  ;Else, check if zero speed left

SetZeroSpeedRight:                 ;Desired speed is 0, so stop motor
    movb      #$00,PWDTY1
    ldx       #integratorRight
    movw      #$0000,2,X+
    movw      #$0000,0,X
    lbra      End_PIDRoutine

CheckZeroSpeedRight:
    ldaa      encoderFlags
    anda      #%00001000
```

```
    cmpa     #%00001000
    beq      ZeroSpeedRight
    bra      CalcSpeedRight

ZeroSpeedRight:
    movw     #$0000,speedRight
    bra      CalcErrorRight

CalcSpeedRight:
    ldd      deltaTRight
    lsrd                          ;Divide deltaTRight by 2
    xgdx
    ldd      #$7FFF
    idivs
    stx      speedRight

CheckNegSpeedRight:               ;Check if speed is negative or positive
    ldaa     encoderFlags
    anda     #%0000100
    cmpa     #%0000100
    bne      SetNegSpeedRight
    bra      CalcErrorRight

SetNegSpeedRight:
    clra
    clrb
    subd     speedRight
    std      speedRight
    bra      CalcErrorRight

CalcErrorRight:                           ;error = speedD   speed
    ldd      speedRightD
    subd     speedRight
    bvs      SaturateErrorRight   ;If two's complement overflow, handle exception
    std      speedRightE
    bra      CalcPIDRight

SaturateErrorRight:
    bmi      SaturateErrorPositiveRight
    bra      SaturateErrorNegativeRight

SaturateErrorNegativeRight:
    movw     #$8000,speedRightE
    bra      CalcPIDRight

SaturateErrorPositiveRight:
    movw     #$7FFF,speedRightE
    bra      CalcPIDRight

CalcPIDRight:
CalcIntegralRight:
    ldx      #kI
    ldy      #speedRightE
    emacs    integratorRight
```

```
CheckSatIntegralRight:
    ldd     integratorRight
    cpd     #$0000                  ;If high word is greater than 0, saturate
positive
    bgt     SaturatePosIntegralRight
    cpd     #$FFFF                  ;If low word is lower than -1, saturate negative
    blt     SaturateNegIntegralRight
    bra     CalcProportionnalRight

SaturatePosIntegralRight:
    movw    #$0000,integratorRight
    movw    #$FFFF,integratorRight+2
    bra     CalcProportionnalRight

SaturateNegIntegralRight:
    movw    #$FFFF,integratorRight
    movw    #$0000,integratorRight+2
    bra     CalcProportionnalRight

CalcProportionnalRight:
    ldx     #integratorRight
    ldy     #outputPIDRight
    movw    2,X+,2,Y+           ;Transfer integratorRight to outputPIDRight
    movw    0,X,0,Y                 ;Transfer integratorRight to outputPIDRight
    ldx     #kP
    ldy     #speedRightE
    emacs   outputPIDRight
    bmi     SetNegOutputRight   ;If result is negative, direction will be negative also
    bra     SetPosOutputRight

SetNegOutputRight:
    ldaa    PORTP
    anda    #%11011111          ;Set negative direction
    staa    PORTP
    ldd     outputPIDRight
    cpd     #$FFFF
    blt     SatNegOutputRight   ;If high word of outputPIDRight is lower than -1,
saturate negative
    ldaa    outputPIDRight+2    ;Else, high byte of low word is the output, but it must
be converted to positive
    coma
    cmpa    #$FF
    bne     UpdateNegOutputRight
    ldaa    #$FE
    bra     UpdateNegOutputRight ;If output is $FF, set it to $FE (special case of HC12
PWM)

SatNegOutputRight:
    ldaa    #$FE

UpdateNegOutputRight:
    staa    PWDTY1
    bra     End_PIDRoutine
```

```
SetPosOutputRight:
    ldaa      PORTP
    oraa      #%00100000          ;Set positive direction
    staa      PORTP
    ldd       outputPIDRight
    cpd       #$0000
    bgt       SaturatePositiveOutputPIDRight
    bra       UpdatePosOutputRight

SaturatePositiveOutputPIDRight:
    movw      #$FEFF,outputPIDRight+2

UpdatePosOutputRight:
    movb      outputPIDRight+2,PWDTY1

End_PIDRoutine:
    rts
```